INFORMATION TO USERS

This manuscript has been reproduced from the microfilm master. UMI films the text directly from the original or copy submitted. Thus, some thesis and dissertation copies are in typewriter face, while others may be from any type of computer printer.

The quality of this reproduction is dependent upon the quality of the copy submitted. Broken or indistinct print, colored or poor quality illustrations and photographs, print bleedthrough, substandard margins, and improper alignment can adversely affect reproduction.

In the unlikely event that the author did not send UMI a complete manuscript and there are missing pages, these will be noted. Also, if unauthorized copyright material had to be removed, a note will indicate the deletion.

Oversize materials (e.g., maps, drawings, charts) are reproduced by sectioning the original, beginning at the upper left-hand corner and continuing from left to right in equal sections with small overlaps.

ProQuest Information and Learning
300 North Zeeb Road, Ann Arbor, MI 48106-1346 USA
800-521-0600

Experimental Study on Two-Phase Flow Regimes and Frictional Pressure Drop in Mini- and Micro-Channels

Korhan Kaan Pehlivan

A Thesis

in

The Department of

Mechanical and Industrial Engineering

Presented in Partial Fulfillment of the Requirements

for the Degree of Master of Applied Science at

Concordia University

Montreal, Quebec, Canada

February 2003

Abstract

Experimental Study on Two-Phase Flow Regimes and Frictional Pressure Drop in Mini- and Micro-Channels

Korhan Kaan Pehlivan

When one designs systems in which there is flow through micro-channels, such as in compact heat exchangers or in small-sized refrigeration systems, it is of utmost importance to possess an extensive knowledge of two-phase flow regimes and pressure drop. The characteristics of two-phase flow in micro-channels differ greatly from the ones found in macro-channels. In order to investigate the frictional pressure drop characteristics as well as the two-phase gas-liquid flow (air-water) regimes found in mini- and micro-channels, a new experimental test facility was designed and built at Concordia University.

The new experimental test facility was designed in order to generate an experimental database for pressure drop and flow regime maps in mini- and micro-channels. The test facility was equipped with state-of-the-art flow meters and differential pressure transducers. Once the test facility was built, three different circular test sections, with diameters of 3 mm, 1 mm, and 800 μm, were used to study the two-phase frictional pressure drop and flow regime transition regions. Most of the experiments for each test section were executed at high local superficial gas velocities (U_{GS} > 10 m/s).

The experimental pressure drop data was compared with the homogenous model, the Friedel (1979) model, and the Chisholm (1967) model. The homogenous model showed the most similarities with the data acquired during the course of this experiment, with an average error of 1.2%, 15.6%, and 24.1% for the 3 mm, 1 mm, and 0.8 mm test sections, respectively. However, it was also observed that the standard deviation of the errors increased as the channel diameter decreased. The Friedel (1979) model over-predicted the pressure drop for every test section, while the Chisholm (1967) model mostly under-predicted the pressure drop data.

The flow regimes were observed for high gas superficial velocities ($U_{GS} \geq 10$ m/s). There were three flow regimes and two transition regions observed in the 3 mm test section, which were in fairly good agreement with the experimental data obtained by Damianides (1987). There were two flow regimes and one transition region observed in both the 1 mm and the 0.8 mm test sections. Finally, the transition region from the annular to the dispersed flow regime in the 0.8 mm test section occurred when the superficial water velocity was approximately 0.9 m/s, which coincides with the results obtained in the 1 mm test tube. A 3CCD analog camera was used for the visualization of images in the present study.

Acknowledgements

I wish to express my deepest gratitude and appreciation to Dr. Ibrahim Hassan for his endless support, valuable advice, guidance, inspiration, and patience along every step towards the achievement of this research.

I am truly grateful to Robert Oliver for his support and help through each stage of the constructing and testing of the experimental facility. Without his help, the construction of the test rig would have been in jeopardy. I would also like to thank John Elliot for his support and guidance during this process as well.

I also wish to express my sincere thanks to Mary Vaillancourt for her help and assistance throughout the preparation of this thesis.

Also, special thanks and sincere gratitude to my family for their support in each step of my studies.

And last, but not the least, I would like to thank Arianne Immarigeon, Mirko Beaudry, Mohammed Abdelgawad, Patricia Phutthavong, and Roland Muwanga for being more than just a research group, but for being a supportive group of friends.

TABLE OF CONTENTS

LIST OF TABLES

LIST OF FIGURES

Nomenclature

A	Cross section area, (m^2)
C	Constant value, ($5 \leq C \leq 20$)
C_C	Area Ratio
Co	Coefficient
D	Diameter, (m)
De	Equi-periphery Diameter, (m)
Fr	Froud number
G	Total mass flux, (kg/m^2s)
g	Gravitational acceleration, (m/s^2)
L	Length of the test section, (m)
P	Pressure, (kN/m^2)
ΔP	Pressure drop, (kN/m^2)
Q	Volumetric Flow Rate, (kg/m^2s)
Re	Reynolds number
U	Velocity, (m/s)
We	Weber number
X	Martinelli parameter
x	Quality

Greek Letters:

α	Void fraction
β	Volumetric quality
ε	Turbulent energy dissipation rate

η	Dimensionless ratio
f	Darcy friction factor
f'	Fanning friction factor
μ	Dynamic viscosity, (Ns/m^2)
ν	Kinematic viscosity, (m^2/s)
ρ	Density, (kg/m^3)
$\overline{\rho}$	Average density, (kg/m^3)
σ	Surface tension, (N/m)
Φ	Two-phase pressure drop multiplier
ψ	Homogenous flow multiplier

Subscripts:

a	Accelerational
atm	Atmospheric
B	Bubble
cr	Critical
exp	Experimental
f	Frictional
G	Gas
GO	Gas only
GS	Gas superficial
H	Hydraulic
L	Liquid

LL	Laminar-laminar
LT	Laminar-turbulent
LO	Liquid only
LS	Liquid superficial
m	Mixture or mean
STP	Standart temperature and pressure
TL	Turbulent-laminar
TP	Two-phase
TT	Turbulent-turbulent

Chapter I

Introduction

During the past decades, micro-machining technology has become available to fabricate micron-sized mechanical parts and micro-machines, which have had a major impact on many disciplines such as aerospace, biology, medicine, and optics. The micro-machining technology that emerged in the 1980s can provide micron-sized sensors and actuators, which can be integrated into signal conditioning and processing circuitry. The result is a micro-electro-mechanical system, which can perform real time distributed control. This capability opens up a new territory for flow control and heat transfer research in micro-systems.

Single-phase forced convection in micro-channels is used to accommodate the extremely high heat fluxes in micro-electronic packages and micro-heat exchangers. However, under some conditions, such as accident or transient conditions, it is known that boiling of the coolant will occur in micro-channels, which changes the flow from single-phase to two-phase. Prediction of the resulting two-phase flow regimes and pressure drop is of great importance for accurately analyzing the system's response during such conditions.

Two-phase micro-channel heat sinks are also an alternative to single-phase micro-channel heat sinks because latent heat can be used to maintain the sink at a uniform temperature. In order to keep the operating temperature constant, the boiling temperature of the coolant must be below the operating temperature. The coolant is initially liquid as it

enters the sink, and through forced convection, the coolant becomes two-phase. Boiling convection is preferable since it requires less pumping power than single-phase liquid convection in order to achieve the same cooling performance. Therefore, it is highly desirable to develop an extensive experimental database for two-phase flow regimes, void fraction, and pressure drop in micro-channels.

This study aims to build an experimental test facility, which will allow for the generation of an experimental database for two-phase flow study, recording the pressure drop, flow regime maps, and void fraction in mini- and micro-channels. Future research may utilize the experimental data obtained in this study in order to generate an appropriate mathematical model for frictional pressure drop and flow regime transition models for two-phase flow in mini- and micro- channels.

First, a new test facility was designed for the purpose of building an experimental database for pressure drop and flow regime maps in mini- and micro-channels. The test facility was equipped with the most precise flow meters and differential pressure transducers available in the market. Once the test facility was built, three different circular test sections with diameters of 3 mm, 1 mm, and 800 μm were used to study the two-phase frictional pressure drop and flow regime transition regions. Most of the experiments for each test section were executed at high local superficial gas velocities ($U_{GS} > 10$ m/s).

Experimental pressure drop data was compared with the homogenous model, the Friedel (1979) model and the Chisholm (1967) model. The homogenous model showed the most similarities with the data acquired during the course of this experiment, with an average error of 1.2%, 15.6%, and 24.1% for the 3 mm, 1 mm, and 0.8 mm test sections, respectively. However, it was also observed that the standard deviation of the errors increased as the channel diameter decreased. The Friedel (1979) model over-predicted the pressure drop for every test section, while the Chisholm (1967) model mostly under-predicted the pressure drop data.

The flow regimes were observed for high gas superficial velocities ($U_{GS} \geq 10$ m/s). There were three flow regimes and two transition regions observed in the 3 mm test section, which were in fairly good agreement with the experimental data obtained by Damianides (1987). There were two flow regimes and one transition region observed in both the 1 mm and the 0.8 mm test sections. Also, the flow regime transition region from annular to dispersed flow observed in the 1 mm test section is in fairly good agreement with the previous experimental data obtained in 1 mm circular test sections in experiments conducted by Damianides (1987), Fukano (1993), and Ekberg (1997). However, in the present experiment, the transition from annular to dispersed flow was observed when the superficial water velocity was slightly higher than that used in the experiments conducted by Damianides (1987) and Ekberg (1997). Finally, the transition region from the annular to the dispersed flow regime in the 0.8 mm test section occurred when the superficial water velocity was approximately 0.9 m/s.

The design and the construction of the test facility was one of the main achievements of this experimental study. It was not anticipated that the problem solving process during the design and construction of the test facility would be as time consuming as it was. As a result, the time designated for the experimental data collection period was limited. However, this study can be extended by using different sizes for the test sections (smaller or bigger), different geometries for the cross-sections (triangular, square, trapezoidal etc.) with an expanded test matrix (higher and/or lower superficial phase velocities), and/or different types of working fluids (such as coolants etc.). Boiling experiments with an addition of heat exchangers would extend the present study by generating a database of the heat transfer characteristics in mini- and micro-channels.

The biggest contribution of this work is the generation of a comprehensive two-phase flow experimental database for mini- and micro-channels under adiabatic and non-adiabatic conditions. The designed and constructed test facility allows almost any experiment pertaining to two-phase flow to be performed by simply varying one or more parameters of the test facility. To perform any of the above-mentioned experimental extensions, the test facility would not require any major modifications.

Chapter II

Literature Review

When one designs systems in which micro-channels flow plays a part, such as compact heat exchangers, small-sized refrigeration systems, or micro-channel heat sinks, it is of utmost importance to have an extensive knowledge of two-phase flow regimes and pressure drop. The reason for this is that gas-liquid two-phase flow is often encountered in micro-channels with diameters of the order equivalent, or smaller than the previously defined Laplace constant. As before mentioned, the characteristics of two-phase flow in micro-channels differ greatly from the ones found in macro-channels. Among the numerous differences, the surface tension, as well as the inapplicability of the hydrodynamic interfacial processes governed by Taylor instability, must be considered. In micro-channels, the large surface tension has a direct impact on the reduction of the slip velocity, as well as on the independence of the micro-channel orientation with respect to gravity. The Taylor instability, though important in interfacial processes inside macro-channels, cannot be applied to micro-channels due to their diameter ranges. Another difference comes from the fact that boiling processes such as bubble nucleation and growth on wall crevices, as well as stable bubble and vapor layers formation on a heated surface are not as likely to occur in micro-channels as in macro-channels.

This research will extensively study the major characteristics of two-phase flow in horizontal micro-channels, namely flow patterns and maps, as well as pressure drop. In the next section, the preexisting work involving two-phase flow regimes in micro-

channels is described. Section 2.2 will give an overview of the most influential maps produced to date. This will be followed, in Section 2.3, by an expansion on the preexisting work focusing on two-phase flow pressure drop in both macro- and micro-channels.

2.1 Two-Phase Flow Regimes in Macro- and Micro-Channels

Martinelli et al. (1944) performed the very first study on two-phase flow in a horizontal glass channel of 1.017 in (25.83 mm) diameter, as well as in a 0.5 in (12.7 mm) diameter galvanized-iron pipe. They were primarily concerned by the static pressure drop existing within the channel. The gas used throughout this experiment was air, while eight different liquids were used. From their study, the first pictures of two-phase flow regimes were made available. Their work was extended when Lockhart and Martinelli (1949) worked with pipes of diameters ranging from 0.0586 in (1.27 mm) to 1.017 in (25.83 mm). The fluids in the two-phase flow were air and either benzene, water, or various oils. From their research, they identified four different flow regimes, namely turbulent flow for both liquid and gas, laminar flow for both liquid and gas, turbulent liquid flow and laminar gas flow, as well as turbulent gas flow and laminar liquid flow. These types of flow pattern were the very first attempt to classify the regimes associated with two-phase flow inside a pipe. It would be ten years before Alves (1954) would define the classical flow regimes recognized today.

One of the first studies conducted on flow patterns was performed by Alves (1954) and investigated the relationship between the two-phase flow pressure drop and the flow

regimes that were observed. The use of several gas and liquid superficial velocities was one of the important characteristics of this experiment, which allowed for the identification of numerous flow patterns. They concluded that the flow patterns, generated when different gas and liquid velocities were combined, depended on gravity, shear stress, and the surface tension present in the pipes. The experiment was conducted inside a 1.042 in (26.47 mm) diameter pipe and utilized an air and water mixture, as well as an air and oil mixture. The data was used to create a flow regime map on which five different flow patterns, namely plug, slug, wavy, annular, and bubble flow, could be identified. Although they were not observed during the course of his experiment, Alves also defined two other patterns: stratified and spray flow. Lastly, the first photographs of two-phase flow regimes were made available from this study, which, along with the data gathered on pressure drop, were found to be similar to the Martinelli correlation. During the same period, Baker (1954) conducted 27 experiments in order to observe different flow patterns. He made use of various gas and liquid superficial velocities in tubes with diameters ranging from 102 mm to 258 mm. The working fluids used to perform this study were oil and gas. As a result, he observed seven flow patterns, namely: bubble, plug, stratified, wavy, slug, annular, and spray flow. Using the data from Gazley, Alves, Kosterin, as well as his own experimental data, Baker created a flow regime map entitled the Baker Chart.

Ten years later, Suo and Griffith (1964) performed a study on both intermittent flow and elongated bubble flow regimes in capillary tubes, with both water and heptanes as the liquid component, along with either air, helium, and nitrogen as the gas component. For

this experiment, tubes with diameters from 1 mm to 1.6 mm were used. The average volumetric flows of the liquid and gas, as well as the velocity of the bubbles, were considered in order to correlate the different transition lines of the flow map define from the experiment. From their analysis, it could be concluded that if the flow was laminar and the gas to liquid ratio was known, the cross-sectional area of the film around the bubbles could be calculated. It could be shown that as the non-dimensional bubble velocity increased, the ratio of the bubble velocity to the average liquid velocity became nearly constant at a value of about 1.19, which is in good agreement with the existing data. It was observed that the bubbles present were cylindrical in shape, and they all traveled at the same velocity. The researchers assumed that the liquid in the film around the bubble was stagnant, while noting that the viscosity of the gas was much lower than that of the liquid. They also extended their study to identify the different flow regimes present in two-phase flow inside circular channels of 0.5 mm and 0.7 mm in diameter. They concluded that slug flow, slug-bubbly flow, and annular flow were the three possible regimes. Using both the Weber and the Reynolds numbers, they formulated expressions to define the transition between the three regimes. The slug to slug-bubbly flow transition was to be characterized by the following relation:

$$\mathrm{Re\ We} = 2.8\times10^{5} \tag{2.1}$$

where:

$$\mathrm{Re} = \frac{\rho_L D U_B}{2\mu_L} \tag{2.2}$$

$$We = \frac{\rho_L D U_B^{\ 2}}{2\sigma} \qquad 2.3$$

$$U_B = 1.2(U_{LS} + U_{GS}) \qquad 2.4$$

The Reynolds (Re) and Weber (We) numbers are functions of the experimental parameters such as the channel diameter (D), the superficial velocities of the gas (U_{GS}) and the liquid (U_{LS}), the liquid density (ρ_L) and viscosity (μ_L), the surface tension (σ), as well as the velocity of the gas bubbles (U_B). One of the most important part of their research was directed towards the study of what they called capillary slug flow. This flow regime could be found, under the following conditions:

$$\frac{\rho_L}{\rho_G} >> 1 \qquad 2.5$$

$$\frac{\mu_L}{\mu_G} > 25 \qquad 2.6$$

$$\Omega = \frac{\rho_L g D^2}{4\sigma} < 0.22 \qquad 2.7$$

and

$$\theta = \frac{2\mu_L^2}{\rho_L \sigma D} \approx 2\times10^{-5} \qquad 2.8$$

The third (2.7) and fourth (2.8) expressions are called the Bond number and the Ohnesorge number, respectively. Even though their correlation accurately predicted the capillary slug flow regime, it could not be used to determine where the capillary slug flow regime would form. It is important to note that the experiments conducted by Suo and Griffith did not reveal the presence of stratified flow. It was proven, in the following years, that stratified flow patterns are not present in gas and water-like liquids, when the channel diameter is less than approximately 1 mm.

In 1970, a group of researchers lead by Al-Sheikh (1970) attempted to gather all the existing experimental data available, and match it to the existing correlations related to flow regime transitions. To do so, they utilized the AGI-API Two-Phase Flow Data Bank. From this theoretical research, it was decided that no single correlation could represent a flow regime transition. Thus, a series of nine correlations was established in order to help define the flow regimes occurring during an experiment performed in a horizontal two-phase flow. It was then used to reduce the number of possible flow regimes that were created with different flow conditions to one or two. However, this experiment did not provide any direct transition correlations. The Reynolds number, the Froude number, the Mach number for the gas phase, and the Weber number were all considered in order to define the flow pattern transitions and compare the area of each flow regime from different maps. From the results and correlations obtained, it was found that this approach was able to distinguish between various flow patterns relatively well. In the worse case scenario, a 60.3% overlap was observed, while in the best case scenario, no overlap between the respective regimes was found. Due to the unique nature

of their statistics-based correlations, the work conducted by Al-sheikh et al. is not widely accepted.

Another attempt to develop a purely theoretical approach for predicting flow regime transitions was performed two years later by Govier and Aziz (1972). They were able to generate a good summary of flow regime transitions, and also performed some work on the continuity balance, as well as on the momentum balance found in different flow regimes. Around the same period, more studies were conducted by research groups such as Agrawal et al. (1973), who conducted the first study of elongated bubble flow. Duckler and Hubbard (1975) developed a model for two-phase slug flow in horizontal and near horizontal tubes, and Nicholson et al. (1978) continued the work of Duckler and Hubbard by extending their model to elongated bubble flow. In their study, Duckler and Hubbard made use of a horizontal pipe with a diameter of 38 mm. The experiments were performed with a mixture of water and air, while the data was gathered using photography, motion pictures, dye tracers, as well as fast-response pressure transducers. They used an analytical solution to gain a better understanding of the bubble velocity inside a two-phase slug flow when the slug flow contained no gas. They were able to generate a simple logarithmic equation for the ratio of the shape-translation velocity to the slug velocity as a function of slug Reynolds number, which was allowed to fluctuate between 30,000 and 400,000. This expression is presented below:

$$\frac{U_{translation}}{U_{slug}} = 0.021\ln(Re_{slug}) + 1.022 \qquad 2.9$$

where $U_{translation}$ is the shape translation velocity, U_{slug} is the slug velocity and Re_{slug} is the slug Reynolds number. From this, the range of velocity ratio found to be from 1.25 to 1.30. In order to complete their work, the researchers worked on the development of expressions for the relative slug length, as well as the pressure loss due to the acceleration of the liquid film trapped between the liquid slugs. The pressure loss determination required the knowledge of various parameters such as the slug frequency, both the liquid and the gas flow rates, as well as the fractional entrainment of gas in the liquid slug.

At the end of the 1970's, Choe et al. (1978) experimented with two-phase flow in order to study the different flow patterns present at different superficial velocities. They were convinced that all the previous researchers had been misled in their observations of minor flow patterns, and that the fluctuations from the main flow patterns were in fact due to the frictional pressure drop taking place inside the channel. They conducted their experiment in 0.45 in (11.43 mm), 1 in (25.4 mm), and 2 in (50.8 mm) diameter pipes with a length of 20 ft (6.096 m). They observed that six flow patterns were possible, namely homogeneous, annular, slug, plug, stratified, and wavy flow. They developed both a primary and a secondary classification for the flow patterns found in two-phase flow. Inside the homogeneous primary category, mist and froth flow are the secondary flow patterns. Stratified and wavy flow are both secondary flows found in the separated flow primary category, while slug, plug, and bubble flow are all secondary flows part of the intermittent primary category. Lastly, the primary category called annular flow comprises the annular and the semi-annular secondary flows. From their experiments, the authors concluded that the flow pattern correlations available to date were not in good

agreement, probably due to the large scatter of the flow pattern observations. For this reason, they developed their own flow regime transition correlations. It could be observed from the maps generated from the data, that the results obtained for the 0.45 in (11.43 mm) pipe differed from the results obtained in the other pipes. First, it was noted that stratified flow was not observed inside the 0.45 in (11.43 mm) pipe at low gas velocities. Some changes in the transition boundaries also took place. The transition from wavy to slug flow was observed to occur at higher liquid velocities. One year later, Weisman et al. (1979) extended the work done by Choe et al. (1978) by investigating the effects of the fluid properties and of the pipe diameter on two-phase flow patterns. They used horizontal lines and worked with diameters ranging between 11.5 mm to 127 mm. The fluids used were varied from one test to the other. They proceeded to vary the liquid viscosity, using a glycerol-water mixture, while the surface tension present in the pipes was kept constant. The surface tension was then allowed to fluctuate, using a solution of water containing a surface agent, while both the gas and the liquid densities were kept constant. The effects of liquid density was tested using a solution of potassium carbonate, while the effects of vapor density were observed using Freon 113 – Freon 113 vapor. Lastly, the effects of diameter were studied using three different channel sizes. From their work, they were able to modify pre-existing correlations for flow regime transitions. They concluded that both pipe diameter and fluid properties have only a mild influence on the transition lines of the flow patterns. The relative volumetric gas and liquid flow rates had the greatest effect on the flow regimes. When compared to the data obtained by Mandhane et al. (1974), the results were found to be in good agreement.

Later, Sadatomi and Saruwatari (1982) studied the different flow regimes found in vertical channels with a rectangular cross section. With the data gathered, they generated a complete flow regime map. From their experiment, they concluded that channel geometry in non-circular channels has very little influence when the hydraulic diameter of the channel in larger than 10 mm. Also, it was noted that three flow regimes were present in the channel, namely bubble, slug, and annular.

In 1983, a group of scientists led by Barnea et al. (1983) was the first to investigate the two-phase flow patterns found in small horizontal tubes. In order to conduct this experiment, the diameter range for the tubes was 4 mm to 12.3 mm. The observations were made using the conductance probe method, as well as visual observations. They classified the different flow patterns observed into four general regimes: dispersed, annular, intermittent, and stratified. It was concluded that all the observed transitions obeyed the Taitel and Duckler (1976) model with reasonable accuracy. The only exception to this is for the stratified to non-stratified transition, which cannot be predicted by that model. In micro-channel flow, the Kelvin-Helmholtz instability looses a lot of its importance when compared with the predominant surface tension and gravitational force. According to Barnea et al. (1983), the transition from stratified flow to slug flow in micro-channels is due to surface tension and gravitational force. From the calculations performed using the results of this experiment, it appears that neither of the expressions presented by Taitel and Dukler (1976) or Barnea et al. (1983) can be successfully applied to micro-channels when determining the flow patterns. This problem has been examined by different groups of researchers, each of which recorded flow patterns according to

several criteria. It was noted that often, under similar conditions, dissimilar patterns were observed. Despite the numerous discrepancies between the different experiments performed on the subject, all the investigations concluded that slug or plug flow was one of the dominant patterns present in micro-channel flow.

In their theoretical work, Annunziato and Grardi (1987) used a statistical approach including the measurement of a differential pressure and local void fraction probes to obtain the flow regime transitions present in 90 mm diameter tubes. With their research, they were able to measure the temporal fluctuations found in the tubes.

Damianides (1987) conducted a study focusing on horizontal two-phase flow of air and water mixtures in small diameter tubes and compact heat exchangers. The pipes used in the experiments had diameters of 5 mm, 4 mm, 3 mm, 2 mm, and 1 mm. The primary goal of the experiment was to determine the effect of the pipe diameter in a two-phase flow inside a channel, investigate the pressure drop inside the channels, and generate flow maps from the gathered data. Also, tests were performed inside a compact heat exchanger in order to determine the accuracy of the 'homogeneous' flow assumption, which states that the flow regimes are a mixture of the two phases, where the two fluids travel at the same velocity. The superficial velocities used during the course of this experiment ranged from 0.0024 m/s to 5.72 m/s for the liquid, while the gas superficial velocities ranged from 0.015 m/s to 125.34 m/s. The author concluded that the effect of pipe diameter is only a factor inside small diameter pipes in two-phase flow. Also, the flow regime transitions were observed for each pipe diameter, enabling the authors to

correctly establish the factors responsible for them, and thus developing the right predictive theory for each of them. Lastly, it was noted that the flow patterns present inside a compact heat exchanger are the following: annular, bubble, as well as intermittent flow. Flow maps for each of the pipe diameters, as well as for the compact heat exchanger, were created and compared to the preexisting maps. The author then proceeded to compare the results obtained with the ones gathered by Lockhart and Martinelli. It was found that the Martinelli correlation does not give accurate results when taking into account the effect of pipe diameter.

In the following year, Damianides and Westwater (1988) performed experiments on two-phase flow patterns in both small tubes and in a compact heat-exchanger. A horizontal plate type apparatus simulated the two-phase flow in a heat exchanger. The patterns were identified using high-speed photography and fast response pressure transducers. The objective of this research was to obtain an accurate flow regime map for plate type heat exchangers. Both the channels and the heat exchanger had an equivalent diameter of 1.74 mm. The gas and liquid superficial velocities fluctuated over ranges of 1.05 m/s to 101.2 m/s and 0.0084 m/s to 8.62 m/s, respectively. To perform the experiment, city water at a temperature ranging between 10 °C and 20 °C was used. The water was pressurized and filtered before it was mixed with air. At the entrance, the air used was also pressurized to about 5 atm, and heated to a temperature of about 15 °C to 25 °C. It was then filtered, and mixed with the water. The measurements for both the water and the air were performed using rotameters. The compact heat exchanger used is a plate type aluminum heat exchanger made by LIMCO Manufacturing Corp. The tubes, on the other hand,

were made out of Pyrex by Wilmad Glass Co. The inside diameters were measured to be of 5 mm, 4 mm, 3 mm, 2 mm, and 1mm. All were placed in a horizontal position during the experiment. Three methods of investigation were selected to gather the information on the flow regimes: the unaided eye, photography, and fast acting pressure transducers. In the heat exchanger, three flow regimes were observed, namely bubble flow at high liquid velocities, intermittent flow at intermediate liquid velocities, and annular flow at low liquid velocities and any gas velocity. One of the major differences between the results obtained in the tubes and in the heat exchanger is the presence of stratified flow instead of annular flow at low two-phase velocities inside the tubes. It was also confirmed that while surface tension plays an important role in small tubes. it is not a major factor in the study of larger tubes. As a general conclusion, it was found that one could not predict the flow patterns found in a plate type heat exchanger from results obtained in straight round tubes.

In the next few years, studies were conducted in tubes of different geometries. For instance, Fukano et al. (1989) conducted experiments in horizontal capillary tubes of 1 mm to 4.9 mm in diameter, investigating the flow patterns and pressure drop in isothermal gas-liquid concurrent flow. They made use of two methods to gather their data, which were visualization and pressure drop experiments. The ratio of the bubble velocity to the slug velocity, in the slug-plug regime, was found to be of 1.2 for each test condition. Also, the authors developed a correlation for the relative slug length as a function of the superficial velocity of the gas and the liquid, with the help of a proportionality constant shown below:

$$\frac{L_{slug}}{L_{slug} + L_{bubble}} = \frac{kU_{LS}}{U_{LS} + U_{GS}} \qquad 2.10$$

where L_{slug} is the length of the slug, L_{bubble} is the length of the bubble, U_{LS} and U_{GS} are the superficial velocities of liquid and gas, respectively, and k is a constant number. Wambsganss et al. (1990), on the other hand, worked on two-phase flow patterns in small, horizontal, rectangular channels. They also investigated the flow regime transitions in the channel. The two aspect ratios used in this experiment were 6 and 1/6, respectively. In order to study the different patterns, the researchers took advantage of both visual observations and photographic data. The cross-sectional area of the channel was measured to be 19.05 mm by 3.18 mm, with a hydraulic diameter of 5.45 mm. The channel was made out of Plexiglas and had a length of 1.14 m. The researchers chose to base their study on six basic flow patterns: stratified, wave, plug, slug, bubble, and annular. To ensure that the results obtained were accurate, they transformed their visual observations using the corresponding root mean square (RMS) values. The RMS was calculated from the dynamic pressure-time signals and was plotted as a function of the mass quality. They were able to show that the transition from plug or bubble to slug flow, and the transition from slug to annular flow could be identified using the plot of the calculated RMS pressure signal versus the mass quality. For the aspect ratio of 6, it was found that the large amplitude waves observed in the wave flow could be associated with annular flow. One of the most tedious tasks in this experiment was distinguishing between wavy flow and annular flow. Throughout history, a lot of researchers have not made the distinction between wavy and annular flow, hence making it very difficult to

accurately compare the results obtained here with previous studies. Also, the plug flow was found to be quite inactive, while the slug flow obtained was characterized by froth in the flow. The bubble flow present in both the 6 and 1/6 aspect ratio tubes comprised clear and uniform bubbles. For the 1/6 aspect ratio, only four of the six flow patterns defined earlier could be observed. The two regimes not observed were the stratified and the wavy flow, which is in accordance with the results obtained by Troniewski and Ulbrich (1984). The goal of this experiment was to extend the knowledge acquired to date on the effects of channel geometry and size on flow patterns, as well as on flow transition boundaries. They concluded that the results differed when the experiments were conducted inside channels of varying diameters. In other words, the flow patterns observed in moderate to large diameter pipes are different from the flow patterns observed in small rectangular channels. The disagreement was found to decrease when the data of two channels of the same geometry were compared.

The following years held multiple developments in the field of two-phase flow in macro- and micro-channels. Mishima et al. (1993) worked on flow regimes, void fraction, bubble velocity, and pressure drop in two-phase flow inside rectangular channels, using a new technology called the neutron radiography technique. Some studies have also been conducted to acquire a better understanding of the different flow regime transitions occurring inside the channels.

Xu et al. (1999) researched the flow transition criteria for bubbly flow to slug flow, as well as for slug flow to churn flow. They also created a new model for the transition

criteria of annular flow. It was found that when the void fraction increased above 0.1 and the frequency reached $\alpha_{cr} = 0.3$, the flow would change from bubbly to slug. Mishima et al. (1993) developed the following criterion for the transition between bubbly and slug flow:

$$U_{LS} = \left(\frac{1}{\alpha_{cr} Co} - 1 \right) U_{GS} - \frac{0.35\sqrt{gDe}}{Co} \qquad 2.11$$

where

$$De = \frac{2(S+W)}{\pi} \qquad 2.12$$

Here, De is called the equi-periphery diameter, and

$$Co = 1.35 - 0.35\sqrt{\frac{\rho_G}{\rho_L}} \qquad 2.13$$

For slug flow to churn flow transition, Mishima et al. (1993) found that the transition occurs when the mean void fraction over the whole region exceeds that found over the slug bubble section. The equation describing the transition is given as follows:

$$\alpha = \frac{U_{GS}}{Co(U_{GS} + U_{LS}) + v_B} \qquad \text{when } \alpha \geq \alpha_m \qquad 2.14$$

where

$$\alpha_m = 1 - 0.813X^{0.75} \qquad 2.15$$

and α is the void fraction, α_m is the mean void fraction, Co is a coefficient, and v_B is the kinematic viscosity of bubble. The formation of annular flow usually occurs when the gas flow rate is high. The flow changes from either slug or churn flow to annular flow. The next criterion described was developed by Taitel (1980), using the force balance between the liquid gravity, the drag force generated by the gas phase, and the surface tension:

$$\frac{U_{GS}\rho_G^{0.5}}{\sigma_G(\rho_L - \rho_G)^{0.25}} = 3.0 \qquad 2.16$$

where σ_G is the surface tension of gas. Note that this criterion does not take into account the channel geometry, which is of great importance as the channel size decreases. For smaller channels, the flow regime transition can be predicted using:

$$1.33U_{GS} - 4U_{LS} = U_{GS}^{n^{1/2}} \sqrt{\frac{(\rho_L - \rho_G)gD_H + 128C_L(\frac{U_{LS}}{v_L})^{-n^2}\rho_L U_{LS}^2}{9.24C_G(\frac{D_H}{v_G})^{-n^{-1}}\rho_G[1 + 1.5(\frac{\rho_L}{\rho_G})^{1/3}]}} \qquad 2.17$$

where $\alpha = 0.75$, D_H is the hydraulic diameter, ν_G is the kinematic viscosity of gas, and both C_L and C_G are the liquid and gas constant, respectively, which have been separately varied to fit the experimental values.

It was concluded that the model presented in this experiment gives a good prediction for the annular flow. This can be explained by the fact that the flow criteria developed takes into consideration the increased wall shear stress and interface shear stress. This model also gives better predictions for the transition from bubbly to slug and from slug to churn flow than the model developed by Mishima et al. (1993), since the present predictions take into account the increased wall shear stress in small gap rectangular channels.

This study was extended in 1998 when Xu (1998) performed experiments on two-phase flow regimes in rectangular channels of 260 mm in length and 12 mm in width. All test sections were similar except for the gaps, which were of 1 mm, 0.6 mm, and 0.3 mm, respectively. This experiment was conducted in order to gain a better understanding of heat transfer with phase change, which is directly related to the structure of the flow in a mini- or micro-channel. In order to study the different flow regimes obtained during the different experiments, a high-speed video camera was used. The results of the tests involving the 1.0 mm and the 0.6 mm gap were very similar to the results obtained previously for medium size channels. The flow regimes observed were: bubbly, slug, churn, and annular. The only major difference noted between the present study and the results for medium channels was the fact that the bubbles observed were flattened (two-dimensional). As for the regimes observed in the channels with the 0.3 mm gap, it was

found that the classical flow structure could not be applied. Instead, cap-bubbly, slug-droplet, churn, and annular-droplet flow were observed. It is important to mention that bubbly flow was never present, and that liquid droplets, pushed by the gas phase, were part of the regimes found at low flow rates.

A recent study performed by Ekberg et al. (1999) explored gas-liquid two-phase flow in narrow horizontal channels. The void fraction, the pressure drop, the flow patterns, as well as the flow regime maps obtained from the gathered data were studied. In order to conduct the experiment, two transparent sections were used. The inner diameter of each is, respectively, 6.6 cm and of 33.2 cm, and the length of the tubes is 46 cm and 43 cm, respectively. The working fluids of this experiment were water and air, and the superficial velocities were varied between 0.02 m/s and 57 m/s for gas, and between 0.1 m/s and 6.1 m/s for liquid. For both test sections, the hydraulic diameter is 2.04 cm. The different flow patterns were observed using a digital video camera. The void fraction for the test section was obtained by averaging the calculated void fractions at ten axial segments along the test section. The void fractions were compared to preexisting correlations, and it was found that the Butterworth (1975) correlation provided the most accurate prediction. The flow patterns observed in the small test section were: slug-plug, stratified-slug, annular-slug, annular, bubbly-plug, dispersed bubbly, and churn. It was noted that no distinction was made between the slug and the plug flow regimes, since the difference could not always be clearly observed. On the other hand, for the large test section, slug-plug, stratified-slug, stratified, annular-slug, annular, bubbly-plug, dispersed-bubbly, and churn were observed.

During the same year Coleman and Garimella (1999) studied the effects of the tube diameter and shape on the flow regime transitions in two-phase flow. They conducted their experiment in horizontal circular and rectangular tubes with hydraulic diameters ranging from 5.5 mm to 1.3 mm. They used air and water as fluids and superficial velocities of 0.1 m/s to 100 m/s for gas, and 0.01 m/s to 10 m/s for liquid. One of the drawbacks, identified by the authors, in studying two-phase flow patterns was the lack of uniformity in the terminology used to describe the different flow regimes found inside a channel. They decided to established specific definitions for each flow regime, and then subdivide these flow regimes into flow patterns. For the round tubes, four flow regimes were observed: stratified, intermittent, annular, and dispersed. The stratified flow regime was subdivided into the smooth flow, as well as the wavy flow patterns. The intermittent flow regime was subdivided into the elongated bubble and the slug flow patterns. As for the dispersed flow regime, it is divided into the bubble flow and the dispersed flow patterns, while the annular flow regime is divided into wavy annular and annular flow patterns. The stratified flows were characterized by a complete separation of the liquid and the gas phases. The stratified smooth flow pattern was defined as a flow in which the liquid and the gas flows were laminar in nature and no fluctuations at the flow interface could be observed. The wavy flow pattern was characterized by an increase in the gas mass flow rate, which in turn brings forth instabilities at the liquid-gas interface due to the interfacial velocity differential. As a reaction of the preceding changes in the flow, interfacial waves formed. For the elongated bubble flow pattern, it was defined by a continuous stream of vapor plugs flowing in the liquid, while the walls of the tube

remained coated by a light film of liquid. When the gas mass flow rate increased, the disturbances inside the tube increased until the aft portion of the plug broke away from the rest of the plug. Smaller bubbles formed from the broken section, which led to the formation of the slug flow pattern. Furthermore, the annular flow was characterized by the nearly complete separation of the liquid and the gas phase along the circumference of the tube wall. The wavy annular flow pattern could be observed when the surfaces of waves in the wavy flow amplified until they touched the top of the tube wall. Annular waves form only when the mass flow rate was increased and the liquid was pushed up around the circumference of the tube wall due to an increase in the gas momentum. Annular flow then occurred when the liquid coated the tube wall completely and the gas flowed through the core of the tube. Finally, for the dispersed flow regimes, the bubble flow pattern could be observed when the liquid flow was turbulent and the gas phase was laminar. Small bubbles were then driven by the buoyancy forces and were found mostly at the top of the tube. The dispersed flow was observed when the Reynolds number of the gas increased while all the other parameters were kept constant. The bubble size decreased, which allowed for the bubbles to be dispersed into the entire cross section of the tube.

2.2. Two-Phase Flow Regime Maps in Macro- and Micro-Channels

One of the first studies ever conducted in the field of two-phase flow regime maps were performed by Bergelin and Gazley (1949). They produced one of the first flow pattern maps using air and water in a pipe of 1 in diameter. The coordinates used were the liquid and gas mass flow rates. They were able to identify five flow regimes, which are bubble,

stratified, wave, slug, and annular flow. However, the authors did not present a formal definition of each flow regime observed. They also noted that a calming section was needed in order to observe the fully developed flow pattern, because the entrance region seemed to affect the flow pattern originally formed inside the pipe. Their research was closely followed by the work of Johnson et al. (1952). This last group proposed a map similar to that produced by Bergelin and Gazley (1949). The data was collected for an air and water mixture in a 0.87 in (22.1 mm) diameter pipe.

A year later, Hughes et al. (1953) performed an experiment in order to produce a flow regime map, based mainly on the data gathered by Kosterin (1949) for two-phase flow of air and water inside a 4 in pipe. From the flow map, five flow patterns could be distinguished, and they are slug, dispersed, froth, stratified, and annular flow. They used the volumetric flow fraction of gas and the mixture's superficial velocity as the coordinates of the map since Kosterin (1949) believed that such a coordinate system partially countered the effects of pipe size. However, it was shown in later studies that the effect of pipe size was much more complex, and could not be accounted for so easily, especially in channels with less than 0.5 in (12.7 mm) diameters, where the surface tension becomes of prime importance.

A short while later, Alves (1954) worked to produce maps for both air-water and air-oil mixtures, and the diameters of the pipes were 1.042 in (26.47 mm). Both systems were presented on a single map with the liquid and gas superficial velocities as coordinates. Alves (1954) theoretically defined a total of seven flow regimes. Five of the seven flow

regimes could be found on this map, and they are bubble, slug, plug, wavy, and annular, while the last two, stratified and spray flow, were never observed. The first photographs of two-phase flow regimes ever produced accompanied his maps.

During the same year, Baker (1954) produced a flow pattern map based on the data found by Jenkins, Gazley, Alves, and Kosterin. Using their data, as well as his own experimental results, Baker created a flow regime map called the Baker Chart. The coordinates used as the axis of this chart, $\frac{G}{\lambda}$ and $\frac{L\lambda}{G}$, and were chosen to take into consideration both the effects of the physical properties and the diameter of the pipe. The variables λ and Ψ were defined as follows:

$$\lambda = \left(\frac{\rho_G}{0.075}\right)\left(\frac{\rho_L}{62.3}\right)^{1/2} \qquad 2.18$$

$$\Psi = \left(\frac{73}{\sigma}\right)\left(\left(\frac{62.3}{\rho_L}\right)^2 \mu_L\right)^{1/3} \qquad 2.19$$

Here, σ is the surface tension. L is the liquid mass velocity, and G is the gas mass velocity in $\frac{G}{\lambda}$ and $\frac{L\lambda}{G}$.

In 1955, White and Hungtington (1955) worked on a tentative flow pattern map for flow in 1 in (25.4 mm), 1.5 in (38.1 mm), and 2 in (50.8 mm) diameter Kraloy plastic pipes which were 70 ft (21.4 m) in length. They used natural gas and kerosene, air and

kerosene, and air and water as their working fluids. The coordinates of their map were the liquid and gas mass velocities, while the regimes observed were the following: slug, stratified, wavy, and annular flow. It was noted that this map could be of used in similar systems operating near atmospheric pressure.

Some four years later, Hoogendoorn (1959) used air and oil, as well as air and water mixtures to observe the effects of pipe diameter, pipe roughness, and liquid properties in two-phase flow. Six flow regimes could be found on this map, namely slug, plug, stratified, dispersed, wavy, and annular flow. Also, the author noted that the flow map could be used for systems with pipes of all sizes since the effect of pipe diameter was found to be very small. The coordinates of their flow maps are the input gas volumetric fraction and the mixture velocity. This last coordinate could be defined as follows:

$$U_m = \frac{4(Q_G + Q_L)}{\pi D^2} \qquad 2.20$$

where U_m is the mixture velocity, Q_G and Q_L are the volumetric flow rates of gas and liquid, and D is the diameter of the channel. Hoogendoorn (1959) also included photographs of the different flow regimes observed during his experiment. These pictures, although not very clear, complemented the results presented in his flow maps.

The previous study was followed by the research of Govier and Omer (1962). They worked with air and water in a 1.026 in (26.06 mm) diameter cellulose acetate butyrate pipe, which was 41 ft (12.5 m) in length. They used the liquid and gas mass velocities as

the coordinates of their map, and were able to distinguish six different flow regimes, which were bubble, slug, plug, stratified, wavy, and annular flow. Govier and Omer (1962) also presented photographs of the flow regimes found on their flow maps, but only for those at lower velocities.

A year later, Scott (1963) hoped to use the data collected by Govier and Omer (1962) and Hoogendoorn (1959) to modify Baker's diagram. Once the experiment was conducted, Scott realized the important role the pipe diameter played in the correct determination of flow regimes in two-phase flow. He therefore used only Hoogendoorn's work, which took into account the effect of pipe diameter in order to improve Baker's chart. The map obtained from this experiment uses the same coordinates as the original Baker's chart. The map's boundaries, on the other hand, are very different from the old map. It was concluded, that the new map was reliable for pipes of diameter greater than 1 in, with its accuracy rapidly decreasing with decreasing diameter.

Eaton et al. (1967) produced data using natural gas and water, natural gas and crude oil, as well as natural gas and distillate mixtures in 2 in (50.8 mm) and 4 in (101.6 mm) pipes of 170 ft (51.8 m) in length. They gathered their data using several different methods such as: visual observations, motion pictures, and static pressure pneumatic transducers. To create the motion pictures, three plastic nipples, each inserted at a different point on the pipes, were used. The static pressure was recorded at eight different points in the two pipes, providing data that covered the entire range of the test section. They created a map, using both the Reynolds number and the Weber number as coordinates, to correlate

the flow regime observations. A general pressure loss correlation was also developed, which was independent of the existing flow regimes. Comparisons between the data gathered by Baker and the results of this experiment were made, but were in poor agreement.

Al-Sheikh et al. (1970) used a sequence of plots to determine the flow regimes in a horizontal pipe. The data used to perform this experiment was extracted from the AGI-API Two-Phase Flow Data Bank, while the range of pipe diameter used was between 1 in and 6.065 in (154.1 mm). In order to completely define the two-phase flow in a horizontal channel, Al-Sheikh et al. (1970) developed a total of nine correlations using heuristic, as well as empirical arguments. One of the drawbacks of the method used to complete their work was the impossibility to absolutely determine what flow regime would be encountered. Finally, because of the statistical nature of their method, the results and correlations obtained by Al-Sheikh et al. (1970) were not accepted at all.

In the following years, extensive work was conducted by Mandhane et al. (1974) in order to test all the previously created maps for two-phase gas-liquid flow against the 5935 flow pattern observations available in the UC Multiphase Pipe Flow Data Bank. Their study was conducted over a wide range of diameters from 12.7 mm to 165.1 mm. The superficial gas and liquid velocities ranged from 0.14 ft/s (0.042 m/s) to 560 ft/s (170.7 m/s), and from 0.003 ft/s (0.0009 m/s)to 24 ft/s (7.32 m/s), respectively. From the comparisons, a new correlation was developed and used to form a new improved flow pattern map for air and water mixtures. Physical property corrections were made in order

to convert the map to systems other than air and water. These corrections could be obtained by multiplying the following expressions by the equations for the transition boundaries.

$$\left(\frac{\rho_G}{0.0808}\right)^{0.2}\left(\frac{\rho_L}{62.4}\frac{72.4}{\sigma}\right)^{0.25}\left(\frac{\mu_G}{0.018}\right)^{0.2} \qquad 2.21$$

$$\mu_L^{0.2}\left(\frac{\rho_L}{62.4}\right)^{0.25}\left(\frac{72.4}{\sigma}\right)^{0.25} \qquad 2.22$$

This new map displays superior overall agreement with all the data points previously mentioned. The data points used in this study were found in the first major compilation of data, for two-phase flow in horizontal, vertical, and inclined pipes, called the AGA-API Two-Phase Flow Data Bank. This data bank was completely updated and rearranged to suit the precise needs of this experiment. Over 4000 data points were added to the bank. The map produced during this research experiment was then compared to the ones created from the work conducted by Baker (1954), Hoogendoorn (1959), as well as Govier and Aziz (1972). It was found that all showed good agreement with the new map and that the effect of the pipes diameter was well accounted for by using the gas and liquid superficial velocities as the coordinate axes of the flow map. To facilitate comparison between the different maps, two parameters were calculated, namely:

$$\alpha_i = \frac{\text{Number of points correctly predicted to lie in flow regime i}}{\text{Number of points which were observed in flow regime i}} \times 100 \qquad 2.23$$

$$\frac{\beta}{100} = \frac{\text{Total observations correctly predicted to lie in respective flow regimes}}{\text{Total of observations}} \quad 2.24$$

It is clear that α_i is the percentage of success of a given flow pattern map with respect to a particular flow regime, and β is the overall percentage of success of a given flow pattern map. A fact worth noting is the constant failure of all the maps to accurately predict the dispersed bubble flow regime. Also, all maps show very accurately the annular-mist flow regime, but poorly predict the wave flow regime. They found that no distinction was made between plug and slug flow, nor between annular and annular mist flow. A new flow map was generated using the logarithm of gas and liquid superficial velocities as coordinates. An attempt was also made to correct for the varying physical properties. It was found that the new map was an "average" of Baker's (1954), Hoogendoorn's (1959), as well as Govier and Omer's (1962) maps. Also, they noticed that the physical properties of the components had very little effect on the flow regimes due to the error present in the position of the transition boundaries. In fact, they noticed that proposed property corrections tended to reduce the reliability of the data. The new map proved to be more accurate for small diameter pipes (less than 2 in (50.8 mm)), but this could be due to the fact that more than 70% of the data points were observed in less that 2 in (50.8 mm) diameter tubes. The authors observed that as the pipe diameter was lowered below 0.5 in (12.7 mm), the effects of the pipe diameter, as well as the effects produced by the surface tension became increasing important in the determination of the existing flow regime. Overall, the map generated during the course of the study yields more accurate results than the ones previously designed.

Simpson et al. (1977) studied the flow maps, void fraction, and pressure drop in a two-phase flow inside large channels. The diameters used were 5 in (127 mm) and 8.5 in (215.9 mm), while the fluids used were water and air. Two distinct maps were produced for each of the two pipe diameters. It was found from the flow maps that there is an effect of pipe diameter present in larger pipes. This effect can be seen from the transition boundaries, which occur at a much higher liquid superficial velocity and at considerably lower gas superficial velocity. In 1981, Simpson et al. (1981) extended their field of study to include observations on pipe diameter effects, as well as on the settling length in pipes with diameters of 5 in (127 mm) and 8.5 in (215.9 mm). It was found that the settling length for the annular, bubble, and stratified flow regimes was less than sixty times the diameter. Also, the authors noted that the wavy and the slug flow were so unstable that it was not possible to observe the settling length within the range of their test sections. Finally, they stated that more work needed to be conducted focusing on the effect of pipe diameter before definite results and conclusions could be drawn.

Taitel and Duckler (1976) developed a theoretical approach to flow regime mapping for air-water mixtures. In order to do so, they used a momentum balance on a stratified flow regime. They then presented four dimensionless parameters, which helped characterize the regime transitions. It was found that this theoretical model was in close agreement with the experimental flow map produced by Mandhane et al. (1974). It was also able to predict the micro-channel data of Fukano et al. (1989) fairly well. It was also the first theoretical attempt to predict the boundaries of the flow regimes on the flow regime

maps. This model assumed that the turbulence in the liquid phase of the two-phase flow was of great enough intensity to maintain the bubbles in a small and spherical shape, as well as to overcome buoyancy, which tended to push the bubbles upwards and cause a phenomenon called creaming. A number of parameters were calculated using various equations. First, when bubble breakup is controlled by turbulence, the stable maximum bubble size is given by:

$$D_B = (0.725 + 4.15\alpha^{1/2})\left(\frac{\sigma}{\rho_L}\right)^{3/5} \varepsilon^{-2/5} \qquad 2.25$$

In the previous equation, the parameter ε represents the turbulent energy dissipation rate, which is expressed:

$$\varepsilon = \frac{f\,(U_L + U_G)^3}{2D_H} \qquad 2.26$$

Here, f is the friction factor. It can be described by the following:

$$f = C_f\left(\frac{(U_{LS} + U_{GS})D_H}{\mu_L}\right)^{-n} \qquad 2.27$$

Also, an expression was developed to determine how long the bubble would remain spherical, which is given below:

$$D_B < 2\left(\frac{0.4\sigma}{(\rho_L - \rho_G)g}\right)^{1/2} \qquad 2.28$$

Finally, bubble creaming would not occur, as long as the following equation held:

$$D_B < \frac{3}{8}\left(\frac{\rho_L}{\rho_L - \rho_G}\right) f \left(\frac{(U_{LS} + U_{GS})^2}{g}\right) \qquad 2.29$$

Here, they assumed that the buoyancy force in an annulus was proportional to δ^3.

Troniewski and Ulbrich (1984) pursued an experiment to determine the flow regimes present in ten rectangular channels, which covered a range of aspect ratios between 12 and 0.1 for the vertical channels, and between 0.1 and 10 for the horizontal channels. An air-water mixture and an aqueous solution of sugar and air were used, where the last mixture was used to study the effect of viscosity. The maps generated here could be used for horizontal and vertical two-phase flow in rectangular channels, respectively. From the tests performed with the sugar-air aqueous solution, the authors concluded that the liquid viscosity, up to 0.040 kg/m^{2}s, had a negligible effect on the flow pattern transitions.

In the late 1980's Damianides (1987) performed a complete research on flow regimes, pressure drop, as well as flow regime maps in two-phase flow inside 5 mm, 4 mm, 3 mm, 2 mm, and 1 mm diameter pipes, as well as in a compact heat exchanger. A flow regime map was obtained for each pipe diameter and for the compact heat exchanger, using the gas and liquid superficial velocities as the coordinates. These maps were then compared

with maps obtained from previous studies. The map obtained for the 5 mm diameter pipe was compared with the Baker chart, the work done by Mandhane et al. (1974), the theoretical map obtained by Taitel and Duckler (1976), and the results of Choe et al. (1978). When the Baker chart and the 5 mm map were put together, some agreement was observed between the wavy flow patterns. However, the rest of the maps were vastly different, most probably due to the fact that the Baker chart was created for pipes larger than 0.5 in (12.7 mm). The Mandhane et al. (1974) map comparison produced the same results, as it was created for pipe diameters ranging between 0.5 in (12.7 mm) and 6.5 in (165.1 mm). In this case, the dispersed and wavy flow patterns were observed at lower liquid velocities, while the absence of stratified flow pattern and the existence of hybrid pseudoslug flow pattern rendered the maps completely different. In the case of the Taitel and Duckler (1976) theoretical flow map, once the corrections for small pipes added by Taitel et al. (1980) were taken into account, it displayed a good agreement with the map obtained by Damianides and Charalambos (1980). The Choe et al. (1978) flow map showed similar trends to the 5 mm map obtained in the present study. A common boundary could be observed between the intermittent and the annular flow, while vast differences could be distinguished between the areas covered by the separated flow. For the 4 mm pipe, the map was compared with the work done by Barnea et al. (1983), who obtained a map for a 4 mm pipe. Good agreement could be seen between the two maps, the only difference being the slope of the annular transition line. This discrepancy could be caused by the subjectivity of the visual observations. The 3 mm diameter pipe was compared to the map created by Taitel and Duckler (1976). It was found that the dispersed flow transition was over predicted by the Taitel and Duckler (1976) map, while

the onset of annular flow was under predicted by the Taitel and Duckler (1976) theory. The 1 mm map was compared with the Taitel and Duckler one, which permitted the authors to compare them. The same behavior, except more pronounced than the one observed for the 3 mm map, was noted in this case.

Damianides and Westwater (1988) studied on two-phase flow patterns in small tubes and in a compact heat exchanger. The objective of this research was to obtain an accurate flow regime map for a precise type of heat exchanger. Another goal was to discover whether both the flow maps obtained for the round tube and the flow map obtained for the heat exchanger were similar or different. The flow maps were determined for tubes with diameters varying from 1 mm to 5 mm. The maps produced from this study were similar in nature, but comprising a number of discrepancies, such as the presence of stratified flow instead of annular flow at low two-phase velocities in the heat exchanger. For the heat exchanger flow map, the superficial liquid velocities ranged from 0.0838 m/s to 8.62 m/s, while the superficial gas velocities varied between 1.05 m/s and 101.2 m/s. From this map, it was noted that the smooth stratified and wavy stratified flows were not observed. Also, the authors found that while the liquid velocity greatly influenced the results, the gas velocity did not have a big impact on the results. For the 1 mm map, the superficial gas and liquid velocities were between 0.715 m/s and 55.3 m/s, and 0.0095 m/s and 1.53 m/s, respectively. Worth noting is the fact that separated flow was never observed, while most of the map was occupied by slug flow. Also, the pseudo regimes only represented a minute part of the map. For the 2 mm map, the authors used superficial velocities ranging from 0.0024 m/s for the liquid, while the gas superficial

velocities were all between 0.593 m/s and 125.3 m/s. The majority of the map was occupied by the intermittent flow patterns, which are slug, plug, and pseudo-slug flow. Also worth mentioning is the fact that the pseudo-slug pattern represented a much larger portion of the map than for the 1 mm map. Transition mechanisms involving surface tension were present for the stratified to annular transition, while plug agglomeration caused the transition in the case of the plug and slug flow. The 3 mm map displayed gas superficial velocities of 0.136 m/s to 64.4 m/s, and liquid superficial velocities of 0.0033 m/s to 5.72 m/s. The transition between wavy and annular flow occurred from the deposition of liquid drops on the tube wall. The transition from slug to annular flow occurred when liquid waves formed on the tube wall. The superficial velocities used for the 4 mm map were between 0.0087 m/s and 3.69 m/s for the liquid, and from 0.0542 m/s to 37.8 m/s for the gas. If the gas velocity was set to the maximum, and the liquid velocities were low and stratified wavy flow was observed. Transition between wavy and annular flow most probably occurred by atomization and deposition of liquid droplets. Finally, for the 5 mm tube, the superficial velocities were between 0.0085 m/s and 2.25 m/s for the liquid, and between 0.0725 m/s and 25.4 m/s for the gas. Plug flow changed into bubble flow from shearing action caused by the turbulence of the liquid, while bubble changed into froth flow by an increased in the number of bubbles. For the transition between annular and dispersed flow, thickening of the liquid film and the formation of waves of liquid on the tube wall occurred. Plug to slug flow changes are achieved from the agglomeration of plugs of gas, while the transition from slug to pseudo-slug occurred due to the presence of roll waves. When compared to the work done by Taitel and Duckler (1976), good agreement was found between the transition

boundaries of their theoretical map and the 5 mm map. However, poor agreement was found between Taitel and Duckler's (1976) map and the 1 mm map. The main conclusion of this experiment was that one cannot predict the flow patterns found in a heat-exchanger from the results obtained in straight round tubes of equivalent hydraulic diameter.

Wambsganss et al. (1990) investigated two-phase flow patterns in small horizontal rectangular channels. They chose the following six flow patterns stratified, wave, plug, slug, bubble, and annular flow. From their results, a preliminary flow pattern map was developed, which they hoped would help deepen the knowledge of the effect of channel geometry and size on flow patterns. The final maps were refined using the pressure measurements, which provided more accuracy than the visual observations used to create the preliminary maps. Six test points were chosen throughout the test section, where a range of six different mass and superficial velocities could be observed in order to obtain data that would cover all of the flow patterns. This method enabled them to create complete maps, and allowed for the identification of all the flow regime transition boundaries of interest. Some discrepancies were observed when the map obtained for the aspect ratio of 6 and the one obtained for the aspect ratio of 1/6 were compared. First, the ratio of 1/6 map produced bubble flow at much lower liquid superficial velocities than the ratio of 6 maps, while the plug to slug transition could be clearly seen at much higher gas superficial velocities. On the other hand, the transition from slug flow to annular flow was more subjective, but showed a better agreement between the two maps. If no distinction was observed between annular flow and wave flow, the transition to annular

flow would be quite identical for the two maps. To refine the map results, the pressure drop measurements, particularly the frictional pressure gradient, were inspected. This investigation helped determine if the indications of flow regime transitions were evident. From this two-phase frictional pressure gradient, it was found that the plug/bubble to slug flow transition was evident, while the slug to annular transition was not. Next, the maps were compared to the maps generated for circular pipes during previous experiments by different authors, namely Mandhane et al. (1974), Govier and Omer (1962), Damianides and Westwater (1988), Fukano et al. (1989), as well as Troniewski and Ulbrich (1984). They concluded that the maps developed from the data for moderate to large diameter pipes could not be directly applied to small, rectangular channels. Also, general agreement was observed between maps for small rectangular channels and larger circular pipes, but the agreement did not hold for all of the flow regimes. For example, the bubble to slug flow transition was not well predicted by any of the maps based on large circular pipe data, while the capillary tube maps yielded good predictions. Also, stratified flow could not be observed on any of the two capillary maps. When compared to the Mandhane et al. (1974) maps, it was noted that the agreement was poor between the magnitude and trends of the transition to slug flow boundaries. Also, major differences could be seen between the liquid superficial velocities at which the transition from plug to stratified flow occurred, as well as when transition from plug to bubble flow occurred. The Fukano et al. (1989) map suggested that the slug to annular transition in the 1 mm capillary tube was in good agreement with the one observed in the tube having an aspect ratio of 1/6. As for the comparison between the present results and the work performed by Troniewski and Ulbrich (1984), it was found to be in very poor agreement.

This could be explained by the large difference in size between the pipes used in the two experiments. Finally, the authors concluded that only sporadic agreement could be noted between the small rectangular channel data and the small or large circular tube data.

In recent years, Xu et al. (1999) studied two-phase flow regimes in rectangular channels to gain a better understanding of heat transfer with phase change in mini- and micro-channels. Flow regime maps were plotted from the data collected, using both the superficial gas velocity U_{GS}, and the superficial liquid velocity U_{LS}. Here, the superficial velocities can be found with the following equations:

$$U_{GS} = \frac{Q_G}{A} \tag{2.30}$$

$$U_{LS} = \frac{Q_L}{A} \tag{2.31}$$

Where Q_G and Q_L are the volume flow rates of gas and liquid respectively, and A is the cross section area of the channels. It could be seen from the maps obtained for the 1.0 mm and 0.6 mm gap that the patterns observed were very similar to those found in medium size channels. It was also observed that the transition lines on the flow regime maps were shifted to the left when compared to the maps for medium size channels. The regimes obtained during the 1 mm gap experiment were similar to those obtained by Wilmarth and Ishii (1994) in channels of 20 mm by 1 mm. For the 0.3 mm gap results, it was noted that the overall map was different from the classical flow structure expected

inside larger size channel. The map was made of new regimes such as cap-bubbly, slug-droplet, churn, and annular-droplet. When the maps were compared to the ones of Mishima et al. (1993), it was observed that the transition lines were shifted to the right. Also, when the channel gap decreased in size, the experimental transition lines shifted to the left, as previously mentioned. Finally, it was noted that bubbly flow could only be observed on a small area of the maps, and was absent from the map created for the channel with the 0.3 mm gap.

A year later, Ekberg et al. (1999) studied gas-liquid two-phase flow in narrow horizontal channels. They extended their study to include the void fraction, the pressure drop, the flow patterns, as well as the flow regime maps. The coordinates chosen to define the maps were the gas and liquid superficial velocities. Different flow patterns were observed depending on the size of the channel used. The researchers noticed that the maps obtained differed from maps obtained in previous macro- and micro-channel experiments in circular channels. It was also found that the major discrepancies between the experimental maps occurred at the transition lines. The maps were compared to maps drawn by Mandhane et al. (1974), and poor agreement was observed. Also, the data in this study was compared to the work done by Wambsganss et al. (1990), as well as by Mishima et al. (1993). In both cases, they found significant differences between the data in two-phase flow in rectangular narrow channels with large aspect ratios (Wambsganss et al. (1990), and Mishima et al. (1993)) and the data from two-phase flow in annuli. When compared to the theoretical work performed by Taitel and Duckler (1976), the experimental data gathered in this experiment was found to be similar for the larger

channels, and dissimilar for the smaller channels. It is important to note that Taitel and Duckler (1976) did not account for micro-channels, which would explain the disagreement encountered in the smaller channels.

During the same year, Coleman and Garimella (1999) also conducted experiments in order to generate flow regime maps. In their study, individual maps were plotted for each of the different tube diameters, which were 5.5 mm, 2.6 mm, 1.75 mm, and 1.3 mm. From this research, it was found that flow regime maps for larger tubes, like the ones created by Mandhane et al. (1974), as well as the transition correlations for larger tubes, such as the one defined by Weisman et al. (1979), were not applicable to small tubes. On the other hand, the present study is in good agreement with the work preformed by Damianides and Westwater (1988). When compared to the theoretical experiments of Taitel and Duckler (1976), the results obtained here showed very poor agreement. More specifically, it was observed that the transition to annular flow was a nearly constant value, which is in agreement with the data found by Damianides and Westwater (1988), as well as by Weisman et al. (1979). When compared to the study made by Damianides and Westwater (1988), it was noted that both studies did not report the presence of stratified flow, while both studies showed a decrease in the size of the wavy-annular flow regime and an increase in the size of the intermittent flow regime as the tube diameter decreased. The most evident discrepancy between the two experiments was the transition from the intermittent pattern to the dispersed pattern. When comparisons were made between this experiment and the work of Taitel and Duckler (1976), the wavy flow pattern was observed at a higher gas velocity than that predicted by the theories of Taitel

and Duckler (1976). The present results were also compared to those of Fukano et al. (1989). Both studies clearly show that the transition to dispersed flow occurred at a higher value of gas velocity, as the diameter of the channel decreased. Lastly, comparisons were made with the correlations designed by Weisman et al. (1979). While some agreement could be found in the predictions made concerning the transitions observed here and the correlations by Weisman et al, especially for the larger diameters, their correlations were not suitable for the predictions of the effect of tube diameter on the shifts in transition. This last affirmation could be explained by the fact that Weisman et al.'s (1979) work was based on large diameter tubes, while the tubes used here were smaller. This difference in diameter potentially leads to wrong assumptions on the effect of tube diameter, surface tension, and liquid viscosity.

One of the most recent studies from which flow maps were generated was conducted by Tabatabai and Faghri (2001). They generated on a new flow map in which the importance of surface tension in two-phase flow in mini- and micro-channels was accounted for. Also, research was conducted to create a transition boundary based on the following: a force balance involving shear, buoyancy, and surface tension. The results obtained were then compared with the data from previous experiments. The flow map developed throughout the course of this experiment helped in determining the relative effects of surface tension forces relative to shear forces. It also determined surface tension effects on the various regime boundaries on the map. The coordinates used to generate the map were the ratio of the pressure drop due to surface tension forces, and the ratio of pressure drop due to the shear forces, as well as the ratio of superficial gas to

superficial liquid velocities. It is therefore implied that both the coordinate axes represent dimensionless parameters. The following equation was used to obtain the ratio of pressure drop due to surface tension and shear forces:

$$\Delta P_{ratio} = \frac{(\frac{dP}{dz})_{surface\ tension}}{(\frac{dP}{dz})_L + (\frac{dP}{dz})_G} \qquad 2.32$$

It was found that the flow regimes dominated by the surface tension are the plug, slug and bubbly flow regimes. On the other hand, the regimes dominated by shear were the annular, mist, stratified, and wavy flow. The results of the experiment were compared with data points taken in pipes of diameters ranging from 15.88 mm to 4.8 mm for condensation runs, and from 12.3 mm to 1 mm for air and water experiments. The researchers concluded that as the diameter of the channel was decreased, the transition boundaries of the map were shifted to the right. Also noted was the surface tension versus the shear boundary, which shifted upwards. The maps obtained were compared with existing models, such as Taitel and Duckler (1976) model, which provided a good prediction of the results for small-diameter tubes. The Mandhane et al. (1974) model, on the other hand, only gave fairly accurate predictions for most applications. To conclude, the map generated by Tabatabai and Faghri (2001) was excellent for small-diameter tubes in which surface tension is the prime acting force. It was also noted that this new map and model gave greatly improved accuracy when determining surface tension dominated regimes.

2.3. Pressure Drop in Two-Phase Flow in Macro- and Micro-Channels

When designing systems in which two-phase flow occurs, a number of specific parameters, such as pressure drop and void fraction, have to be considered. Pressure drop in two-phase flow channels has been the primary subject of numerous researches and experiments. The first part of this section will be dedicated to the previous work conducted involving pressure drop in both macro- and micro-channels.

For practicality, some of the most well known correlations related to pressure drop in channels are considered to be flow regime independent. As a result, some of these correlations may not yield accurate results under certain conditions. The most relevant correlations and models for pressure drop in macro- and micro-channels will be discussed in a later subsection. The first model of importance here is the Homogeneous Mixture Model, which is also the simplest model enabling one to measure the pressure drop in two-phase flow. One of the main aspects to be considered when studying pressure drop in micro-channels is the drop due to friction. As a result, many experiments have been conducted in order to predict the frictional pressure drop in channels of all sizes. From these experiments, a number of models and correlations have been developed. The second model described here will be the Separated Flow Model, followed by the Two-Fluid Model. A short section on the different experimental correlations developed will end the pressure drop review.

2.3.1. Previous Work Done on Pressure Drop in Macro- and Micro-Channels.

One of the first studies conducted on pressure drop in macro-channels, along with the work done by Jenkins (1947), was performed by Lockhart and Martinelli (1949). They investigated the possibility of an empirical relationship between the superficial gas velocity and the pressure drop in two-phase flow. The size of tubes used ranged from capillary to 25.4 mm in diameter. For the purpose of their research, they defined a parameter X, which is in fact the ratio of the liquid pressure drop upon the gas pressure drop:

$$X^2 = \frac{\left(\frac{\Delta P}{\Delta L}\right)_L}{\left(\frac{\Delta P}{\Delta L}\right)_G} \qquad 2.33$$

Next, their parameter X was correlated to the parameters Φ_L and Φ_G, which were defined by the following:

$$\Phi_{L,G}^2 = \frac{\left(\frac{\Delta P}{\Delta L}\right)_{TP}}{\left(\frac{\Delta P}{\Delta L}\right)_{L,G}} \qquad 2.34$$

In this last expression, $(\Delta P/\Delta L)_{TP}$ represents the pressure drop per unit length during two-phase flow. Some work was also performed on the void fraction, in which they related it to the parameter X.

This study was closely followed by Bergelin and Gazley's (1949) work on pressure drop in macro-channels. The bulk of their study was based on pressure drop measurements in a 2 in (50.8 mm) copper pipe. When their results were compared to the data obtained by Lockhart and Martinelli (1949), there were large discrepancies. They concluded that the Martinelli correlation was providing a conservative prediction of the pressure drop observed in the stratified flow, and that the prediction of the pressure drop found in annular flow was in better agreement with their data. It was also noted that the results obtained by Lockhart and Martinelli (1949) for the void fraction in stratified flow differed from their own results. Some years later, Baker performed an experiment enabling him to create the first flow pattern map. He also studied the pressure drop in tubes with diameters ranging from 102 mm to 258 mm. The two-phase components were oil and gas. The superficial pressure drops were calculated using a modified Fanning equation. The pressure drop observed in pipes of more than 200 mm were found to be 40% to 60% less then the ones measured by Lockhart and Martinelli (1949). From these results, it was concluded that the large influence of pipe diameter on flow patterns has to be taken into account when developing pressure drop correlations.

Johnson and Abou-Sabe (1952) conducted some of the earliest work on the static pressure drop present in two-phase flow inside a horizontal brass channel of 1 in

diameter, 15 in length, and 16 gauge. The different flow patterns could be observed with the help of an observation glass inserted at the end of the test section. Their results were then transferred onto a flow regime map, and then separated into four different regimes, namely bubble, annular, slug, and stratified. However, the flow regimes identified were arbitrary and subjective, as the observations made were purely visual. The data obtained during both the isothermal and the non-isothermal experiments were then compared to the work done by Martinelli et al. (1944). It was found, from this comparison, that even though the pressure estimate of the Martinelli et al. (1944) data was conservative, it was in agreement with their results.

Baker (1954) is one of the first researchers to develop separate correlations for pressure drop in the different flow regimes. He extended his work to produce a modified version of the correlations originally presented by Martinelli (1944). In order to achieve his goal, 0.87 in (22.1 mm), 1 in (25.4 mm), 3 in (76.2 mm), 4 in (101.6 mm), 6 in (152.4 mm) , 8 in (203.2 mm), and 10 in (254 mm) diameter pipes were used. Data was gathered, and a correlation was developed for each pipe diameter. According to his work, the two-phase pressure drop can be determined by:

$$\Delta P_{TP} = \Delta P_G \Phi_{GTT}^2 \qquad 2.35$$

Here, the term Φ_{GTT} takes on a different value according to the flow pattern and ΔP_G represents the superficial gas pressure drop. The following table presents the flow regimes observed, as well as the value of the parameter Φ_{GTT}.

Annular flow	$\Phi_{GTT} = (4.8 - 0.3125D)\, X^{(0.343 - 0.021D)}$
Stratified flow	$\Phi_{GTT} = 15400X / L^{0.8}$
Plug flow	$\Phi_{GTT} = 27.315X^{0.855} / L^{0.17}$
Slug flow	$\Phi_{GTT} = 1190X^{0.815} / L^{0.5}$
Bubble flow	$\Phi_{GTT} = 14.2X^{0.75} / L^{0.1}$

In the preceding expressions, D represents the pipe diameter, X is the Martinelli parameter, and L is the liquid mass velocity. Although the extent of his work is quite vast, Baker realized that, when compared to his experimental data, his correlations were not very accurate. It was concluded that this lack of agreement was most probably due to the inadequate amount, and low quality of the experimental data gathered.

White and Hungtington (1955) worked on the pressure drop found in two-phase flow, and proposed an improved correlation. They used three liquids and two different gases to conduct their experiments in tubes with diameters ranging from 25.4 mm to 50.8 mm. Their correlation gave a better approximation of both their results and Jenkins' results. It was however very limited since it was based on the following restrictions: the flow regimes were stable in nature, low pressures were maintained, and the viscosity of the liquid was always less than 120 cp.

During the same period, Hoogendoorn (1959) conducted a study on two-phase flow, taking into account both the pipe diameter and roughness. The data produced by his

experiments were compared to the correlation designed by Martinelli (1949). It was found that Martinelli's (1949) correlation was in agreement for the plug, slug, and dispersed flow, under atmospheric conditions. However, the correlation was not valid for the data gathered on annular, stratified, and wave flow, as well as on plug, slug, and dispersed flow under non-atmospheric conditions. Hoogendoorn (1959), therefore, produced his own pressure drop correlations for the regions in disagreement with the one generated by Martinelli (1949). Also, a hold-up correlation was developed.

$$\frac{\alpha}{1-\alpha} = 0.6\left(U_{GS}\left(1 - \frac{\alpha}{1-\alpha}\frac{U_{LS}}{U_{GS}} \right) \right)^{0.85} \qquad 2.36$$

where α was the void fraction, U_{GS} was the gas superficial velocity, and U_{LS} was the liquid superficial velocity. Govier and Omer (1962) performed experiments involving air and water in horizontal pipes with 1.026 in (26.06 mm) of diameter. Several flow patterns, as well as the pressure drop were observed. The pressure drop correlation generated was based on a superficial Reynolds number related to liquid properties, as well as on the friction factor f_{TP}:

$$\left(\frac{\Delta P}{\Delta L} \right)_{TP} = \frac{2 f_{TP} U_{LS}^2 \rho_L}{gD} \qquad 2.37$$

Govier and Omer (1962) decided to use the Fanning equation to express the pressure drop, while substituting the Fanning friction factor by their two-phase friction factor. The results were found to be approximately the same as the data previously obtained by

Johnson and Abou-Sabe (1952). Also, when compared to the Martinelli correlation, it was found that the experimental results were very similar when the two-phases were in a turbulent state. The previous research was followed, by a study of the elongated bubble flow regime in capillary tubes performed by Suo and Griffith (1964). For this experiment, tubes with 1 mm to 1.6 mm of diameter were used. The average volumetric flows of the liquid and gas, as well as the bubbles' velocity, were considered in order to correlate the different transition lines defined by the experiment.

This experiment was closely followed by study of Baroczy (1966). He gathered all of the data obtained by Johnson and Abou-Sabe (1952) in order to develop an empirical two-phase flow pressure drop correlation. This correlation, however, was only valid in the presence of a turbulent-turbulent flow regime, and was based on both air-water and mercury-nitrogen data. The parameters used are presented below:

$$\Phi_{LT}^2 = \Phi_L^2 (1-x)^{1.8} = \left(\frac{\Delta P}{\Delta L}\right)_{LT} \qquad 2.38$$

$$\frac{(\frac{\mu_L}{\mu_G})^{0.2}}{(\frac{\rho_L}{\rho_G})} \qquad 2.39$$

In the above expressions, Φ is the Martinelli parameter.

Here, $[dP/dz]_f$ is the frictional pressure gradient, G is the mass flux, μ_{TP} is the two-phase viscosity, and ρ_{TP} is the homogeneous density. The homogeneous void fraction is given by the following:

$$\beta = \frac{\rho_L x}{\rho_L x + \rho_G (1-x)} \qquad 2.47$$

A hybrid definition was used to find the two-phase viscosity:

$$\mu_{TP} = \mu_L (1 - \beta)(1 + 2.5\,\beta + \mu_G \beta) \qquad 2.48$$

To test the theoretical method, a comparison was made between the data taken from various flow patterns. This data was found in a data bank, which covered adiabatic horizontal and vertical up flow in round tubes. Since the model yielded good results, they concluded that errors due to the neglect of the mass flux effects are not as significant as errors due to the neglect of other effects, such as the entrance effect.

At the beginning of the 1990's, Mishima et al. (1993) performed a very complete study on flow regimes, void fraction, bubble velocity, and pressure drop in two-phase flow using the Newton radiography technique in rectangular channels.

Recently, Pfung et al. (1998) performed an experiment which obtained for the measurements for the pressure drop, and used flow visualization inside a single-phase

flow in a micro-channel. Surface roughness data was obtained. The objective was to distinguish the differences between macro- and micro-channel flow measurements. To obtain the experimental results, a test section was built in which a channel with a depth varying from 100 to 500 microns was used. The working fluid flowing through the channel was water. A single channel was built, formed of a spacer and two plates, where the spacer's thickness determined the depth of the channel. The length of the channel was 10 cm, and its width was 1 cm. The channel parameters were such that the flow could be assumed to be two-dimensional. To measure the pressure drop, miniature pressure transducers were used. The flow rates were obtained with miniature turbine meters. Measurements of the surface roughness were made using an interferometer. Approximately 10,000 data points were recorded for each test, from which it was found that the surface roughness tended to increase the laminar friction factor inside the channel. The friction factor was calculated and it was noted that no significant differences between the sizes of the channels were observed. Measurements were made to verify the linearity of the pressure drop in the micro-channel, as well as to verify whether the entrance and exit effects were present or not. It was concluded that the pressure drop was in fact linear, and that as the flow rates increased, an exit loss could be observed. Also, the transition between laminar and turbulent flow was studied with a dye stream injection method. It was found that the critical region began at a flow rate of about 450 ml/min (Re = 2080).

A year later, Ekberg et al. (1999) worked on a project that involved gas-liquid two-phase flow in narrow horizontal channels. Many parameters were studied, such as the void

fraction, the flow patterns, the flow maps, as well as the pressure drop. The tubes used here had diameters of 6.6 cm and 33.2 cm, and lengths of 46 cm and 43 cm, respectively. The pressure drop in the test section was calculated and compared to several well-known correlations, such as the ones designed by Beattie and Whalley (1982), Friedel (1979), and Chisholm and Laird (1958). The Beattie and Whalley (1982) correlation, although very simple, was found to accurately predict pressure drop data found inside thin rectangular channels, while the Friedel correlation was based on a wide range of parameters, and accounts for a vast range of data. The Friedel correlation is shown below:

$$\left(\frac{-dP}{dz}\right)_{f.TP} = \Phi_{LO}^2 \left(\frac{dP}{dz}\right)_{f.LO} \qquad 2.49$$

where

$$\left(\frac{-dP}{dz}\right)_{f.LO} = \left(\frac{2f_{LO}}{R}\right)\left(\frac{G^2}{2\rho_L}\right) \qquad 2.50$$

As for the Chisholm and Laird correlation, it is described below by:

$$\Phi_L^2 = 1 + \frac{C}{X} + \left(\frac{1}{X}\right)^2 \qquad 2.51$$

Here, the parameter $(-dP/dz)_{f.L}$ represents the single-phase frictional pressure drop if pure liquid flows in the channel, and if its mass flux is G(1 – x). The X symbolizes for the Martinelli factor, while C had a value ranging between 10 and 20. Also, it could be seen that:

$$\left(\frac{-dP}{dz}\right)_{f.TP} = \Phi_L^2\left(\frac{-dP}{dz}\right)_{f.L} \qquad 2.52$$

From all the comparisons made with the various correlations, it was noted that the accuracy of them all depended highly on the flow regime studied. It was found, that the homogeneous mixture model accurately predicted the frictional pressure drop inside the micro-channels. On the other hand, the homogeneous model under predicted the experimental data obtained during the course of this experiment, particularly for the churn and the annular flow patterns. The correlation that best predicted the data collected was the Friedel (1979) correlation, as it showed general reasonable agreement with the data. While the Beattie and Whalley (1982) correlation provided a small overall scatter of the data, its general agreement with the experimental data remains inferior to the Friedel correlation. As for the prediction of the Chisholm and Laird correlation, its performance highly depended highly on the value of the parameter C, which, for small channels, could be a function of the channel hydraulic diameter.

Garimella et al. (2002) conducted one of the most recent studies on two-phase flow. They created an experimentally validated model for pressure drop during intermittent flow. The fluid used was R-134a refrigerant in horizontal micro-channels. The channels

had hydraulic diameters ranging from 0.5 mm to 4.91 mm. The focus of the experiment was to model the pressure drop existing inside a round tube during condensation, in a particular flow regime. The intermittent flow regime was chosen for the research.

In order to make the experimental pressure drop measurements, three selectable differential pressure transducers with maximum ΔP values of 6.22 kPa, 62.2 kPa, and 248.2 kPa were used. It was found that the pressure drop data could be represented by:

$$\Delta P_{measured} = \Delta P_{frictional} + \Delta P_{expansion\&contraction} + \Delta P_{deceleration} \tag{2.53}$$

where

$$\Delta P_{contraction} = \frac{G^2}{2\rho_L}\left[\left(\frac{1}{C_c - 1}\right)^2 + 1 - \gamma^2\right]\Psi_H \tag{2.54}$$

In this last equation, C_c is the function of the area ratio, γ^2 is the area ratio, and ψ_H is the homogeneous flow multiplier.

$$\Delta P_{expansion} = \frac{G^2\gamma(1-\gamma)\Psi_H}{\rho_L} \tag{2.55}$$

$$\Delta P_{acceleration} = \left(\frac{G^2x^2}{\rho v\alpha} + \frac{G^2(1-x)^2}{\rho_L(1-\alpha)}\right)_{x+xout} - \left(\frac{G^2x^2}{\rho v\alpha} + \frac{G^2(1-x)^2}{\rho_L(1-\alpha)}\right)_{x=xin} \tag{2.56}$$

In the previous equation, α is the void fraction and G is the total mass flux. Also, note that only the data points from the intermittent flow regime were included for the pressure drop model.

It was found that smaller diameter tubes display a much higher pressure drop than the one observed in larger tubes. Also, the relationship between the pressure drop and the quality was found to be nearly linear, while the pressure drop was found to increase with increasing mass flux. The results obtained were in an approximately $\pm$ 13.4% margin around the measured data. While 88% of the predictions turned out to be within $\pm$ 25% of the 77 measured data points, it was concluded that the experimental results were far more accurate for smaller diameter tubes.

2.4. Summaries

2.4.1. Summary for Flow Regimes

Influence of the channel diameter:

Most of the experiments performed on two-phase flow inside channels of various geometries used mainly diameters in the macro-size range. The earliest studies provided an introduction to the parameters of two-phase flow inside channels of diameters of the order of one inch. Overall, a vast quantity of studies have been conducted with diameters ranging from around 0.03 in (0.762 mm) to 8 in (203.2 mm), all of which yielded different results where the flow regimes were concerned. Some research was specifically conducted by different groups in order to study the effects of tube diameter and channel dimension on flow regimes. In recent years, it was proven that diameter does indeed play a significant role in the flow regimes found inside small tubes. Later, other experiments helped prove that not only were the flow regimes changing inside different size of channels, but the discrepancies were much more obvious as the size of the channel decreased to near micro sizes. Also, an experiment preformed very recently showed that while the diameter effects are huge in small diameter tubes, the impact on larger diameter tubes is less significant.

While experiments performed on macro-channels are prevalent, studies using mini- and micro-channels are much more scarce. Worth mentioning is the work of Weisman et al. (1978), which focused on the effect of pipe diameter in pipes with diameters of 0.45 in (11.43 mm), 1 in (25.4 mm), and 2 in (50.8 mm). This study was the first to conclude that

within that range of macro-channels, the pipe diameter effect had only a moderate impact on the results. Following this study, Damianides and Charalambos (1998) performed experiments on the relative importance of these same effects on channels of 5 mm, 4 mm, 3 mm, 2 mm, and 1 mm in diameter. His results greatly contributed in proving that the pipe diameter effects are significant in the regimes found inside horizontal two-phase flow for that range of diameters. Thus, while the results obtained for macro-channels are numerous and quite precise, those results cannot be applied to mini- and micro-channels. An extension of their studies for smaller channels would be of prime importance for the advancement of two-phase flow regime observation. Xu et al. (1999) performed one of the only studies on the effects of diameters in macro-channels. Their research was however aimed more towards discovering the reason behind the discrepancies observed between the micro-channels and macro-channels results. It was concluded that for channels of diameters of 1 mm, 0.6 mm, and 0.3 mm, the cause for the change in flow regimes was the increase in wall shear stress, as well as the increase in interface shear stress. From these studies, it is obvious that the properties of two-phase flow are greatly affected by the diameter effects as the diameter size decreases, which makes it imperative to obtain more data within this range of diameters.

Influence of geometry:

The influence of the channel geometry is an aspect that was not covered in great depth over the history of research on two-phase flow. While some experiments were performed in triangular, rectangular, and circular channels, very few experiments used ellipsoidal, trapezoidal, and irregular shaped channels. The most common channel geometry used is

the circular geometry, while rectangular is the second most commonly used geometry. While the basic flow regimes, (bubbly, slug, and annular) remain the same for both circular and rectangular channels, some discrepancies can still be observed in the flow regimes present.

Sadatomi and Saruwatari (1982), determined that channel geometry has little influence in noncircular channels when the hydraulic diameter is greater than 10mm. This experiment was further explored in more recent years by Coleman and Garimella (1999), which extended the research to pipes of smaller diameters, ranging between 1 mm and 10 mm. It was observed that while the diameter, geometry, and surface tension have a moderate effect in pipes with diameters larger than 10 mm, they have a huge impact in the flow pattern formation inside smaller channels. Extending the work of Coleman and Garimella (1999) with sizes of diameters in the micro-range is a possible future research direction. Also, Wambsganss et al. (1990) observed that the difference in flow regimes as the channel diameter is changed (in a range of diameters below 10 mm) is much more pronounced when two channels of dissimilar geometry are compared. It can be concluded that while the data and correlations developed for macro-, mini-, and micro-channels is fairly extensive for circular channels, an enormous lack of data pertaining to other geometries greatly restricts the expansion of two-phase flow knowledge.

Influence of fluids:

From the numerous experiments performed on gas-liquid two-phase flow, only a small portion was actually performed with other fluids than water and air. Though the liquids

were occasionally varied, practically all the experiments thus far have involved air as the gas component of the two-phase flow. Obviously, there is a need to perform experiments in which a gas other than air is utilized. In addition, very few experiments observed the actual effects of fluid properties on the regimes formed in two-phase flow inside channels. Most researchers performed experiments focusing on other aspects, and stating that the effects of fluid properties as negligible. However, when the effects of fluid properties were studied, the main parameters investigated were the viscosity, surface tension, liquid density, and vapor density. Due to the very small number of studies that took into account the effects of fluid properties, not every range of diameters or any channel geometry has accompanying data pertaining to these effects. This lack of data is another obstacle in the exploration of two-phase flow.

One of the most important experiments in studying the effects of fluid geometry was performed by Weisman et al. (1979). The components of the two-phase flow were glycerol-water solutions, water containing a surface active agent, potassium carbonate solution, and freon 113- freon 113 vapor. Results showed that the effects of fluid properties were not significant for the flow regimes observed in macro-channels. White and Hungtington (1955), in the earlier years of the development of two-phase flow, investigated the behavior of two-phase flow using three liquids and two different gases (natural gas and kerosene, air and kerosene, and air and water) in channels of macro-size. In recent years, however very little development has occurred on the subject, and extension of experiments such as the one performed by Weisman et al. (1979) are needed in order to account for the effects of fluid properties in a wider range of pipe diameter

and geometry, which includes the mini- and micro- ranges. Also, the different flow regimes observed varied greatly with the studies conducted. The most common ones observed were slug, stratified, wavy, and annular flow. However, it is not yet possible to clearly distinguish which of the parameters studied introduces the most the discrepancies found in the different flow regimes.

2.4.2. Summary for Flow Regime Maps

Coordinate systems:

Very few researchers decided to present their results in another form other than flow regime maps. These maps are the fastest and easiest way to examine the results obtained during the course of an experiment, and to extrapolate conclusions from the data acquired. Some basic differences can be observed between the maps produced to date with earlier maps. The most obvious of them is the coordinate system used to classify the results in the map. In earlier maps, it was believed that the effects of diameter and geometry could be accounted for by using the volumetric flow fraction of gas and the mixture superficial velocity as the coordinates of the map. Several maps were generated in this way, including the Baker (1954) Chart, one of the most important maps produced, which represented macro-channel two-phase flow. However, it is now known that these effects cannot be accounted for so easily. Nowadays, nearly all experiments pertaining to two-phase flow inside channels use the superficial velocities of the gas and the liquid components as the coordinate system of their flow regime maps. One of the results of this uniformity is the greater ease with which the results of different studies can be compared. Great improvements have changed the layout of the maps over the years, but

this uniformity is on of the best changes that occurred, facilitating the process of comparing results and extrapolating trends between experiments.

Influence of diameter:

Earlier experiments produced flow regime maps, that were believed to be applicable for all diameters. This belief has since been refuted, and researchers now know that the maps produced for macro-channels can never be applied to two-phase flow inside mini- and macro-channels. As mentioned before, the number of experiments performed with mini- and micro-channels is relatively small compared to the amount of research that was performed in macro-channels. For this reason, very few maps are available with data pertaining to mini- and micro-channel two-phase flow. To date, it is believed that the main cause of the discrepancies between macro-, mini- and micro-range maps is due to the surface tension inside smaller channels.

Scott (1963) was the first to comprehend the importance of the diameter effect in identifying the correct flow regimes inside a pipe. Consequently, he was able to produce a map that yielded better results than all the previous ones generated by that time, but restrained its use to pipes with diameters greater than 1 in (25.4 mm). Recently, Damianides and Westwater (1988) were able to prove that the data collected inside circular tubes cannot be applied to plate-type geometries, such as the one of a heat-exchanger. Their conclusion was based on the different maps generated in their study for diameters ranging from 1 mm to 5 mm. Wambsganss et al. (1990) conducted a study which helped concluded that maps designed for circular pipes of moderate to large

diameters could not be directly applied to small, rectangular channels. Ekberg (1997) confirmed that even in the macro-range (between 6.6 mm and 33.2 mm), maps produced for a specific diameter could not be used to extrapolate results for other diameters, due to the difference in flow regimes observed. A recent study, performed by Xu et al. (1999), studied vertical channels of 0.3 mm and 0.6 mm. From their maps, they determined that while the flow regimes inside the 0.6 mm channel still showed characteristics of classical flow regimes, the regimes in the 0.3 mm channel displayed distinctively different characteristics from the classical patterns, in that bubbly flow never occurred. Coleman and Garimella (1999) were the ones to confirm that the flow regime maps obtained previously for larger tubes could not be applied to tubes smaller than 10 mm in diameter due to the due to the effect of surface tension inside smaller channels.

Transition boundaries:

One of the major aspects relating to the flow regime maps in two-phase flow concerns the positioning of the flow regime transition boundaries. Unfortunately, this aspect of the flow regime maps is still quite ambiguous, and generates large errors in the design of the maps. One of the important discrepancies that occurs when the diameter of the pipes is varied a shift in the transition boundaries between the different classical flow regimes. Several theoretical and experimental attempts have been made to determine the exact location of the transition boundaries on flow regime maps. It was concluded, that numerous parameters were responsible for the position of the transition boundaries, such as the viscosity of the fluids, the channel geometry, as well as the diameter of the pipe.

The most significant parameters affecting the position of the transition boundaries, however, are the superficial velocities of both the gas and the liquid components.

Mandhane et al. (1974) conducted an experiment in which they concluded that errors in the position of the transition boundaries almost annihilated whatever physical property effects that might have been present. Taitel and Duckler (1976) developed a theoretical approach to flow regime mapping in order to predict the boundaries of the flow regimes on the flow regime maps. Also, Simpson et al. (1977) presented two flow regime maps in which the effects of pipe diameter could be observed. This effect could be seen from the transition boundaries, which occurred at a much higher liquid superficial velocity and at a considerably lower gas superficial velocity. Troniewski and Ulbrich (1984) investigated the effects of viscosity on the transition boundaries, and found that the liquid viscosity up to 0.040 kg/m^2s had negligible effect on the flow pattern transitions. More recently, Xu et al. (1999) performed a study on two-phase flow inside vertical mini- and micro-channels. They observed that the maps created for those channels differed from the maps obtain for macro-channels in previous experiments, in that the transition boundaries on the micro- channel maps were shifted to the left. Also, it was found that with the decrease of gap size, the transition between the regimes occurred at lower gas flow rates. Ekberg et al. (1999) investigated the two-phase flow inside mini-channels, and concluded that the largest source of discrepancies between the flow regime maps created was related to the location of the transition lines. They also found that the flow patterns and the transitions fluctuated greatly with the change in the tube diameter and the tube shape. Finally, Tabatabai and Faghri (2001) recently developed a model for a

transition boundary separating the surface tension dominated regimes from the shear dominated regimes. This was achieved using a surface tension, buoyancy, and shear force balance. The proposed map and model provide significant improvement on determination of surface tension dominated regimes.

2.4.3. Summary for Pressure Drop

Influence of diameter:

Several studies have been conducted, investigating the variation of pressure in two-phase flow. Most studies aimed to establish the relation between the effects of diameter and the pressure drop inside a channel. To date, the research performed has been in the macro-channel range, while very few studies pertain to the mini- and micro-channel ranges. In the macro-range, studies were performed in channels of diameters ranging from approximately 0.87 in (22.1 mm) to 10 in (254 mm). It was found that of all the correlations developed, none were able to predict the pressure drop for all flow regimes and all diameters, rendering it extremely difficult to extrapolate results on this subject. In the future, it would be of extreme importance to develop a single correlation for every flow regime observed at a specific channel diameter. Also, more data on pressure drop inside mini- and micro-channels is needed for the progression of research on two-phase flow.

Baker (1954) was the first to understand the need for different pressure drop correlations for each flow pattern that was observed. As a solution to this problem, he generated separate correlations for the flow regimes observed in 0.87 in (22.1 mm), 1 in (25.4 mm),

3 in (76.2 mm), 4 in (101.6 mm), 6 in (152.4 mm), 8 in (203.2 mm), and 10 in (254 mm) pipes. In recent years, Coleman and Garimella (1999) developed an experimentally validated model for the pressure drop during the intermittent flow of condensing fluid. The main focus of the work was the measurement and modeling of two-phase pressure drop during condensation in the intermittent flow regime for round tubes of varying diameters. It was concluded that as the diameter decreased, the pressure drop increased. However, this model becomes less accurate when applied to regimes other than intermittent.

Influence of geometry and fluid properties:

The pressure drop is one of the most highly studied parameters inside two-phase gas-liquid flow. In most cases, the data acquired pertained to circular or rectangular horizontal and vertical channels. Evidentially more studies have been conducted in channels of macro-size, with very few studies actually focusing of the pressure drop inside micro and mini-channels. Also, the fluids used to form the two-phases of the flow were most often air (as the gas), and water (as the liquid). Very few studies used components other than air and water, which implies that the effects of fluid type on the pressure drop in two-phase flow are not well known. Also, there is a significant lack of channel geometry variation in the studies accomplished previously. Very few research was been conducted with triangular, ellipsoidal, and irregular channel cross-section, limiting the knowledge of two-phase flow pressure drop. In addition, the angle of the test section has been limited to either 0 or 90 with respect to the horizontal, restraining the

knowledge of the effects of test section angle on the pressure drop inside channels of various sizes.

White and Hungtington (1955) investigated the behavior of two-phase flow using three liquids and two different gases. Their study was however limited by the numerous assumptions made to obtain their correlations. Some of these assumptions referred to the stability of the flow, the pressure range, and the viscosity of the fluids used. Also, Baroczy (1966) generated an empirical correlation for the pressure drop occurring in air and water flow, as well as mercury and nitrogen flow. From his work, a chart was created, which predicted the pressure changes occurring in a two-phase flow. More recently, Coleman and Garimella (1999) developed an experimentally validated model for the pressure drop during the intermittent flow of condensing fluid. The fluid used in this experiment was refrigerant R-134a, and the pressure was measured inside fourteen channels with different geometries. A pressure drop model was developed for a unit cell in the channel using the individual phase friction factors. The approach used by the researchers accounted for the variation in flow patterns as the quality changed. Some of the problems encountered during this experiment were the omission of the effects of gravity when compared to the surface tension forces, weakness in the calculation of the unit cell length, and the incomplete collapse of the data into a single trend upon application of the correlation.

2.5 Future Directions

Thus far, a state-of-the-art literature review covering the research performed to date on the subject of gas-liquid two-phase flow inside channels of different diameters has been presented. Although the amount of data gathered thus far is indeed impressive, there are many future directions linked to the field of two-phase flow that have yet to be explored. In the present section, a brief summary of the possible future directions that could be followed to expand the knowledge in this area is given.

There is a significant lack of data pertaining to two-phase flow inside channels in the mini- and particularly the micro-range. In order to advance the research on two-phase flow, it is important to explore the mini- and micro-range since the effects of pipe diameters have a great impact on the flow regimes. Due to the fact that flow regime maps obtained for channels with diameters in the macro-range cannot be used for the data found in the mini- and micro-channels, and also because of the scarcity of the data available in the mini- and micro-ranges, there is a great need for further elaboration of flow regime maps for the mini- and micro-ranges. The creation of flow regime maps for the mini- and micro-ranges of diameter will be necessary for the advancement of research in the field of two-phase gas and liquid flow inside channels. In fact, the elaboration of maps depicting the data obtained using ranges of diameters not covered in the past could be a turning point in the research in this field. The one major factor influencing the pressure drop inside a channel is the diameter of the channel. Since none of the correlations generated to date were able to predict the pressure drop for all flow regimes and for all diameters, it would be highly beneficial to develop a single correlation for

every flow regime observed for a specific channel diameter. Also, more data on pressure drop inside mini- and micro-channels is needed for two-phase flow.

Future studies involving channel geometries with cross-sections that are triangular, ellipsoidal, as well as irregular shapes would expand the knowledge of gas-liquid two-phase flow regimes inside channels. While the effects of pipe diameters were covered to some extent in previous work, very little research has been conducted using geometries other than circular and rectangular. A wider knowledge of the effects of geometry can become of crucial importance, especially when design considerations are to be taken into account. Also, the effect of the channel angle has, to date, not been extensively studied and thus requires further attention. In addition, more research needs to be conducted on the impact of fluid properties and channels geometry on the pressure drop in two-phase flow. Future studies using varying viscosity, for example, would be of crucial importance for the advancement of the two-phase flow pressure drop research.

Another aspect that needs further attention concerns the effects of fluid type. Almost all the studies performed used water and air, limiting the data relating the effect of fluid type on the flow regimes. Thus, future studies using other fluids other than water and air will help gain a better understanding of the effects of fluid type on the flow regimes found in channels of all diameters, particularly in the mini- and micro-ranges. Also, fluid properties such as the fluid viscosity and fluid density need to be extensively studied to understand how such parameters affect the flow regimes found in the channels. Further determination of the main parameters affecting the results obtained in macro-, mini-, as

well as micro-channels is of great importance for the advancement of the research. Also, channels that are triangular, ellipsoid, and irregular shapes, mounted on tests rigs at different angles with respect to the horizontal, should be studied extensively in the future in order to gain a wider range of pressure drop data, taking into account both the effects of channel geometry and the effects of channel angle with respect to the horizontal.

For the flow regime maps, future work needs to be performed in order to find either a new, more efficient coordinate system, or to find some new means of collecting all the data. The goal would be to generate maps that will be even more universal than the current flow regime maps used. A milestone in research occurred when all researchers decided to use the same coordinate system in order to facilitate the comparison of data from one experiment to another. However, the major problem with these maps, which use the superficial velocities of both the gas and the liquid as the coordinates, is the difficulty in determining the location of the transition boundaries on the map. Unless a system that reduces the error produced by the positioning of the transition boundaries is developed, most of the effects of the fluid properties, as well as other minor effects will never be fully understood.

Therefore, future work pertaining to the positioning flow transition boundaries on the flow regime maps is important for the advancement of the two-phase flow research field. It would be extremely useful to be able to accurately predict the exact location of the transition boundaries between each flow regime observed.

The progression of the research on this particular topic greatly depends on the discovery of a single correlation that would accurately predict the transition boundaries between all flow regimes.

The present research will generate data for mini- and micro-channels by providing information on flow regimes observed in channels with diameters in both the mini- and micro-ranges, more precisely diameters of 3 mm, 1 mm, and 0.8 mm. The data obtained in the present study is presented in the form of flow regime maps. Flow regime maps were drawn for all three diameters studied here, namely 3 mm, 1 mm, and 0.8 mm. The purpose of this study purpose was not aimed at creating a new system for the flow regime maps, thus the coordinate system was similar to that used by the majority of the other researchers. The coordinates of the map are the superficial velocities of the gas and the liquid. Therefore, the comparison with other studies will be facilitated. The frictional pressure drop inside channels with diameters in both the mini- and micro-range will be studied and analyzed. The data collected in this study will become a part of an experimental database for pressure drop and flow regime maps in mini- and micro-channels.

Chapter III

Experimental Investigation

3.1. Overview

Designing and constructing the test facility was the most challenging part of this project. The process included designing and determining the necessary devices, searching for the available products and manufacturers, as well as ordering them from the manufacturers. It is important to note that the test rig will not only be used in this experimental investigation, but also in future studies, which will help establish two-phase flow research at Concordia University. Therefore, provided a few alterations are made to the structure of the test rig, other experimental studies could be performed using the same apparatus.

Once the devices had been received, the assembly of the different components of the test rig initiated. This part of the research was very interesting since further knowledge was acquired on the subject of hydraulic, pneumatic and mechanical connections. The long delays in the shipping of various components caused the most problems, thus retarding the commencement of the experimental process. However this delay was beneficial, in that it permitted the completion of the literature survey, as well as the construction of the test matrix for the defined test sections.

The test facility was designed to supply without any leak, the desired flow rates of both air and water into the test sections. It also enabled the measurements of the frictional pressure drop, which occurred through the test section during the test runs. Also, the frame of the test rig was chosen specifically so that the attachment and detachment of any experimental device would be a simple and effortless task, allowing one to make any desired changes to the test facility easily. The body structure of the test rig was built from frames fabricated by MayTec. These frames have two rails on each side, permitting them to be connected to one another by the edges, as well as allowing any other device to be mounted on these rails. Also, the mounted devices will slide easily to any position on the rails by the simply loosening the screws. In addition, mounting elements needed to hang up the devices and the mixer and test section holder frame were built from aluminum and Plexiglas, respectively.

The test rig was assembled in the Concordia University Hall Building H-027-1, where there is a supply of air and water readily available to be connected to the test facility. The test rig has two main supply lines. One provides air while the other provides water. Each line has its own separate pressure regulators, control valves, and flow meters. The two lines merge together in the mixer and leave the mixer from a single line containing the two-phase mixed flow. Afterwards, the two-phase flow enters the test section where the experimental investigation of the frictional pressure drop and flow regime determination is conducted. Finally, the flow discharges into the drain line located after the test section.

3.2. Experimental Test Facility

The goal of the experimental apparatus is to mix the two-phase components, air and water, within the predetermined range of superficial velocities. The purpose is also to observe the flow regimes and measure the pressure drops occurring in the test section. Two of the test sections were circular mini-channels with hydraulic diameters of 3 mm and 1 mm, while the last test section was a circular micro-channel of 800 μm. The volumetric flow rates were the key parameters in determining the superficial velocities of the two-phase components. The superficial velocity of water ranged from 0.02 m/s to 1 m/s, while the local superficial velocity of air ranged from 10 m/s to 100 m/s.

The test facility was designed once the test parameters and the main components of the apparatus were determined. The main components were the flow meters, both for air and water, as well as the differential pressure transducer, which was used to measure the pressure drop across the test sections. The auxiliary components were the pressure regulators, pressure gauges, and the needle valves. A schematic of the test rig is shown in Figure 3.1, followed by Table 3.1, which contains the description of all devices.

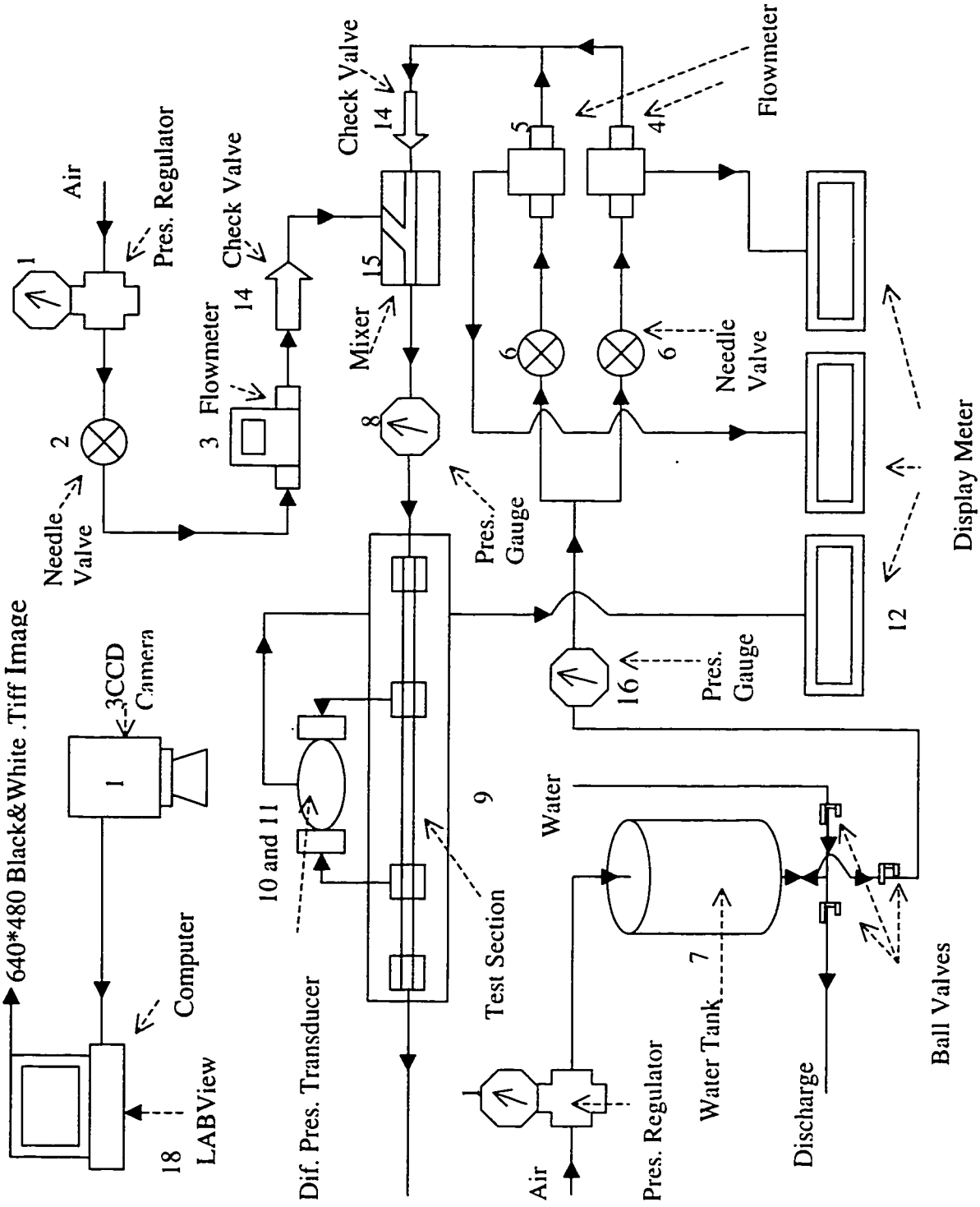

Figure 3.1. Schematic of the designed Test Facility.

Table 3.1. Major Components of the Experimental Test Facility.

NO	DESCRIPTION	MANUFACTURER	PART NO	RANGE
1	Pressure Regulator	Parker	06E12A13A*SB	0-160 psi
2	Needle Valve	Parker		
3	Air Flow Meter	Omega	FMA-1609	0-50 slpm
4	Water Flow Meter	Omega	FPR-1503	50-500 cc/min
5	Water Flow Meter	Omega	FPR-1501	13-100 cc/min
6	Needle Valve	Parker	N200S/N400S	
7	Precharged Water Tank	Teel	4P833A	
8	Pressure Gauge	Omega	PGS-25L-160	0-160 psi
9	Test Section	Wilmad Glass	On request	
10	Differential Pressure Transducer	Omega	PX821-005DV	0-5 psi
11	Differential Pressure Transducer	Omega	PX821-075DV	0-75 psi
12	Display Meter	Omega	DP-41S	
13	Display Meter	Omega	DPF-64	
14	Control Valve	Parker		
15	Mixer	Home-made		
16	Pressure Gauge	Omega		0-100 psi
17	3CCD Camera	Sony	DXC-9000	
18	Computer	Dell		

3.2.1 Test Sections

The test sections are circular mini- and micro-channels with diameters of 3 mm, 1 mm, and 800 μm. The test tubes are made of borosilicate glass tubing, and have a length of 450 mm each. The test section begins at 150 mm and ends at 350 mm of the test tubes. A tolerance of 150 mm at both ends was applied to ensure that the investigated flow was completely steady, turbulence free and free from non-homogenous effects, which are all induced by the restriction area of the flow. This restriction appeared as a result of the change in diameter from the transfer tubes to the test tube. The advantage of this procedure was the possibility to neglect all the minor pressure losses, and thus concentrate only on the frictional pressure drop. The borosilicate tubes were supplied by Wilmad Glass USA, which manufactured tubes with diameters almost exactly equal to their nominal values. The nominal values are 3 mm, 1 mm, and 800 μm, and the exact values are 2.999 ± 0.005mm ID, 0.9906 ± 0.005 mm ID, and 0.7996 ± 0.005 mm ID.

The homemade brackets for the test section were designed and manufactured to secure the test section safely, and allowed easy removal and replacement of the test section. As shown in Figure 3.3., two of the brackets were positioned at the inlet and outlet of the test tube, while the other two were placed at the inlet and outlet of the test section. These two last brackets also supply the input pressure to the pressure transducers. The inlet pressure was used to calculate the local superficial velocity of the gas, and the inlet-outlet pressure difference was used to measure the frictional pressure drop across the test section.

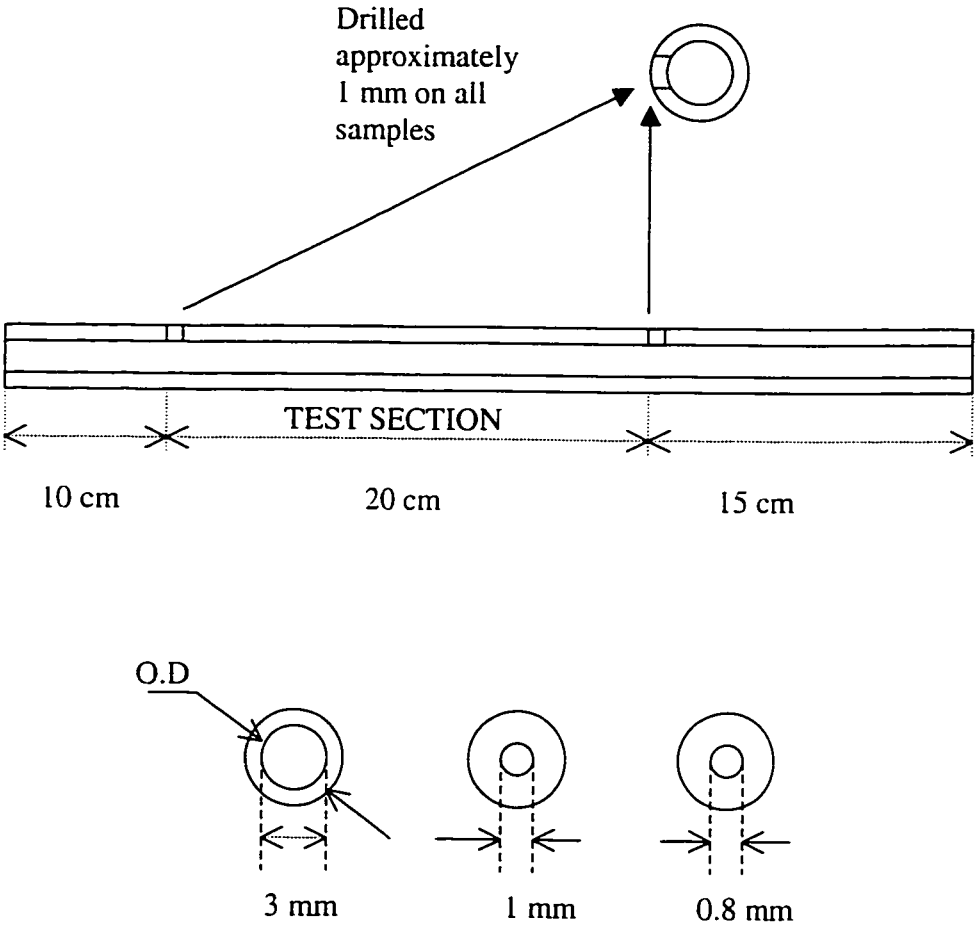

Figure 3.2. Geometry of the Experimental Test Sections.

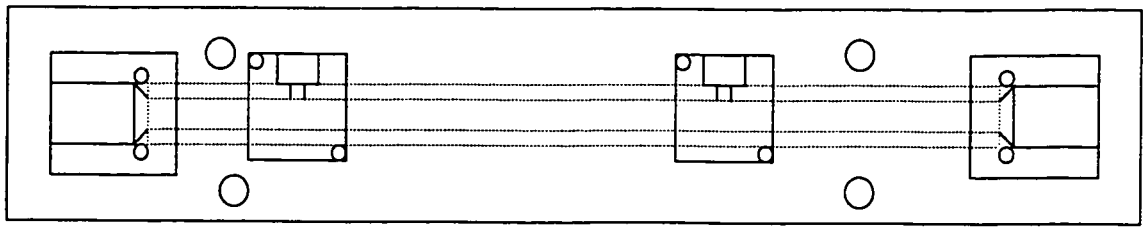

All main connection sizes are ¼" NPT

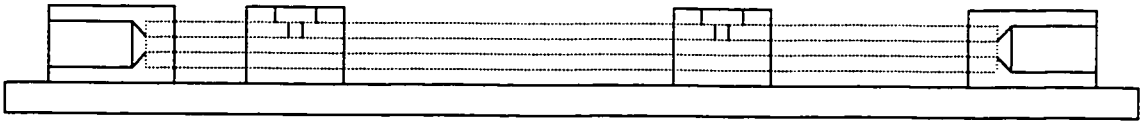

Figure 3.3. Schematic of the Brackets to Hold the Test Sections.

The test section had to be placed carefully through the brackets before it could be mounted onto the test rig. First, the glass tube is gently installed inside the brackets. Then, screws were used to secure the glass tube. Once the installation was complete, sealing between the glass and the metal was applied. At first, wax was used as a sealing material since it is solid at cold or at room temperature, and is liquid when heated to a higher temperature. This versatility in hardness was advantageous and was applied to the joints of the test rig. However, in high-pressure situations, for example greater than 10 psi (68.96 kPa), the wax seal began to fail and water began leaking at the inlet of the test tube, especially for the 1 mm test section. The wax was melted and reapplied numerous times, and while the result was satisfactory for the 3 mm diameter test section, the wax could not properly bond the connections of the 1 mm test section, for which there was a serious leakage. Finally, a bonding mechanism developed, using properly-sized o-rings between the joints and mounting the joints together with screws. The results were satisfactory, annihilating the leaks observed previously for the 1 mm and 800 μm test sections.

3.2.2 Flow Measurements

Air and water were the fluids chosen for the two-phase flow experiments. The test results of the two-phase flow experiments depend on the flow rates of both the air and water, the sources of these fluids, and the mixture quality.

An air and water supply provided the fluids for the experiments. The water supply was a Teel Precharged Water Well Tank Model 4P833A, which was supplied by Auckland's-

Grainger Inc., St Laurent, Canada. It is important that the water supply be pressurized. This tank model has a capacity of 8.5 gallons (32.18 L), with a maximum working temperature of 160 °F (71.11 °C) and a maximum allowable pressure of 100 psi (689.6 kPa).

The tank possessed an internal rubber diaphragm, which was used to contain and store the water. Air surrounding the diaphragm was used to adjust the pressure of the water. The diaphragm was filled with water from the faucet supply in the laboratory. During this period, the relief valve of air was open, which allowed the diaphragm to be filled with water without any resistance. The inlet and outlet of fluid into and leaving the tank were maintained with three ball valves. One of them was used to control and supply the water into the system while the other ball valves were closed. When the second ball valve was open, the other ball valves were closed in order to discharge the water from the tank. When the third one was open, the two first were closed, and pressurized water was supplied to the test rig. The opposite side of the tank is connected to the air supply from the university's source and is equipped with a pressure regulator and a relief valve, which will pressurize the tank and pump the water at any desired pressure within the range of 1 psi (6.9 kPa) to 100 psi (689 kPa). The ball valves as well as the pressure regulator equipped with a filter and a gauge, were supplied by Wainbee Ltd. Canada. The part number for the ball valves is XV500P-4, and the pressure regulator was made by Parker (PN 06E12A13A*SB). Once the pump was filled, all the ball valves, as well as the relief valve were closed, preparing the pump for supplying fluids to the test rig. When this was accomplished, the pressure regulator was adjusted to the desired pressure. This operation

forced the diaphragm to pump the water into the system with an even pressure. The ball valve was finally opened to release flow into the system. Note that while the water was stored in the diaphragm, it is possible that air particles coming from the faucet supply were collected at the top of the rubber. Pumping an air-water mixture into the water line was avoided, since the supply line was in the middle of the diaphragm.

The main compressed air line provided in Concordia University supplied air to the test rig. The inlet pressure of the system was always approximately 105 psi (± 3) (724 kPa). The experiments were mostly performed in the basement of the Hall Building, while the air supply is normally generated on the 9^{th} floor. The contaminant particles, such as oil, water etc., were removed before releasing the air into the test rig through the filter placed on the pressure regulator. Also, since the inlet pressure was only relatively steady at approximately around 105 psi, a pressure regulator was installed to maintain the pressure level of the air. The pressure regulator and the filter were placed at the inlet of the air line. The ball valve was installed immediately before the pressure regulator and was used to initiate and stop air intake from the university's pressurized air supply. This ball valve was acquired from Wainbee Ltd. Canada (PN: 2BVL-2004B). For safety reasons, and in order to measure the inlet pressure, a pressure gauge was placed between the ball valve and the pressure regulator. The pressure gauge was supplied by Omega Canada and has a range of 0 to 160 psi (0-1103 kPa) (PGS-25L-160).

The air supply line is similar in design to the water supply line. The pressurized air supply was controlled by the pressure regulator and purified with the help of the filter.

The regulated and purified air entered the needle valve where the flow rate of air was adjusted before entering the air flow meter. The air then passed through the air flow meter, where the flow rate, the pressure, and the temperature were recorded. Finally, the air was inputted to the mixer where it was mixed with the water.

Today, there are many different kinds of flow meters with different flow ranges available. However, before choosing one, the flow range necessary for this experiment was determined. The determining process began with the expected superficial velocity of water, which is one of the most important parameters for the two-phase flow regime determination. The superficial velocity of water was chosen to range between 0.02 m/s and 10 m/s, while the hydraulic diameters of the test sections were chosen to have a maximum of 3 mm and a minimum of 500 μm. From this information, the flow rate was determined to be within a minimum of 17 cc/min and a maximum of 424 cc/min. Two flow meters of the same kind, but with different ranges, supplied by Omega Canada Inc. (PN: FPR-1501 and FPR-1503), were used. The FPR-1501 liquid sensor was able to measure the volumetric flow rate within a range of 13 cc/min to 100 cc/min, while the FPR-1503 liquid sensor was able to measure the volumetric flow rate of water within a range of 50 cc/min to 500 cc/min. These devices both have a full-scale accuracy of ± 3% and a full-scale repeatability of ± 0.2%. The FPR1500 series use a pelton-type turbine wheel to determine the flow rate of the liquid. The rotation of the wheel is linear over a wide range of flow. The electro-optical signals, which are proportional to the turbine wheel speed, are converted to an analog signal varying from 0 to 5 VDC.

Since the flow meter yields an analog output, it is necessary to use a device that converts these voltage outputs into the appropriate flow rate values. The flow meter instruments chosen to combine with the FPR1500 series flow meters were supplied by Omega Canada, since they were already compatible with the flow meters used (PN: DPF64). The DPF64 digital rate meter is a unit that accepts analog signal inputs and converts them into the 6 digits of bright, 7-segment LED displays. This programmable unit needs to be properly set up in order to combine with the device supplying the analog signals. Some examples of the main steps in the programming procedure are: defining the input signal range, defining the number of decimals desired to be displayed on the screen, defining the input either as linear or square root extraction, etc. Each flow meter was connected to a DPF64 and programmed using the required parameters. These rate meters feature 6 digits of bright, 7 segment LED displays and the unit is an integrating rate meter, which accepts accepting analog signal inputs. Programming is necessary for identifying the unit connected. There are more than a hundred parameters to enter. However, the key parameters are the input characteristics, which are defined as follows: 1- Assignment of the type of input that the unit will be using (0-20mA, 4-20mA, 0- 5 V, 0-10 V, 1-5V, linear, or square root extraction), 2- Set low: the rate value for the lowest input (Etc. 0 V- 0 ml/min), and 3- Set high: the rate value for the highest input (etc. 5 V- 100 ml/min).

Since there were two flow meters, the water supply line was separated into two lines. One entering the FPR1501 and the other entering the FPR1503. Note that because of the connection requirements of the flow meters, the tubing for the FPR1501 was chosen to be $0.125''$ and the tubing for the FPR1503 was chosen to be $0.25''$. The air flow meter was

supplied by Omega Canada (PN: FMA-1609 Mass flow meter), and offered a range flow rate varying between 0 slpm and 50 slpm, as well as a ± 1% of full scale of accuracy. This device utilizes a full graphic display that enabled simultaneous viewing of all operating parameters.

Generating a pressure drop across a unique internal restriction is known as Laminar Flow Element (LFE), and measuring the differential pressure across it determines the volumetric flow rate. The device's principle of operation uses the Poiseuille Equation:

$$Q = \frac{(P_1 - P_2)\,\pi R^4}{8\,\eta L} \tag{3.1}$$

Note that Q is the volumetric flow rate, P_1 and P_2 are the static pressures at inlet and outlet respectively, R is the radius of the restriction, L is the length of the restriction, and η is absolute viscosity of the fluid. Since π, R, and L are constants in the device, the previous equation can be rewritten as:

$$Q = K(\Delta P / \eta) \tag{3.2}$$

where K is a constant determined by the manufacturer as a function of the geometry of the restriction. The working fluid (gas) can be chosen from the menu of the device, which means that η is also known. The device measures the pressure drop across the inlet and the outlet and converts that value into the volumetric flow rate using the

Equation 3.2. The device is able to work with air, argon, methane, carbon monoxide, carbon dioxide, ethane, hydrogen, helium, nitrogen, neon, oxygen, and propane. One of the important features of this device is its ability to give the mass flow rate that corresponds to the volumetric rate corrected to a standard temperature and pressure (101.3 kPa and 25 °C).

To obtain the expected flow rate of the water from the flow meters and to adjust the flow to a desired value, two needle valves were used, which were supplied by Wainbee Lte. Canada and manufactured by Parker. The model part numbers were VLV Needle Valve Parker Colorflow N200S (with a connection size of 0.125" NPT) and VLV Needle Valve Parker Colorflow N400S (with a connection size of 0.25" NPT). The needle valves were placed at a length of fifty times the diameter of the tube, far before the flow meters in order to avoid any disturbance that could be produced in the readings of the flow meters.

The mixer was one of the most important tools needed for the two-phase flow experiments. The purpose of this device was to mix the air and the water in an easy and continuous way, without any back flow. The mixer used in this experiment was made, at the university, from Plexiglas. The water line entered the mixer from the side and the air line entered the mixer with a 45 degree angle, as shown in Figure 3.4 both lines merge into one inside the mixer and the mixture exists from opposite ends, directing the two-phase flow mixture towards the test section.

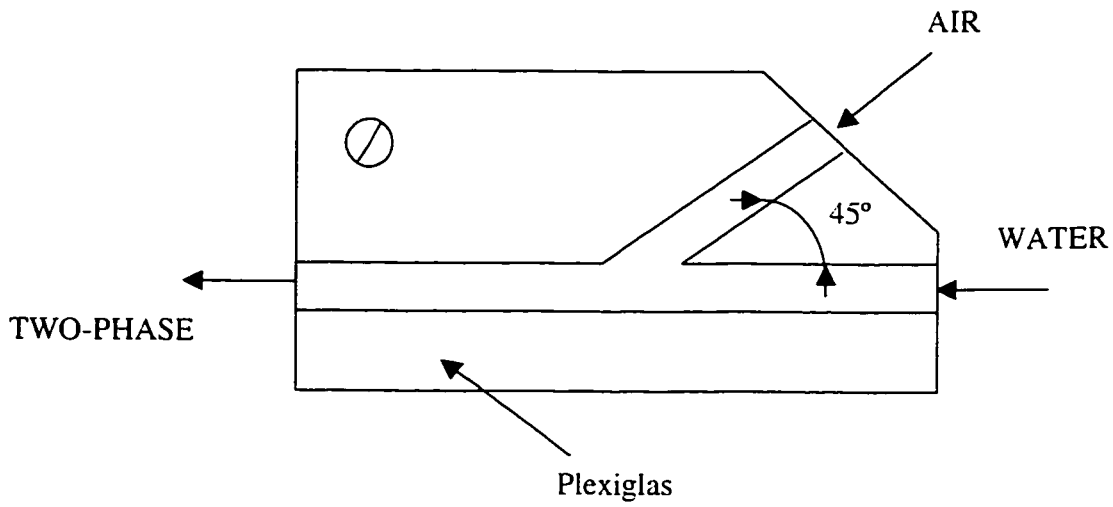

Figure 3.4. Schematic of the Air/Water Mixer.

Non homogeneous effects, turbulence effects, and unsteadiness of the mixture were expected inside the mixer, but these effects were also expected to dissipate after traveling a certain length inside a tube placed at the exit of the mixer. From the literature, it was found that a length of approximately fifty times the diameter would annihilate these effects (Fukano, 1989). At the exit of the mixer, tubing was used to link it to the test section, giving more than the necessary length to negate the unwanted effects. Another problem that was expected a back flow in one of the lines when the two fluids were mixed. This problem might be caused by the high-pressure difference between the phases. It was expected that when the pressure of one line was higher than the pressure of the other one, then the phase at lower pressure will return to the line from which it originated, due to the influence of the fluid higher pressure. Safety issues with the devices must also be considered. Since the fluids enter to the mixer after they have passed through the flow meters, and since these flow meters have only one working direction

stated, an opposite flow could damage the devices, affect the calibration data, cause mechanical problems, and/or shorten the life of the devices. On the other hand, the service manuals, for the devices do not mention any harmful consequences due to an opposite flow occurring for a very short period of time. The two check valves were supplied by Wainbee Ltd. Canada and manufactured by Parker. These check valves were placed between the mixer inlet lines and the flow meters, which allowed the flow to travel in the desired direction, and inhibited any flow in the opposite direction.

3.2.3 Pressure Measurements

The instruments used for the pressure measurements were pressure regulators, used to adjust the inlet pressure of air and water, pressure gauges, used to check the pressure at certain points, and a differential pressure transducer, used to measure the pressure drop through the test section. The air supply of the university provides a steady pressure averaging around 105 psi. The task of regulating the pressure to a steady constant value was performed by a Parker pressure regulator (supplied from Wainbee Ltd. Canada PN:06E12A13A*SB). The model, which was also chosen because it contained a filter placed under the regulator, which was used to purify the air. Such a device had the advantage of accomplishing two functions at once. A pressure gauge was installed on the pressure regulator to manage and regulate the desired pressure level at the outlet. The entire process described above could provide a pressure supply between 0 and 105 psi (0-724 kPa).

A pressure gauge was placed at the entrance of the air supply line to check the pressure of the air supply, as well as to check for fluctuations occurring in the system. It was important to check for fluctuations since there were many parameters that could affect the steady and continuous supply of air to the test rig. Another pressure gauge was placed immediately after the water pump to measure the pressure of the supplied water. Normally the water tank is to pump the water into the system at a pressure equal to the air pressure surrounding the water balloon. However, when the balloon was completely filled with water, no air could surround it, thus the water was pumped at a pressure caused by its inertia. This pressure decreased with time and a small amount of water needed to be removed from the tank in order to allow the surrounding air to control the pumping pressure once again. As long as air surrounded the balloon, the air pressure maintained with the pressure regulator was equal to the water pressure in the system. Another pressure gauge was at the outlet of the mixer in order to measure the pressure of the mixed two-phase flow. The gauges mentioned previously indicated the inlet pressure of the two-phases into the system, while this one indicates the inlet pressure of the mixed flow into the test section. Since the flow entering this pressure gauge contronted many minor losses, it was anticipated that the pressure reading at this point be lower than any other inlet pressure measurement.

The measurement of the pressure drop across the test section was one of the main purposes of this research. The process of choosing the differential pressure transducer was very important and a key parameter in the design of the test rig. Omega PX821 series wet/wet differential pressure transducers were found to be the best differential

pressure transducers for the desired purpose. These series of differential pressure transducers are highly accurate and lightweight, and are manufactured by Hastelloy C276 and 316L stainless steel. They are compatible with a number of liquid and gaseous media. In addition, the welded construction ensured excellent resistance to shock, vibration, and overload. Since the test section diameters were 3 mm, 1 mm, and 800μm, the expected range of the pressure drop was very large for the determined flow rates.

It was found that one of the differential pressure transducers was not satisfactory the for this experiment. Two models of PX821 series transducers were therefore supplied by Omega Canada. One was the PX821-005 DV with a range of 0 to 5 psi, while the other was the PX-821-075DV with a range from 0 to 75 psi. The full-scale accuracy was 0.1% for both devices, which gave a $\pm$ 0.005 psi reading for the PX821-005DV and a $\pm$ 0.075 psi reading for the PX821-075DV. Both devices were installed on the test rig, with the PX821-005 V connected to the test sections where the pressure drop was expected to be less than 5 psi, and the PX821-075 DV connected where the pressure drop was expected to be more than 5 psi. As for the differential pressure transducers, the DP41 series high performance strain gauge indicators were supplied by Omega Canada. The DP41-S strain gauge meter has a programmable front panel to accept unipolar and bipolar DC voltage inputs and 0 mA to 20 mA or 4 mA to 20 mA inputs. The DP41 meter can be used with transmitters, pressure transducers, and potentiometers. The DP41-S has 6 digit LED display, 0.005% accuracy of reading is able to obtain 13 readings per second has 12 DC input ranges and possesses many other attributes. Programming was necessary to use

the menu and input options. The most important inputs were the reading scale, the reading offset, and the number of decimal places to be displayed.

3.3. Experimental Procedure

The test section being used for a particular set of experiments was installed on the test rig. After the installation was completed, a leak test was performed. For the leak test, the outlet of the test section was sealed, the system was pressurized, and the valve at the front of the air flow meter was closed. The pressure was measured from the air flow meter after a waiting period of ten to fifteen minutes. If the pressure of the closed system did not change, then the leak test was successfully completed and the experimental process could commence.

All the valves were closed before beginning the experimental procedure. The water tank was filled with water, and all the valves at the exit of the water tank were closed. The tank was slowly pressurized, and the valve directing the flow to the test rig was opened. At the inlet of the water flow meters, before the control valves, the pressure gauge indicated the pressure of the water, which had to be equal to the pressure of the regulator. After obtaining the desired pressure, a control valve (depending on which flow meter was to be used) was opened slowly, until the desired flow rate was supplied. At this point, the air supply was initiated and the pressure was regulated to the desired pressure. Afterwards, the control valve was opened until the desired flow rate was obtained. Once steady flow was obtained, the data from the air and water flow meters, as well as from the differential pressure transducer, were recorded. The previously mentioned devices, used

to measure the flow rates and pressure drops, all have an output to a computer, based on the board acquisition systems. Usually, it is more convenient to use a computer acquisition system with numerous inputs and where more than one data point must be collected by each device every minute. However, for this research, the readings could only be recorded after all parameters reached steady state, which corresponds to an approximate elapsed time of 5 to 10 minutes. Therefore, only one data point needs to be recorded from each device every 5 to 10 minutes, thus eliminating the need to build an onboard computer acquisition system. Please note that for each run, two pressures were measured, namely, the test section inlet pressure and the pressure drop. The inlet pressure of the test section was used to calculate the local superficial velocities through the test section.

For the flow regime map determination, the same procedure was followed. A 3CCD analog camera was used to capture images from the test section. The camera was set to capture 20 pictures for each run. Due to the relatively high speed of the flow, a stroboscope was used with an adjustable frequency in order to obtain a slow motion image. These images were stored in the computer along with the flow configuration, such as the flow rates, temperature, and the inlet pressure. The system pressure was constantly controlled and supervised in order to avoid any dangerous situations that may arise due to the high pressures used in the system.

3.4. Experimental Uncertainty

In this section, the error analysis of the data collected during this investigation is presented. The percentage of errors associated with the liquid and gas superficial velocities have been calculated.

The liquid superficial velocity is a function of the liquid volume flow rate and the channel diameter. The error function can be determined from:

$$\sigma_{U_{LS}}^2 = \left(\frac{\partial U_{LS}}{\partial Q_L}\right)^2 \sigma_{Q_{LS}}^2 + \left(\frac{\partial U_{LS}}{\partial D}\right)^2 \sigma_D^2 \qquad 3.3$$

The liquid volumetric flow rate was measured by two water flow meters. The error associated with the liquid volume flow rate and the channel diameter is based on the accuracy of the flow meters and the accuracy of the channel diameter, respectively. The relations for the partial derivatives of the superficial liquid velocities can be given by:

$$\frac{\partial U_{LS}}{\partial Q_L} = \frac{4}{\pi D^2} \quad \text{and} \quad \frac{\partial U_{LS}}{\partial D} = \frac{-8Q}{\pi D^3} \qquad 3.4$$

The accuracy of the water flow meters is 3% in full scale, and the accuracy of the test section diameters is ± 0.005 mm. Therefore, using Equations 3.3 and 3.4 along with the accuracy values, the maximum error for the liquid superficial velocities is determined to be no more than 3.3%, in all test sections.

A similar error analysis can be performed for the local gas superficial velocity. The gas superficial velocity is a function of gas volume flow rate, channel diameter, and the test section inlet pressure. The error function for the superficial gas velocity can be written as:

$$\sigma_{U_{GS}}^2 = \left(\frac{\partial U_{GS}}{\partial Q_G}\right)^2 \sigma_{Q_G}^2 + \left(\frac{\partial U_{GS}}{\partial D}\right)^2 \sigma_D^2 + \left(\frac{\partial U_{GS}}{\partial P_1}\right)^2 \sigma_{P_1}^2 \qquad 3.5$$

The accuracy of the air flow meter is 1% in full scale, the accuracy of the test section diameters is ± 0.005 mm, and the accuracy of the differential pressure transducers is 0.1% in full scale. Therefore, using Equation 3.5 along with the accuracy values, the maximum error for the gas superficial velocities is determined to be no more than 4.22%, in all test sections.

Since the pressure drop measurements were taken directly from the differential pressure transducers, the uncertainty of the pressure drop measurements is only a function of pressure drop itself. The differential pressure transducers have both 0.1% accuracy in full scale. The maximum error obtained from the present experimental data is 1.05%, where the minimum error remained as low as 0.29%.

CHAPTER IV

RESULTS & DISCUSSION

4.1. Overview

After the successful completion of the test facility, experiments were performed for both single and two-phase flow. The tests consisted of pressure drop measurements and comparisons, as well as two-phase flow regime determination in all three of the test sections. To perform the single phase flow experiments, the mixer was disabled so that only air or water was supplied to the test section. The single-phase flow experiments were executed to verify that the test facility could be used for other research purposes. It permitted to establish a good relationship between the flow meters and the differential pressure transducers. Their relationship was observed and verified by comparing the results obtained using the known frictional pressure drop correlation:

$$\Delta P = f \frac{L}{D} \frac{\rho U^2}{2} \qquad 4.1$$

where ΔP is the pressure drop, f is the friction factor, D is the diameter of the test tube, U is the velocity of the fluid and ρ is the density. After obtaining satisfactory results from the single-phase experiments, the test facility was verified and the two-phase pressure drop experiments were performed with circular test sections 3 mm, 1 mm, and 800 μm in

diameter. Three widely used pressure drop correlations: the homogenous flow model, the Friedel correlation, and the Chisholm correlation, were used to compare the experimental pressure drop results.

Flow regime experiments were performed once the pressure drop experiments were completed. The flow regime maps were defined with the help of many other experimental studies and transition models. After the determination of the flow regimes for the entire test sections was completed, the experimental regions containing the data acquired during this experiment were compared with some of the experimental flow regime maps defined in other studies using 3 mm and 1 mm test sections. However, the experimental flow regimes found with the 800 μm test section could not be compared since no other experimental results have been obtained for this diameter thus far. These results and comparisons are detailed in sub-sections of this chapter.

The range of the local superficial velocities of the gas and liquid used during the pressure drop experiments varied from 11.8 m/s to 95.5 m/s and 0.222 m/s to 1.174 m/s, respectively for the 3 mm diameter test section, from 21.2 m/s to 106.1 m/s and 0.488 m/s to 1.655 m/s, respectively for the 1 mm diameter test section, as well as from 25.9 m/s to 94.2 m/s and 0.625 m/s to 2.148 m/s, respectively for the 800 μm diameter test section. The range of the local superficial velocities of the gas and liquid used during the flow regime experiments varied from 9.5 m/s to 75.4 m/s, respectively and 0.221 m/s to 1.144 m/s, respectively for the 3 mm diameter test section, from 20.2 m/s to 99.7 m/s, respectively and 0.272 m/s to 3.145 m/s, respectively for the 1 mm diameter test section,

as well as from 27.5 m/s to 98.8 m/s, respectively and 0.621 m/s to 2.234 m/s, respectively for the 800 μm diameter test section.

4.2. Single-Phase Experiments

Single-phase experiments were performed to compare the experimental frictional pressure drop with theoretical pressure drop. Water and air were separately used as working fluids for the single-phase experiments. While only the 3 mm and 1 mm circular borosilicate glass tubes were used for water, plastic tubes of 6.25 mm and 4.318 mm in diameter, as well as 3 mm and 1 mm circular borosilicate glass tubes were used for air. Single-phase experiments were performed with water first in order to verify the readings of the differential pressure transducers. Afterwards, single phase experiments using air were executed to verify the accuracy of the air flow meter.

Fifty-eight different experimental runs, where the Reynolds number varied between 195 and 3138, were performed using the single-phase (water) flow in the 3 mm diameter test section. Seventy different experimental runs, where the Reynolds number varied between 607 and 7157, were performed with the single phase (water) flow in the 1 mm diameter test section. The comparison between the experimental and the theoretical frictional pressure drop of single-phase water are given in Figure 4.1 to 4.4. As shown in these figures, the theoretical pressure drop and friction factor expectations from the experimental input, are in good agreement with the experimental output, as anticipated for the smooth pipes. These experiments helped ensure that the water flow meters, differential pressure transducers, as well as the reading devices of these components were

working properly and accurately. Also, the water flow meters and the differential pressure transducers were calibrated before any experiments were performed (Appendix A). After obtaining satisfactory results with the water experiments, the water line was disabled and the air line was enabled. This step of the research was executed in order to verify the readings of the air flow meter, since its calibration could not been made in house at Concordia University.

The air experiments were performed using 6.35 mm and 4.318 mm diameter pipes, each having a length of 3.6 m, as well as the 3 mm and 1 mm diameter borosilicate glass tubing test sections. Fifteen experiments were executed with the 6.35 mm diameter, where the Reynolds number varied between 529 and 11125. Twenty-three experiments were executed with the 4.318 mm diameter, where the Reynolds number varied between 341 and 9482. In the 3 mm test section, 23 experiments were performed for Reynolds numbers varying from 510 to 21291, while in the 1 mm test section, 11 experiments were performed for Reynolds numbers varying from 2050 to 24615. Results are shown in Figure 4.5 and Figure 4.6 for the 3 mm and 1 mm test sections, respectively.

The experimental frictional pressure drop was found to be in good agreement with the theoretical results, especially for the 6.35 mm, 4.318 mm, and 3 mm test sections. Please note that, for all these experiments, the frictional pressure drop was calculated using the assumption that the velocity of the air was the average local velocity of the air, which had been calculated as a linear average of the inlet and the exit velocities. However, in the 1 mm test section, the experimental pressure drop was slightly higher than the theoretical

frictional pressure drop, especially when higher Reynolds numbers were used. This difference can be explained by the accelerational pressure drop occurring across the test section. When both the frictional and the accelerational effects are present, the accelerational effects can be neglected, when the Reynolds number remains small. However, when the Reynolds number is relatively high, the accelerational pressure drop effect can be related to the frictional pressure drop component, by:

$$\Delta P_f = f \frac{L}{D} \frac{\rho U^2}{2} \tag{4.2}$$

$$\Delta P_a = \frac{\overline{\rho}}{2}\left(U_2^2 - U_1^2\right) \tag{4.3}$$

$$\Delta P = \Delta P_a + \Delta P_f \tag{4.4}$$

Once all experiments using the single-phase flow of air were completed, the satisfactory results indicated that the air flow meter was highly reliable. Therefore, it was concluded that the test facility as a whole, along with its various components is excellent.

4.3. Two-Phase Experiments

Two-phase flow experiments were performed once the completion of the single-phase experiments ensured the accuracy of the test facility. The mixer was installed in the system and connected to the air and water lines. Two-phase frictional pressure drop

measurements and flow regime determination were performed in the 3 mm, 1 mm, and 800 μm diameter test sections.

Seventy pressure drop measurements were carried out with the 3 mm diameter test section, while thirty pressure drop measurements were carried out with the 1 mm and 800 μm diameter test sections. Ninety-seven different run configuration images were captured for the 3 mm diameter test section, fifty different run configuration images were captured for the 1 mm diameter test section, while thirty different images were captured for the 800 μm test section. These images formed the basis for the flow regime determination process.

4.3.1. Two-Phase Pressure Drop Experiments

The experimental pressure drop measurements were compared with three of the most widely used pressure drop models, namely, the homogenous model, the Friedel (1979) model, as well as the Chisholm (1967) model. Experimental data obtained by Ekberg (1997) for 1 mm diameter circular and semi-triangular channels were also compared with the present 1 mm diameter data.

The homogenous model is one of the simplest models defined for two-phase pressure drop calculations. The homogeneous model considers the two phases as a single phase, and assumes that the two phases from a well-mixed mixture. The model works on the basis that both the vapor and the liquid have the same velocity, that a thermodynamic equilibrium exists between the phases, and that the friction factor of the mixture can be

treated as a single-phase friction factor for the two-phase flow. However, in multiphase flow, the phases are not exactly in thermodynamic and mechanical equilibrium. The homogeneous model is moderately acceptable as an initial estimator over a wide range of data comparisons (Corradini, 2002). The homogenous flow model describes the frictional pressure drop inside a test section in which the quality is constant:

$$\Delta P_f = f_{TP} \frac{L}{D} \frac{\rho_{TP} U^2}{2} \tag{4.5}$$

where f_{TP} and ρ_{TP} are given by:

$$f_{TP} = 64 / \mathrm{Re}_{TP} \text{ (Laminar)} \tag{4.6}$$

$$f_{TP} = 0.3164\, \mathrm{Re}_{TP}^{-0.25} \text{ (Turbulent)} \tag{4.7}$$

$$\mathrm{Re}_{TP} = \frac{\rho_{TP} U D}{\mu_{TP}} \tag{4.8}$$

$$\rho_{TP} = \left(\frac{x}{\rho_G} + \left(\frac{1-x}{\rho_L} \right) \right)^{-1} \tag{4.9}$$

$$\mu_{TP} = \left(\frac{x}{\mu_G} + \left(\frac{1-x}{\mu_L} \right) \right)^{-1} \tag{4.10}$$

Friedel's (1979) correlation is empirically derived from a vast pool of experimental data, covering very wide parameter ranges. The Friedel (1979) correlation should be used for $\mu_l / \mu_g << 1000$ (Corradini, 2002). The frictional pressure drop for two-phase flow can be written using the two-phase flow multiplier:

$$\left(-\frac{dp}{dz}\right)_{f.TP} = \Phi_{LO}^2 \left(-\frac{dp}{dz}\right)_{f.LO} \tag{4.11}$$

where

$$\left(-\frac{dp}{dz}\right)_{f.LO} = \frac{2f_{LO}}{D}\frac{G^2}{2\rho_L} \tag{4.12}$$

For horizontal and vertical upward flow configurations, Friedel (1979) suggested the following:

$$\Phi_{LO}^2 = A + 3.21x^{0.78}(1-x)^{0.234}\left(\frac{\rho_L}{\rho_G}\right)^{0.91}\left(\frac{\mu_G}{\mu_L}\right)^{0.19}\left(1-\frac{\mu_G}{\mu_L}\right)^{0.7} Fr^{-0.0454} We_{TP}^{-0.035} \tag{4.13}$$

where

$$A = (1-x)^2 + x^2\rho_L f_{GO}(\rho_G f_{LO})^{-1} \tag{4.14}$$

$$Fr = \frac{G}{gD\rho_{TP}^2} \tag{4.15}$$

$$We_{TP} = \frac{G^2 D}{\rho_{TP}\sigma} \qquad 4.16$$

Chisholm's (1967) correlation can be expressed as:

$$\Phi_L^2 = 1 + (\frac{C}{X}) + (\frac{1}{X})^2 \qquad 4.17$$

where

$$\left(-\frac{dp}{dz}\right)_{f.TP} = \Phi_L^2 \left(-\frac{dP}{dz}\right)_{f.L} \qquad 4.18$$

The $\left(-\frac{dp}{dz}\right)_{f.L}$ represents the single phase frictional drop in pure liquid, where a mass flux of G (1-x) flows in the channel and X represents the Martinelli factor, where C may have values in a range of 5 to 20. As an example C = 20 for turbulent-turbulent, C = 12 for laminar-turbulent (Re_L and Re_G), C = 10 for turbulent-laminar, while C = 5 for laminar-laminar. In these cases, the Reynolds number were calculated as:

$$Re_L = \frac{G(1-x)D}{\mu_L} \qquad 4.19$$

$$Re_G = \frac{G(x)D}{\mu_G} \qquad 4.20$$

$$Re_{GO} = \frac{GD}{\mu_G} \tag{4.21}$$

$$Re_{LO} = \frac{GD}{\mu_L} \tag{4.22}$$

However, Corradini (2002) suggested that the Chisholm (1967) correlations should be mostly used for $\mu_L / \mu_G > 1000$ and $G > 100$ kg/m^{2}s.

Two-phase frictional pressure drop measurements were first performed in the 3 mm diameter test section. Seventy different configurations were used in these experiments. The experimental results were compared with three pressure drop models, as shown in Figures 4.7 to 4.9. The average error observed between the experimental data and the homogenous model was 1.2% with a standard deviation of 21%. The homogenous model was found to be the best model to predict the experimental results in the 3 mm diameter test section. Two-phase frictional pressure drop measurements were then performed in the 1 mm diameter test section with thirty different configurations. The experimental results are shown in Figures 4.10 to 4.12. In addition, experimental data obtained by Ekberg (1997) for 1 mm diameter circular and semi-triangular channels were also compared with the present 1 mm diameter data. The average error observed between the experimental data and the homogenous model was 15.6% with a standard deviation of 26.8%. The homogenous model was found to be the best model to predict the experimental results in the 1 mm diameter test section.

Similarly, the two-phase frictional pressure drop measurements were performed in the 800 μm diameter test section. Thirty different configurations were used in these experiments. The experimental results were compared with three pressure drop models in Figures 4.13 to 4.15. The average error observed between the experimental data and the homogenous model was 24.1% with a standard deviation of 39%. The homogenous model was also found to be the best model to predict the experimental results in the 800 μm diameter test section.

4.3.2. Flow Regimes Determination

Flow regime experiments were performed with a 3CCD analog camera, which was added to the test facility. Ninety-seven different run configuration images were captured for the 3 mm diameter test section, fifty different run configuration images were captured for the 1 mm diameter test section, while thirty different images were captured for the 800 μm test section. The experiments were performed using the same procedure used to perform the pressure drop measurements. The camera was installed a certain distance (approximately 1.6 m) from the test section, and the lens was adjusted to focus on the test section. The lightning was adjusted to obtain the best possible flow visualization. The stroboscope was also used so that slow motion pictures could be captured.

The flow regimes were observed for high gas local superficial velocities ($U_{GS} \geq 10$ m/s). For each velocity, twenty images were taken and analyzed. There were two transition regions and three flow regimes observed in the 3 mm test section, namely, pseudo-slug, annular, and dispersed. One transition region, as well as two flow regimes, namely,

annular and dispersed, was observed in the 1 mm and the 800 μm test sections. Pseudo-slug regime occurred as a transition regime from slug to annular flow, where the slug particles inside the flow intended to transfer to a gas bulk similar to the annular flow. Since the superficial gas velocity was not high enough to produce annular flow, only a pseudo-slug regime was observed. Please, note that the pseudo-slug phase was only observed in the 3 mm diameter test section, for a chosen test matrix. The dispersed flow region was observed in the three test sections. This was caused by an increase in liquid velocity, which caused turbulence in the thin liquid film layer, and consequently created instability in the gas bulk.

Images of the 3 mm test section were captured when the local superficial gas velocity varied between 9.5 m/s and 75.3 m/s, and when the superficial liquid velocity varied between 0.151 m/s and 1.144 m/s. The observed flow regime maps are presented in Figure 4.16 and Figure 4.17, respectively. The presented experimental flow regime map for the 3 mm diameter circular test section was compared with the experimental flow regime map obtained by Damianides (1987). In was found that the flow regime transitions for the specified area studied in the course of this experiment was in fairly good agreement with the results of Damianides (1987). However, the transition from pseudo-slug to annular flow occurred at higher superficial gas velocities, while the transition from annular to dispersed flow was observed at higher liquid superficial velocities.

Figures 4.18 to 4.20 present the flow regimes observed in the 1 mm test section, taken while the local superficial gas velocity varied between 20.2 m/s and 99.7 m/s, and the superficial liquid velocity varied between 0.272 m/s and 3.820 m/s. The results of the flow regimes were compared with the experimental flow regime map of Damianides (1987), Fukano (1993), and Ekberg (1997). It was found that the flow regime transitions for the specified area studied in the course of this experiment was in fairly good agreement with the results obtained by both Damianides (1987) and Ekberg (1997). However, the transition from annular to dispersed flow was observed at higher superficial liquid velocities in this experiment. Even though the test matrix for the present data coincides with Fukano's (1993) for small areas, Fukano did not observe any dispersed flow. Note also that in Ekberg's (1997) study, the definition of the dispersed flow is the same as that for churn flow. Please, note that the definition of churn flow is mostly used for vertical up flow in two-phase studies. However, the characteristics of the churn flow and dispersed flow are not very different.

Images of the 800 μm test section were captured when the local superficial gas velocity varied between 27.5 m/s and 98.8 m/s, and when the superficial liquid velocity varied between 0.582 m/s and 2.234 m/s. For each case, twenty images were captured and analyzed. The test matrix and the flow regime map are presented on Table 4.10 and Figure 4.22, respectively.

The flow regime map obtained for the 800 μm diameter test section could not be compared with any previous experimental data, since no experimental work using this

diameter could be found in the known literature. Therefore, a comparison was made between the 3 mm, 1 mm, and 800 μm diameter test sections. The transition from annular to dispersed flow was observed at higher superficial liquid velocities for the 3 mm diameter test section. However, the transition region was observed at almost the same superficial liquid velocities for the 1 mm and the 800 μm diameter test sections.

4.3.3. Discussion on Pressure Drop and Flow Regimes

In summary, the two-phase pressure drop experiments were performed for 3 mm, 1 mm and 800 μm diameter circular test sections, using air and water as the working fluids. The pressure drop measurements were performed over a length of 200 mm. Since the inlet of the test sections were placed at a distance of 250 mm from the actual inlet of the flow in the tubing, the measured pressure drops were considered to consist only of the frictional pressure drop component. Also, it was assumed that, because of the design of the test sections, the accelerational pressure drop and the minor losses were negligible compared to the frictional pressure drop. The measured experimental pressure drops were compared with the theoretical models mentioned earlier, namely, the homogenous, the Friedel (1979), and the Chisholm (1967) model. In addition, experimental data obtained by Ekberg (1997) for 1 mm diameter circular and semi-triangular channels were also compared with the present 1 mm diameter data. The homogenous model showed the most similarities with the data acquired during the course of this experiment, with an average error of 1.2%, 15.6% and 24.1% for the 3 mm, 1 mm, and 800 μm test sections, respectively. However, it was also observed that the standard deviation of the errors increased as the channel diameter decreased. The Friedel (1979) model over-predicted

the pressure drop for every test section, while the Chisholm (1967) model mostly under-predicted the pressure drop data. Ekberg (1997) observed that when compared to the homogeneous model and the Friedel (1979) model, the homogenous model was superior in predicting his experimental results for 1 mm and 1.5 mm hydraulic diameter test sections.

When possible, the flow regimes were observed and compared with existing experimental data. Three different kind of flow regimes (pseudoslug flow, annular flow, and dispersed flow) were observed for the 3 mm diameter test section, and two different kind of flow regimes (annular flow and dispersed flow) were observed for the 1 mm and 800 μm diameter test sections. Some sample images are presented in Figure 4.23, Figure 4.24, and Figure 4.25 for the 3 mm diameter test section. However, due to the small size of the channel diameters of 1 mm and 800 μm test sections, the images captured were very small in sizes. These flow regimes were determined by using the photo editing software on the computer, but since the quality deteriorated each step of zooming, and subsequently after printing the images for the 1 mm and 800 μm cases are not presented.

Pseudoslug flow was observed in the 3 mm diameter test section. This flow regime is a transition from slug flow to annular flow. Slug particles in the two-phase flow begin to merge together as the superficial gas velocity increases. Therefore, the flow is no longer slug flow, where the slug particles travel separately. Instead, the slug particles have merged together. Also, the superficial gas velocity is not high enough to attain annular flow (Figure 4.23).

Annular flow was observed in all test sections. Annular flow always occurred at high gas superficial velocities. The gas phase passes through the liquid phase, where the liquid phase exists as a very thin film layer surrounding the gas phase (Figure 4.24).

Dispersed flow was also observed in all test sections. This flow regime was observed at high superficial gas and liquid velocities. In dispersed flow, increasing superficial liquid velocity causes turbulence in the thin liquid film layer, which consequently generates instability in the gas bulk, and begins separating the gas bulk into different gas particles, such as slugs, bubbles, and partial bulks (Figure 4.24).

The flow regime map comparisons made with the present and existing experimental data are in fairly good agreement. However, one should keep in mind that the flow regime definitions and maps, whether experimental or theoretical, vary greatly among the studies in the field of two-phase flow. The differences are mostly due to either different techniques or the complex nature of the gas-liquid interface. Also, because of the high velocities that are associated with the annular and the dispersed flow, the visual observation enabling the flow regime determination becomes very difficult.

Different flow regime determination techniques were used in the above mentioned researches, a pressure trace method was used by Damianides (1987) for small channels, a high-speed digital camera was used by Ekberg (1997) for the visualization of images, and a 3CCD analog camera was used for the visualization of images in the present study. The

different techniques, as well as the human effects present in the observation and interpretation of the images, could cause the discrepancies mentioned above.

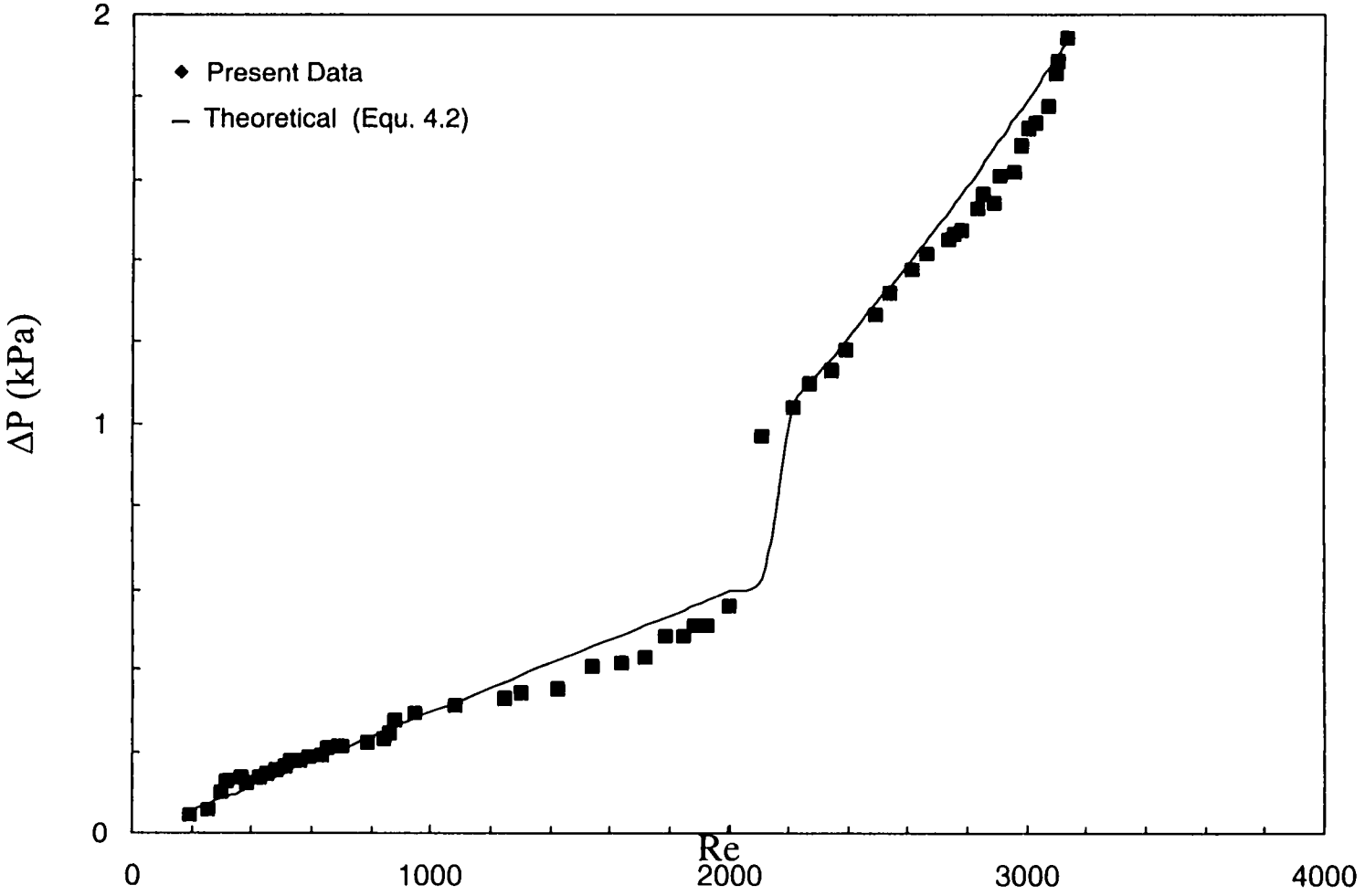

Figure 4.1. Measured and Predicted Pressure Drops for Single-Phase (water) Flow of 3 mm Diameter Test Section.

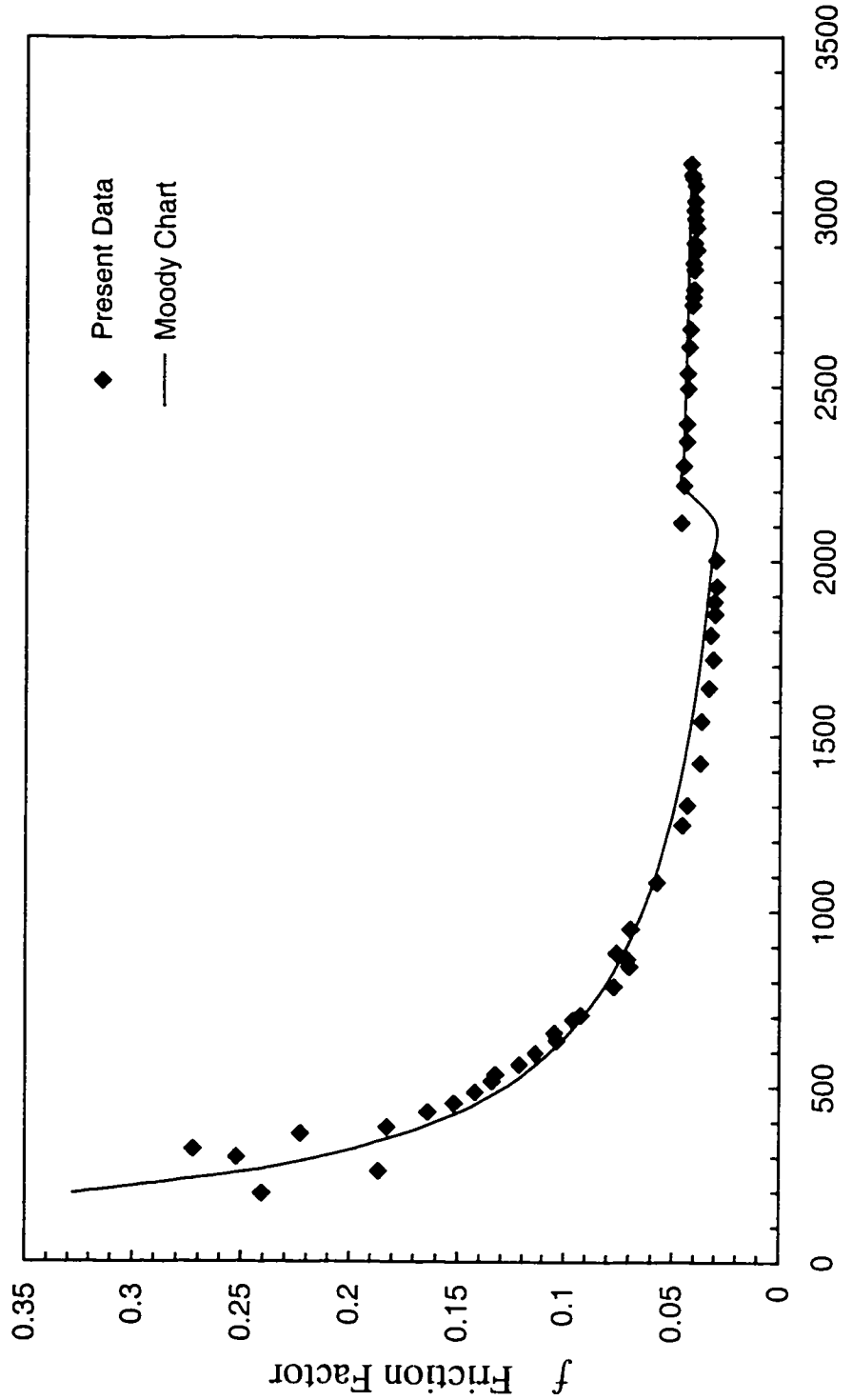

Figure 4.2. Measured and Predicted Friction Factors for Single-Phase (water) Flow of 3 mm Diameter Test Section.

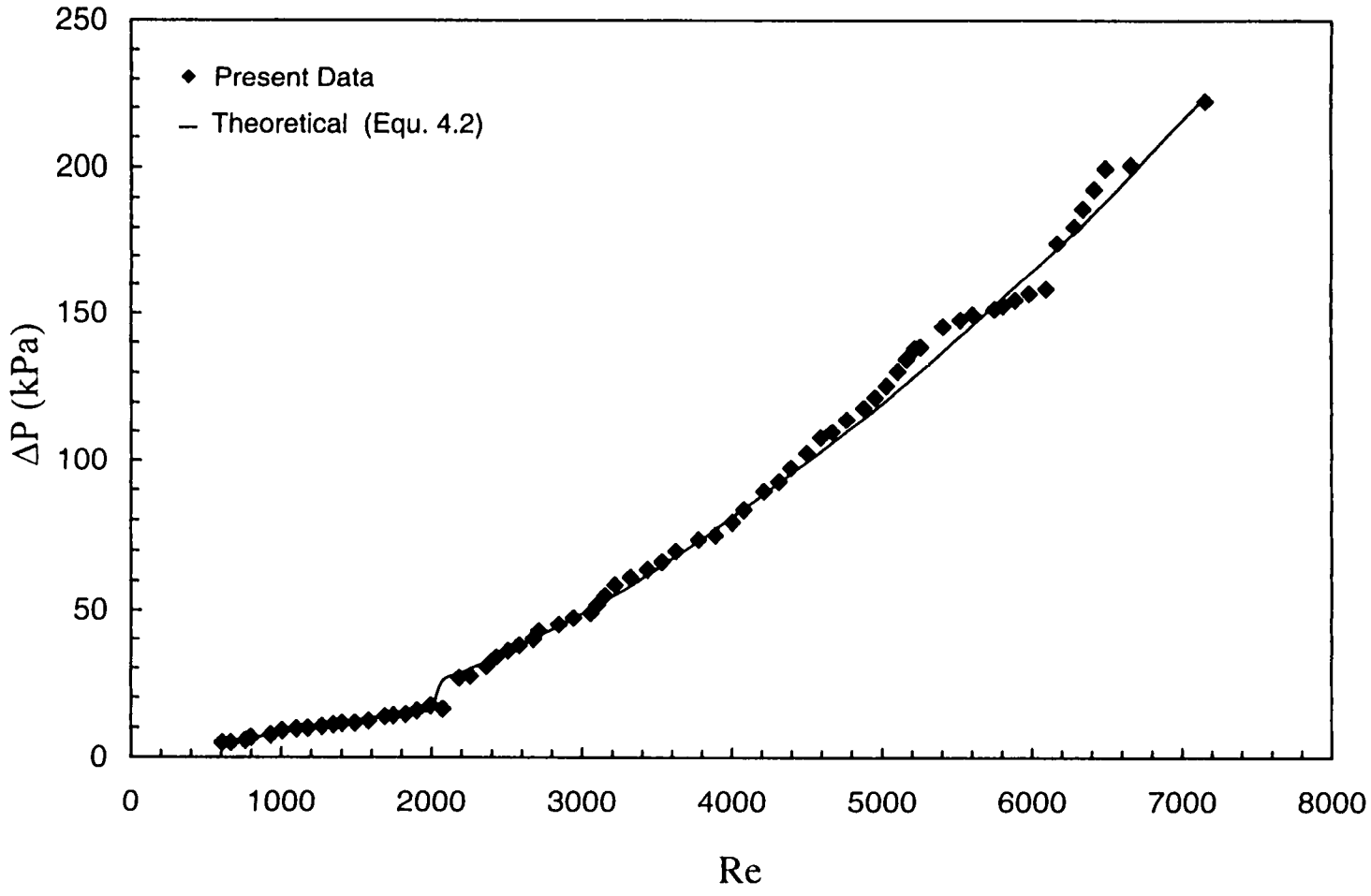

Figure 4.3. Measured and Predicted Pressure Drops for Single-Phase (water) Flow of 1 mm Diameter Test Section.

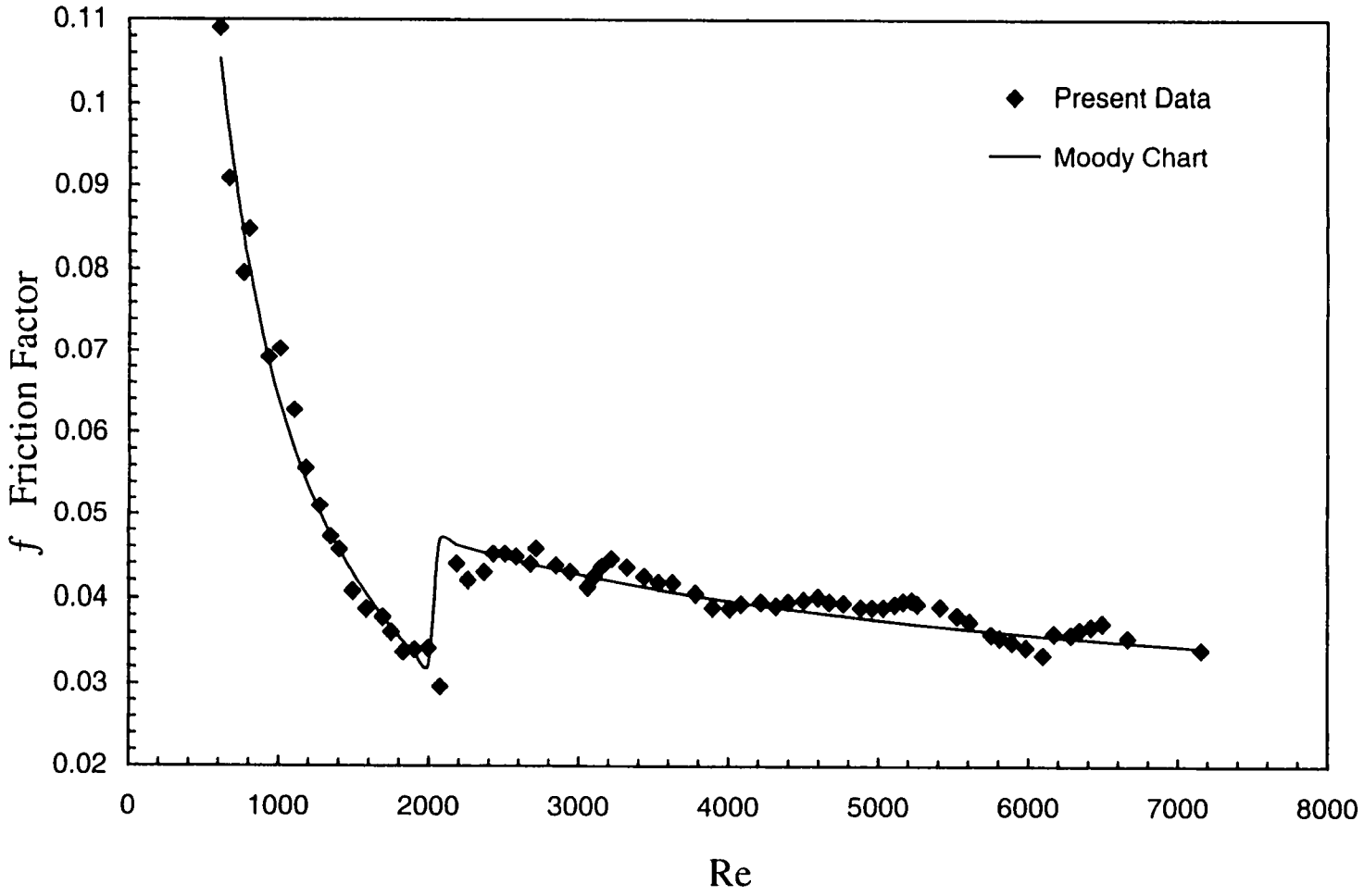

Figure 4.4. Measured and Predicted Friction Factors for Single-Phase (water) Flow of 1 mm Diameter Test Section.

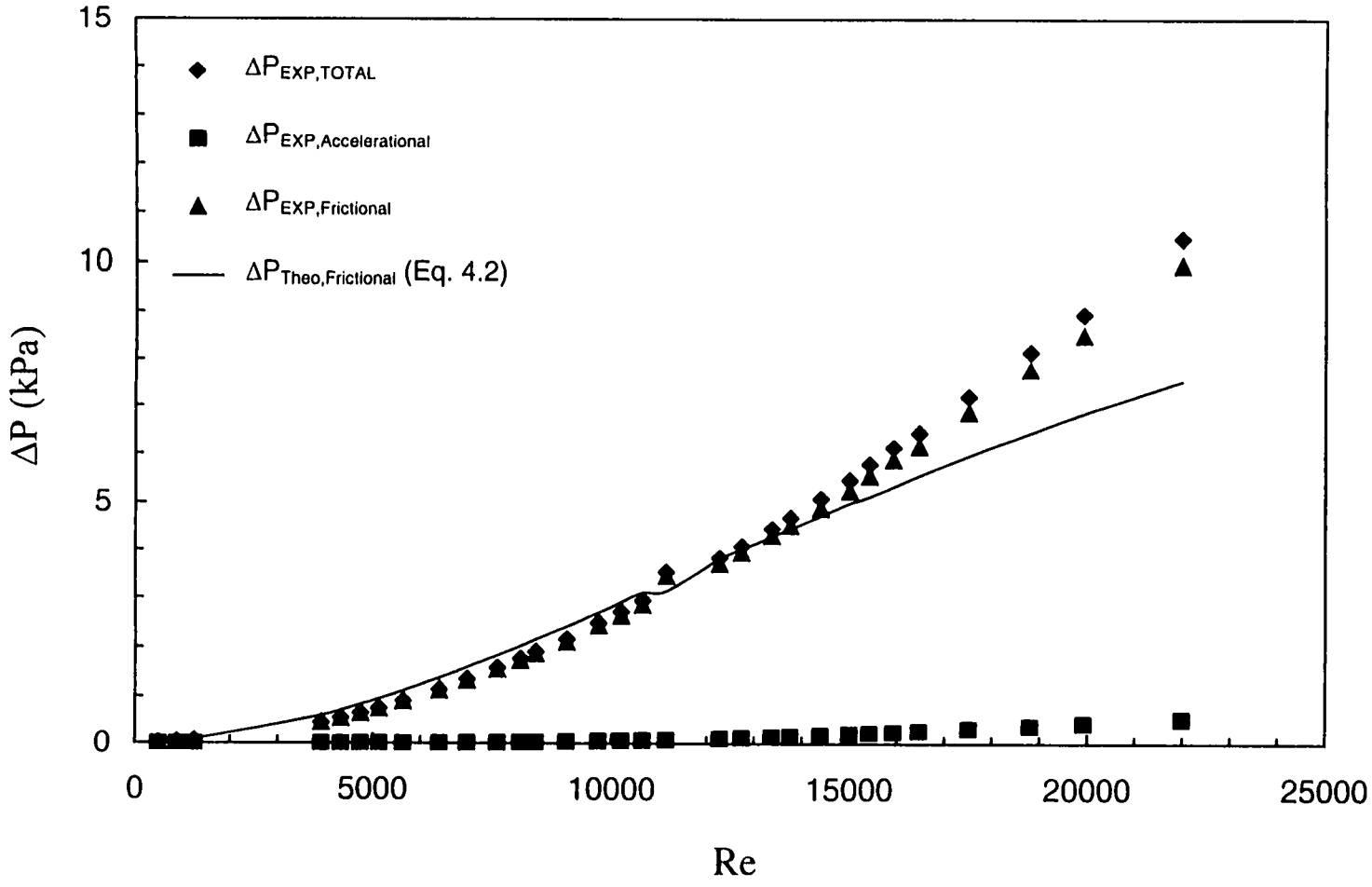

Figure 4.5. Measured and Predicted Pressure Drops for Single-Phase (air) Flow of 3 mm Diameter Test Section.

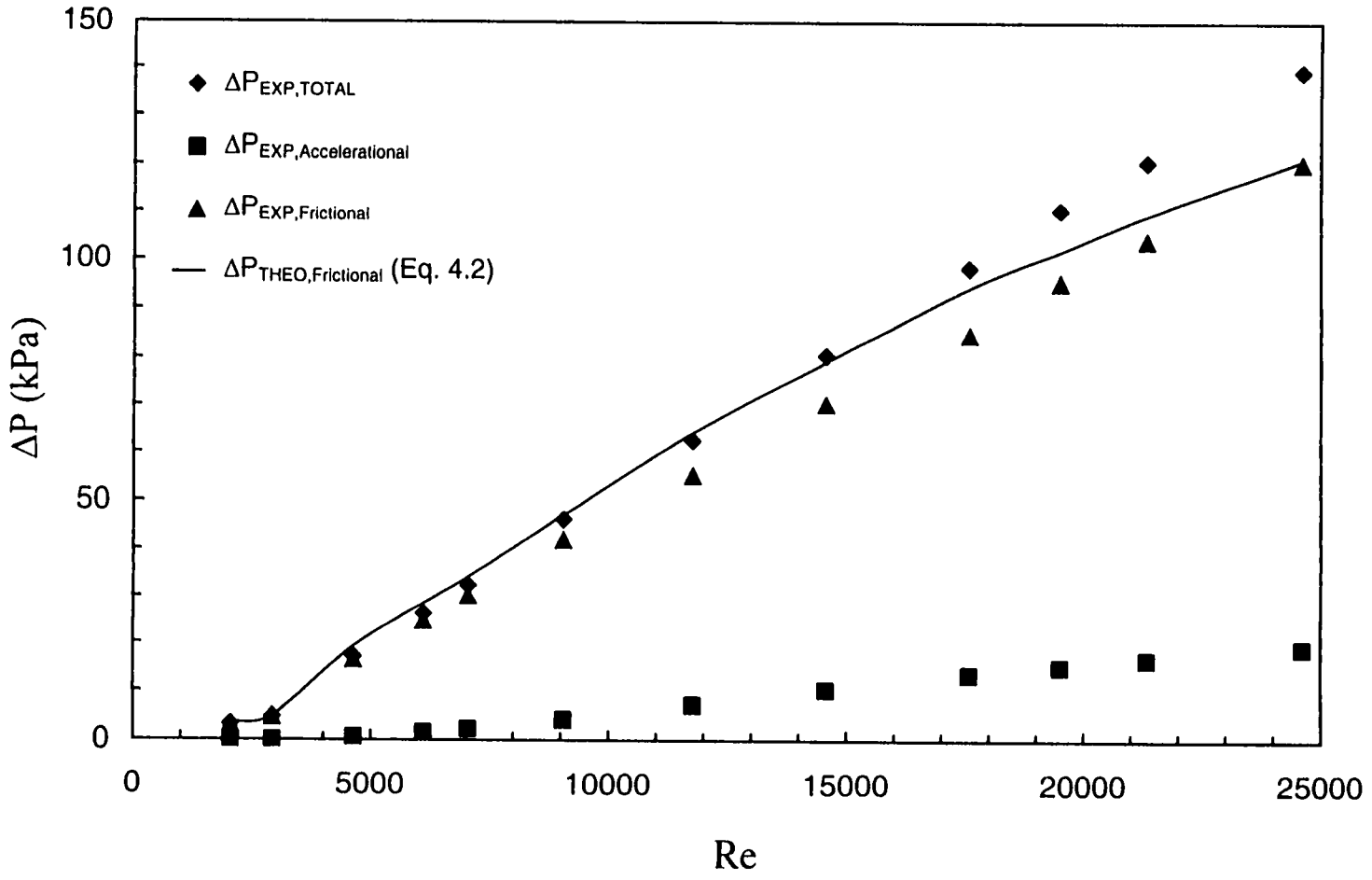

Figure 4.6. Measured and Predicted Pressure Drops for Single-Phase (air) Flow of 1 mm Diameter Test Section.

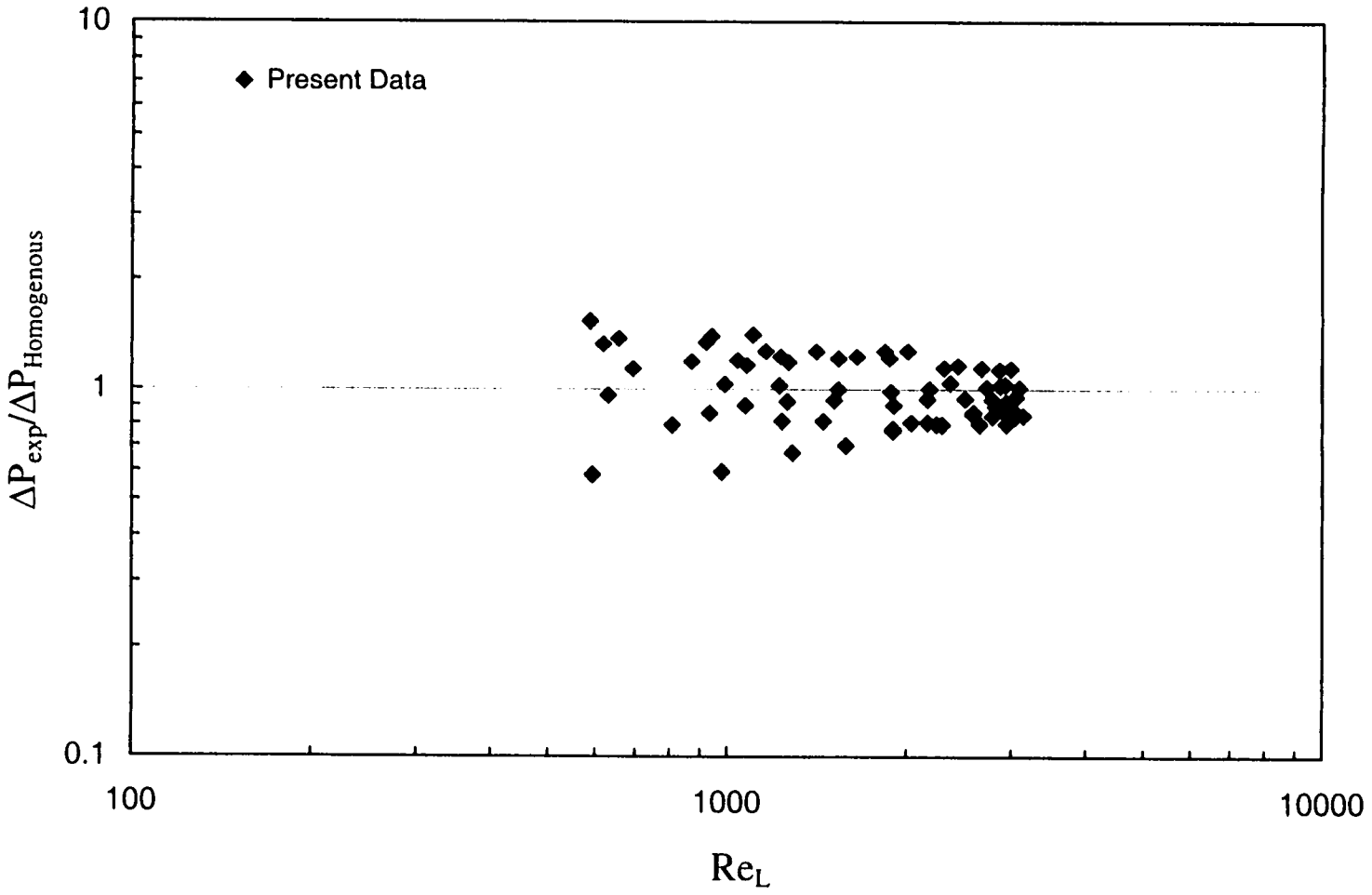

Figure 4.7. Experimentally Measured Pressure Drops Normalized with Predicted Pressure Drops (using Homogenous Model) for 3 mm diameter Test Section.

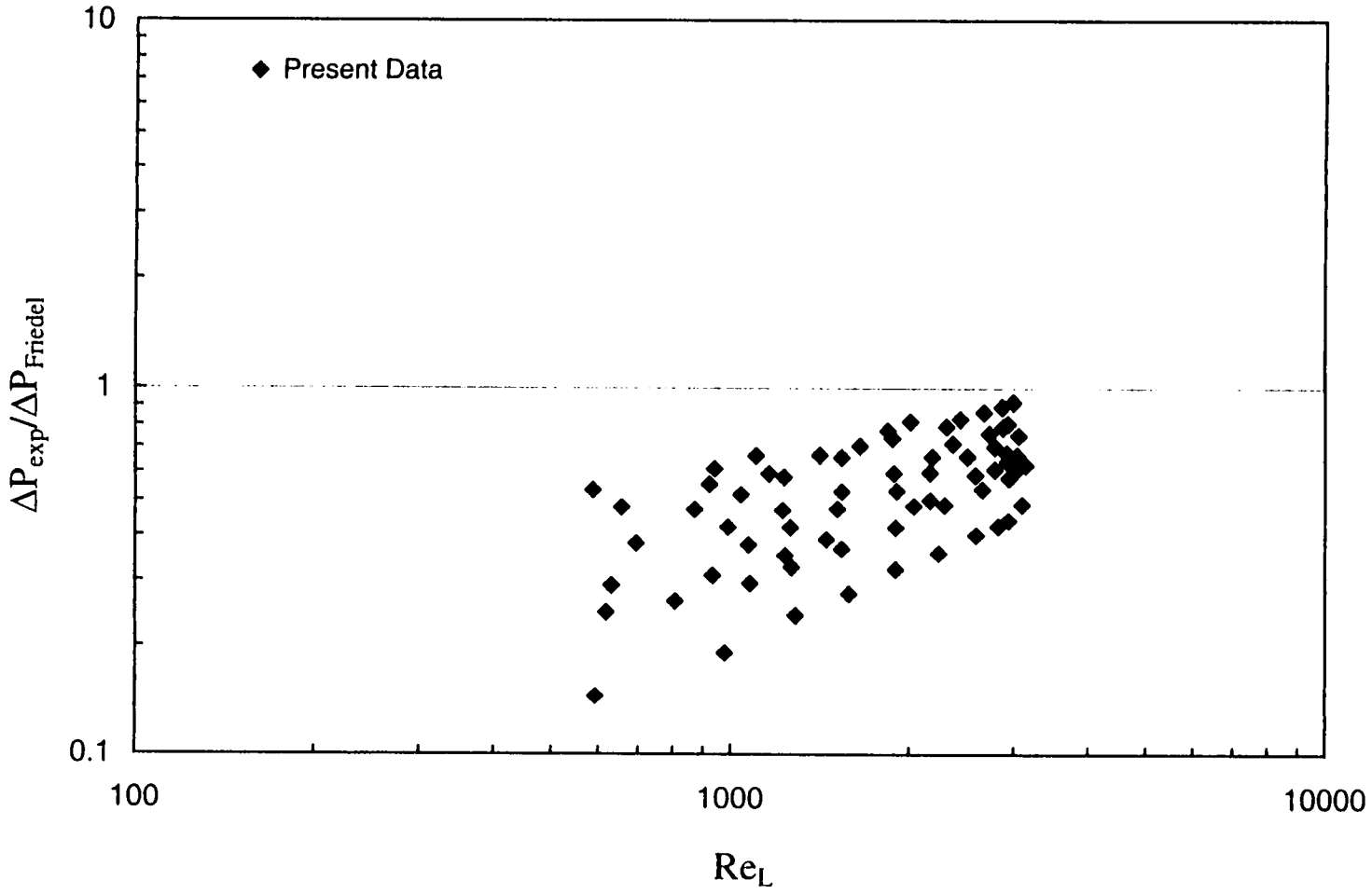

Figure 4.8. Experimentally Measured Pressure Drops Normalized with Predicted Pressure Drops (using Friedel Model) for 3 mm diameter Test Section.

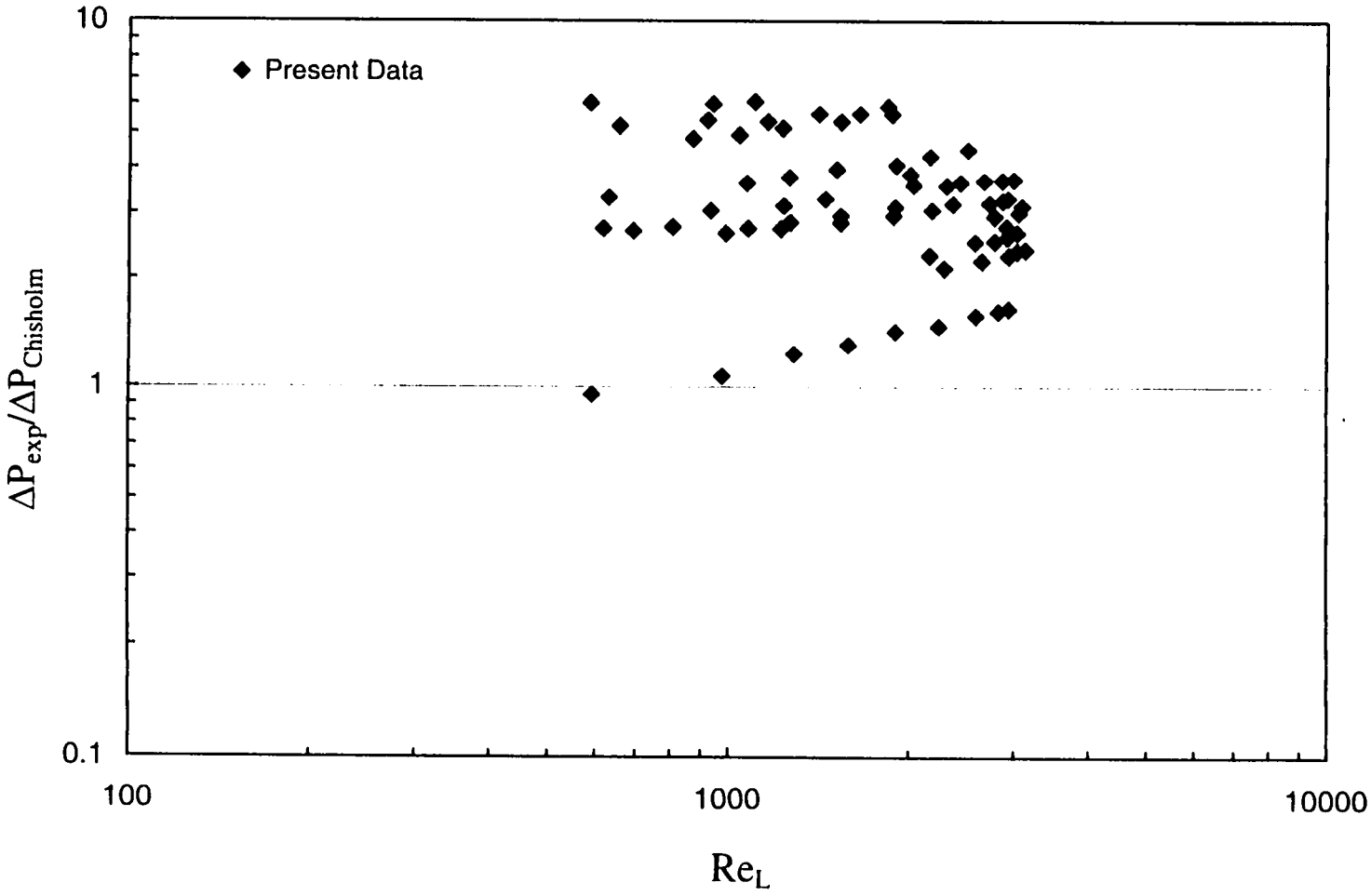

Figure 4.9. Experimentally Measured Pressure Drops Normalized with Predicted Pressure Drops (using Chisholm Model) for 3 mm Diameter Test Section.

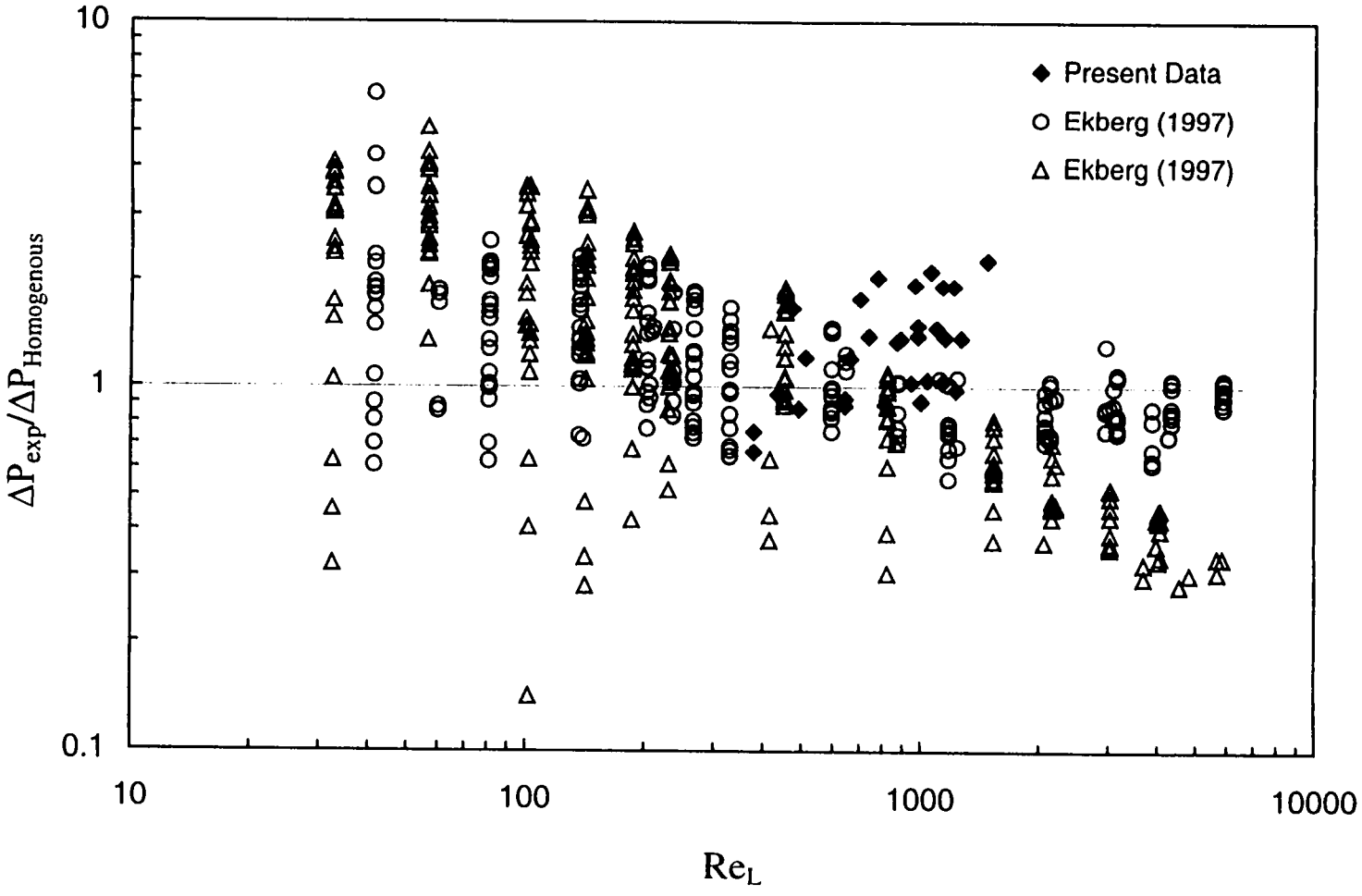

Figure 4.10. Experimentally Measured Pressure Drops and the Experimental Data of Ekberg (1997) [for 1 mm Circular (○) and 1 mm Hydraulic Diameter Semi-Triangular (△) Test Sections] Normalized with Predicted Pressure Drops (using Homogenous Model) for 1 mm Diameter Test Section.

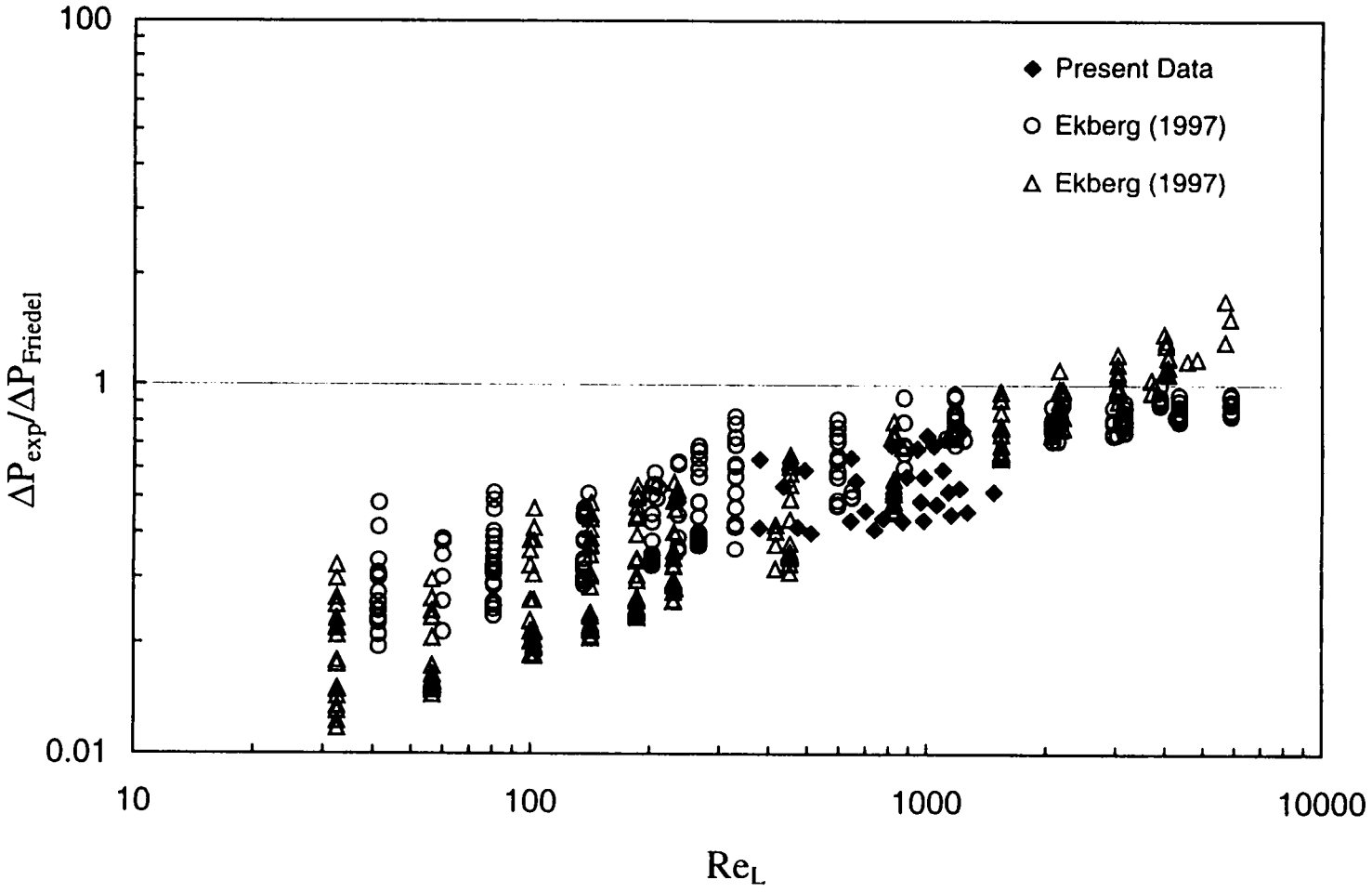

Figure 4.11. Experimentally Measured Pressure Drops and the Experimental Data of Ekberg (1997) [for 1 mm Circular (○) and 1 mm Hydraulic Diameter Semi-Triangular (△) Test Sections] Normalized with Predicted Pressure Drops (using Friedel Model) for 1 mm Diameter Test Section.

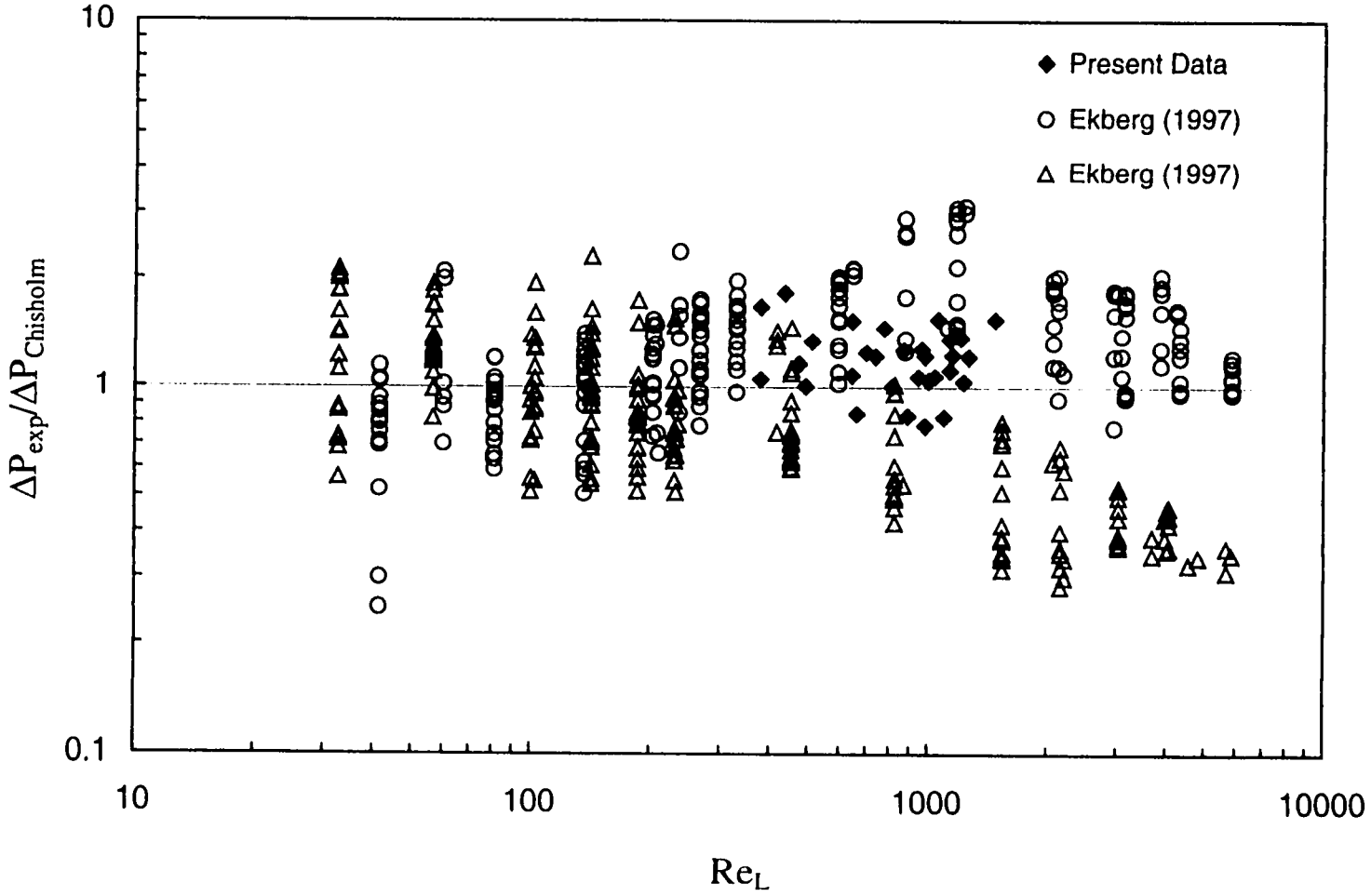

Figure 4.12. Experimentally Measured Pressure Drops and the Experimental Data of Ekberg (1997) [for 1 mm Circular (○) and 1 mm Hydraulic Diameter Semi-Triangular (△) Test Sections] Normalized with Predicted Pressure Drops (using Chisholm Model) for 1 mm Diameter Test Section.

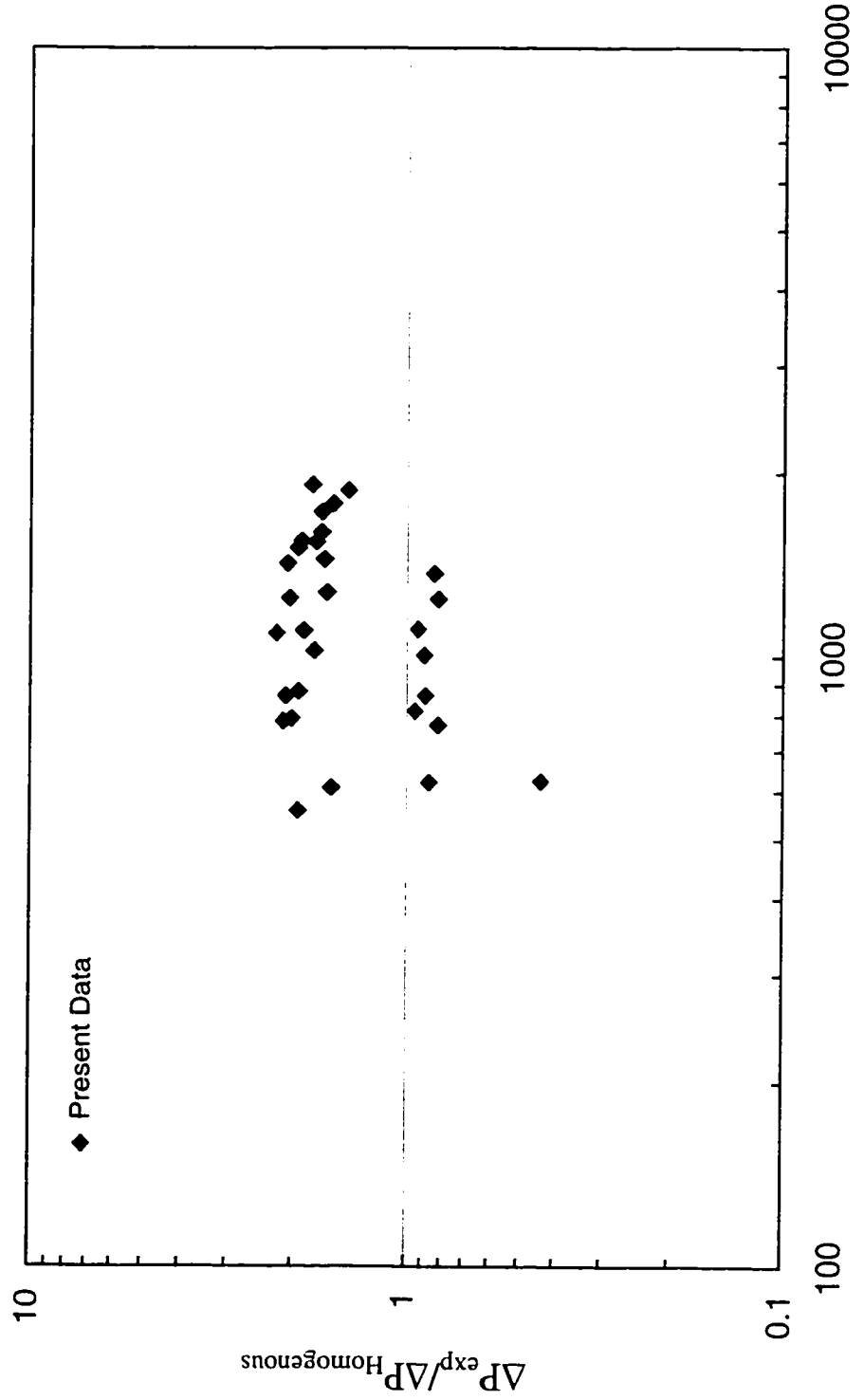

Figure 4.13. Experimentally Measured Pressure Drops Normalized with Predicted Pressure Drops (using Homogenous Model) for 800 μm Diameter Test Section.

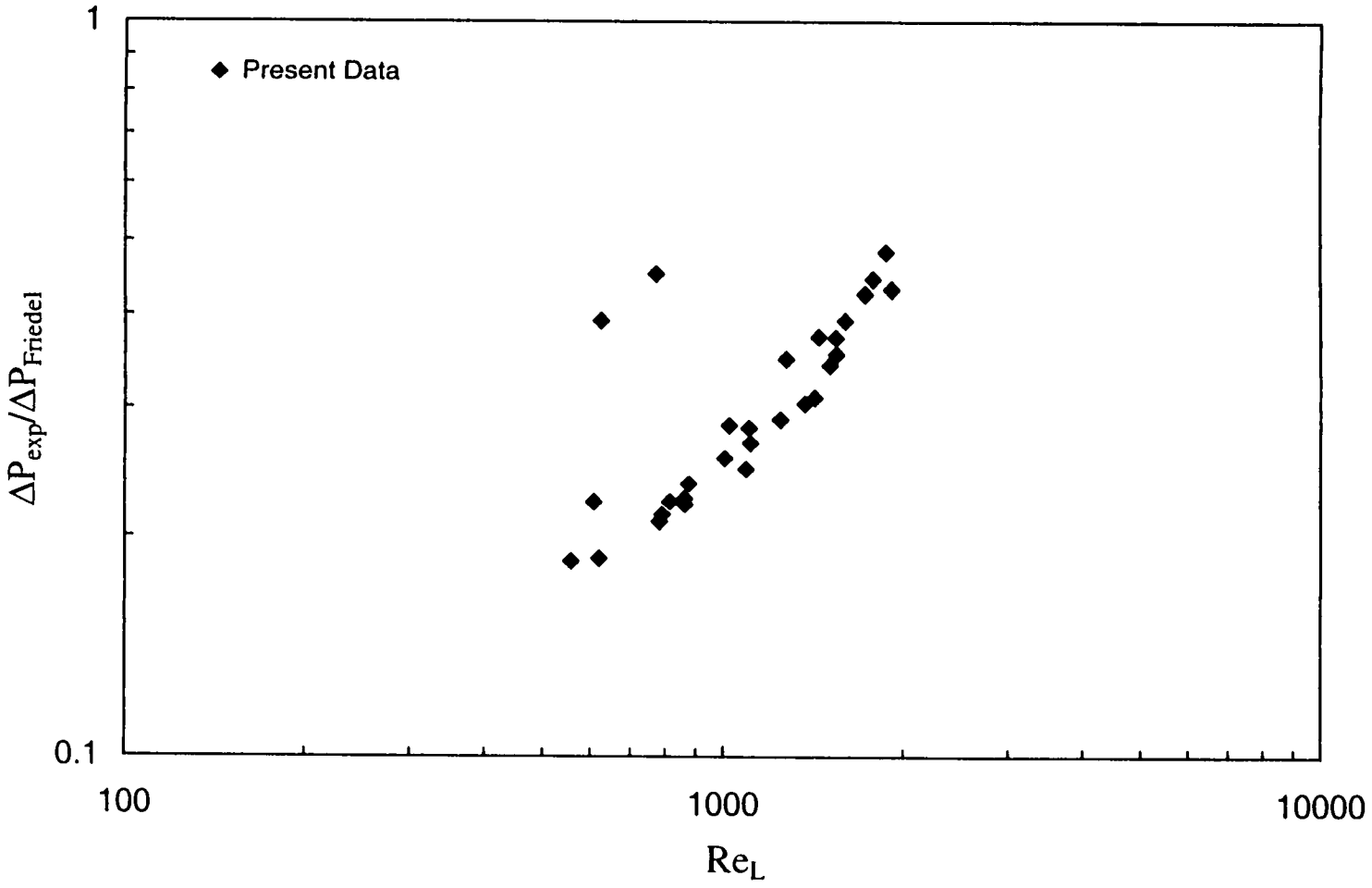

Figure 4.14. Experimentally Measured Pressure Drops Normalized with Predicted Pressure Drops (using Friedel Model) for 800 μm Diameter Test Section.

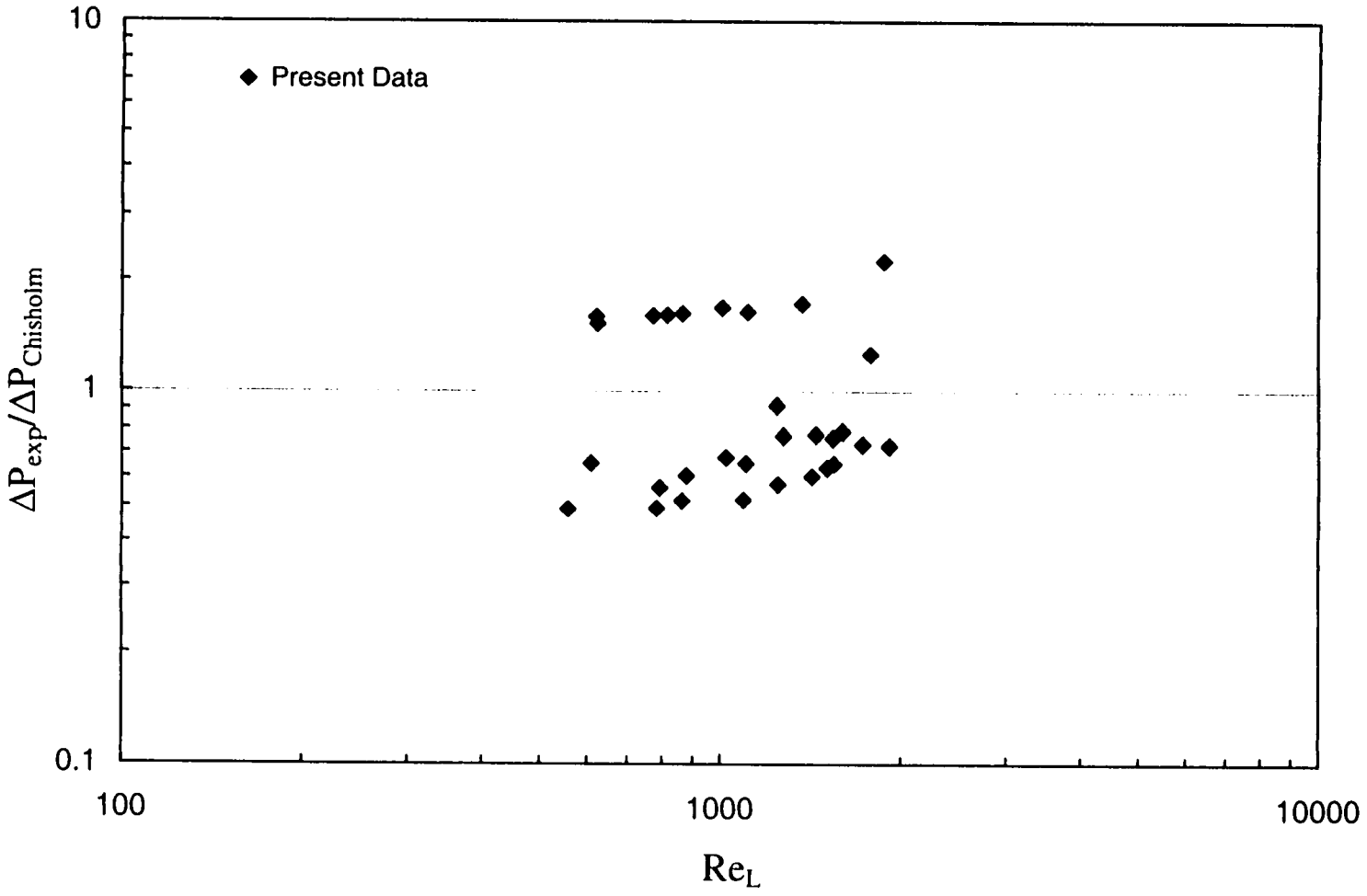

Figure 4.15. Experimentally Measured Pressure Drops Normalized with Predicted Pressure Drops (using Chisholm Model) for 800 μm diameter test section.

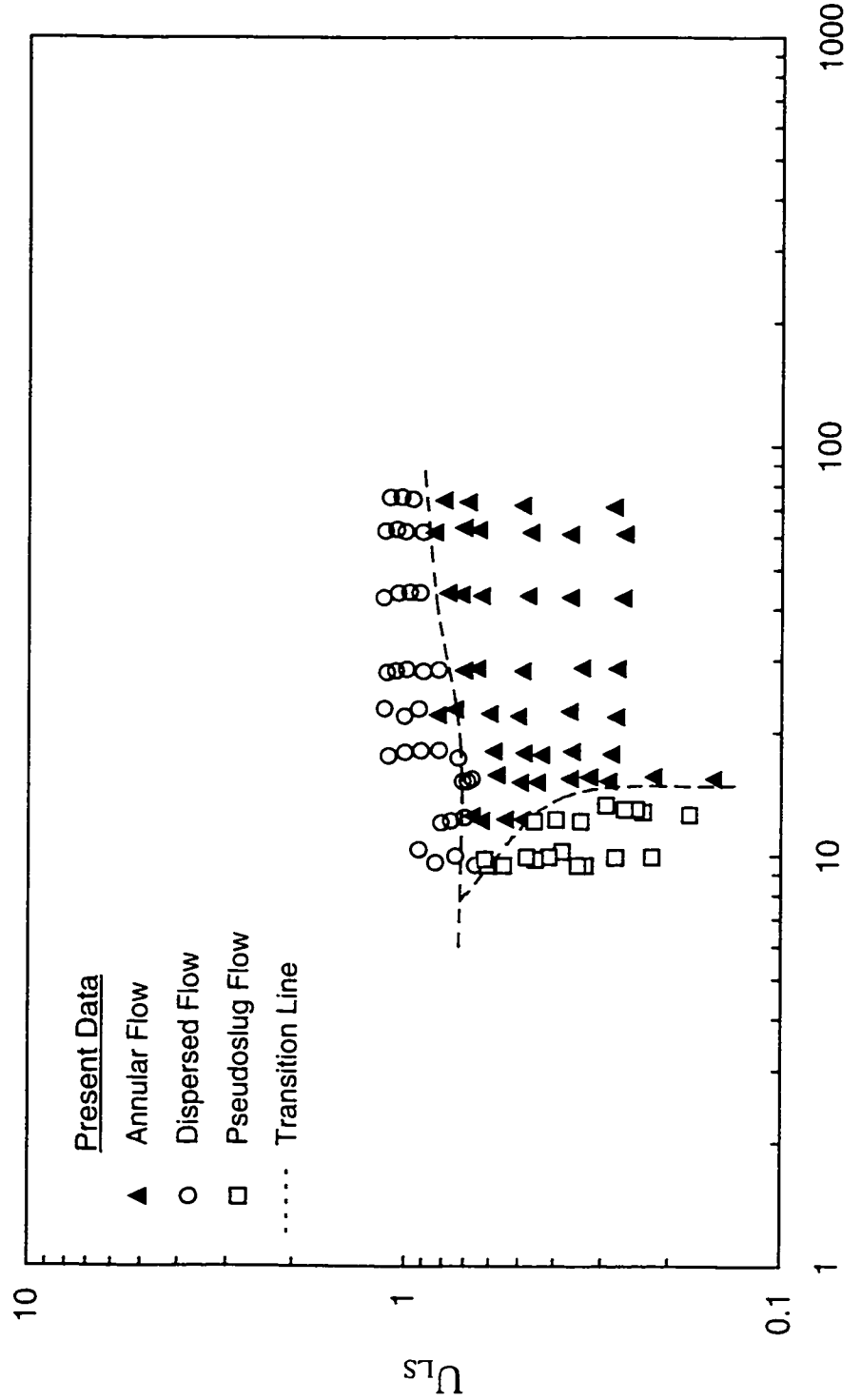

Figure 4.16. Flow Regimes and Flow Pattern Transition Lines for the 3 mm Diameter Test Section.

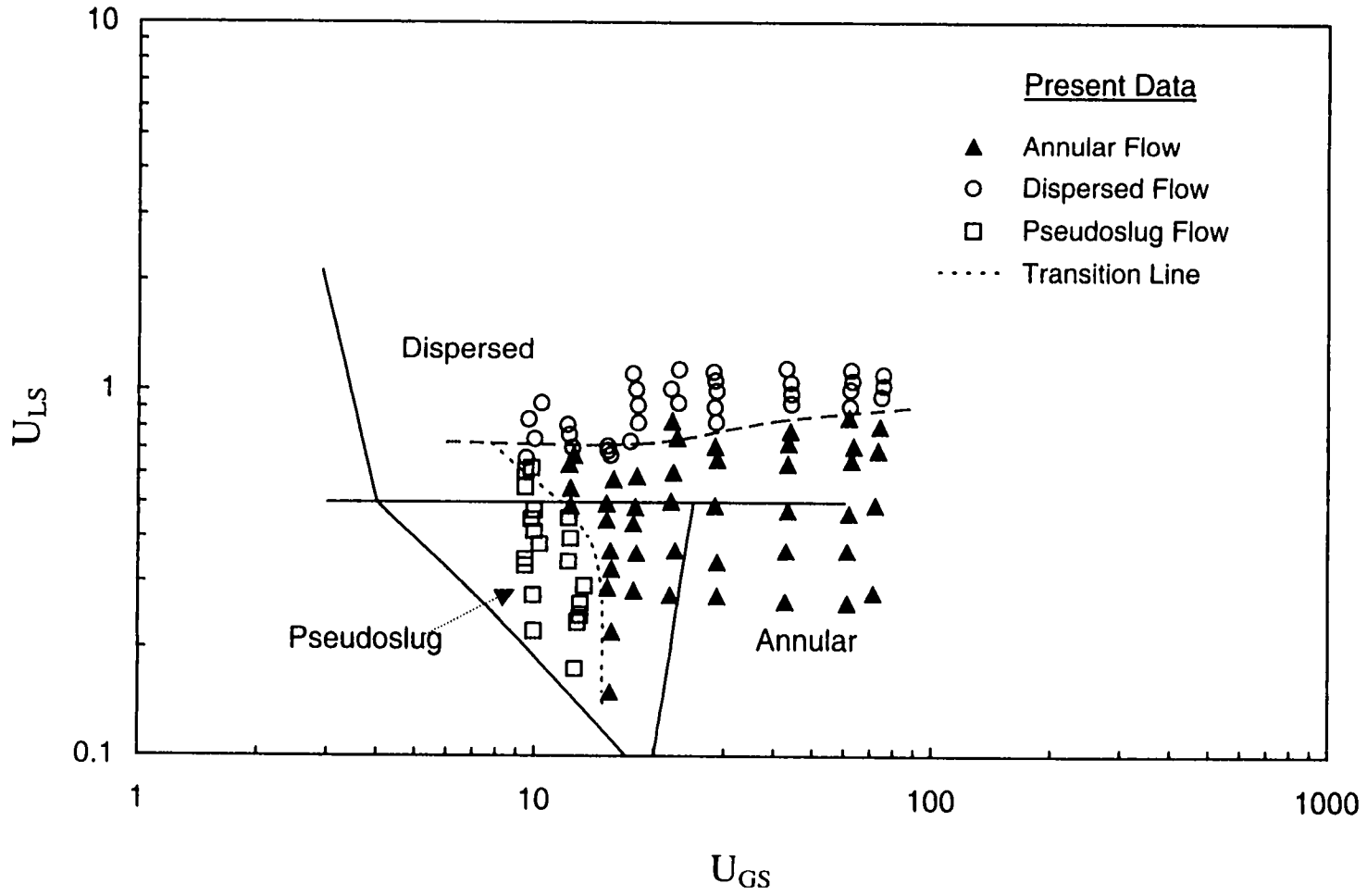

Figure 4.17. Comparison of Present Flow Regimes and Flow Pattern Transition Lines to the Flow Regimes and Transition Lines of Damianides (1987) for the 3 mm Diameter Test Section.

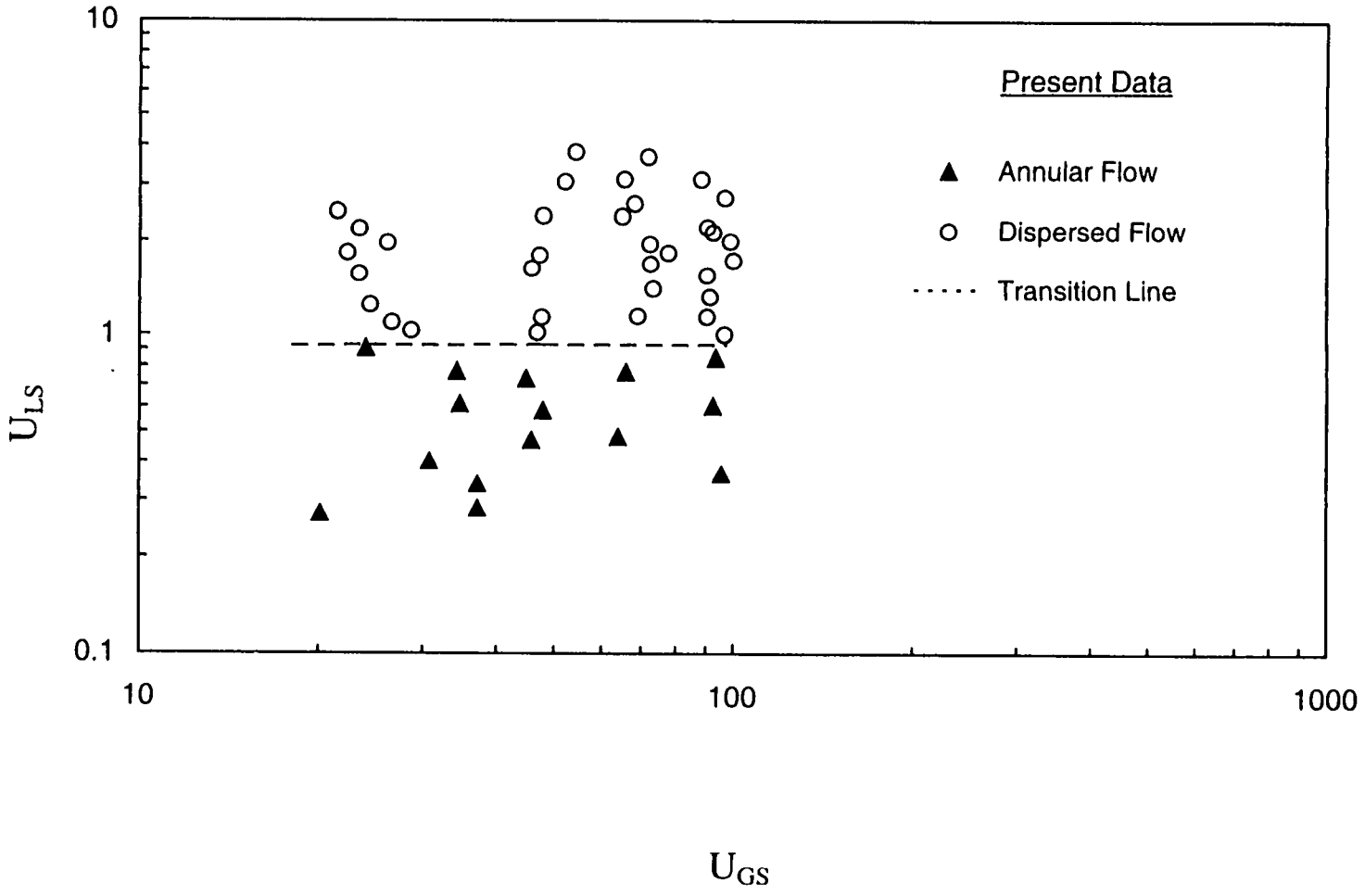

Figure 4.18. Flow Regimes and Flow Pattern Transition Line for the 1 mm Diameter Test Section.

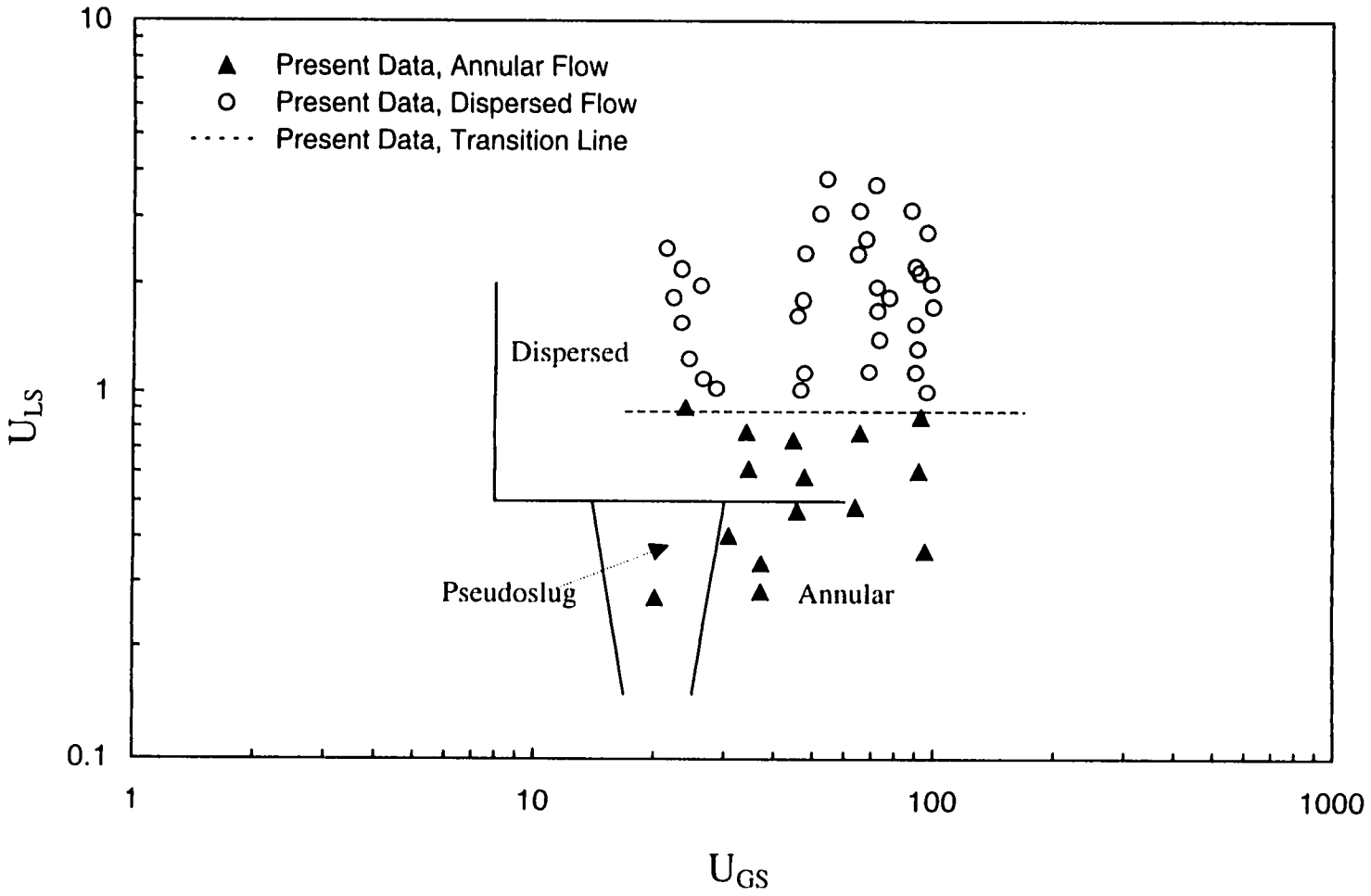

Figure 4.19. Comparison of Present Flow Regimes and Flow Pattern Transition Lines to the Flow Regimes and Transition Lines of Damianides (1987) for the 1 mm Diameter Test Section.

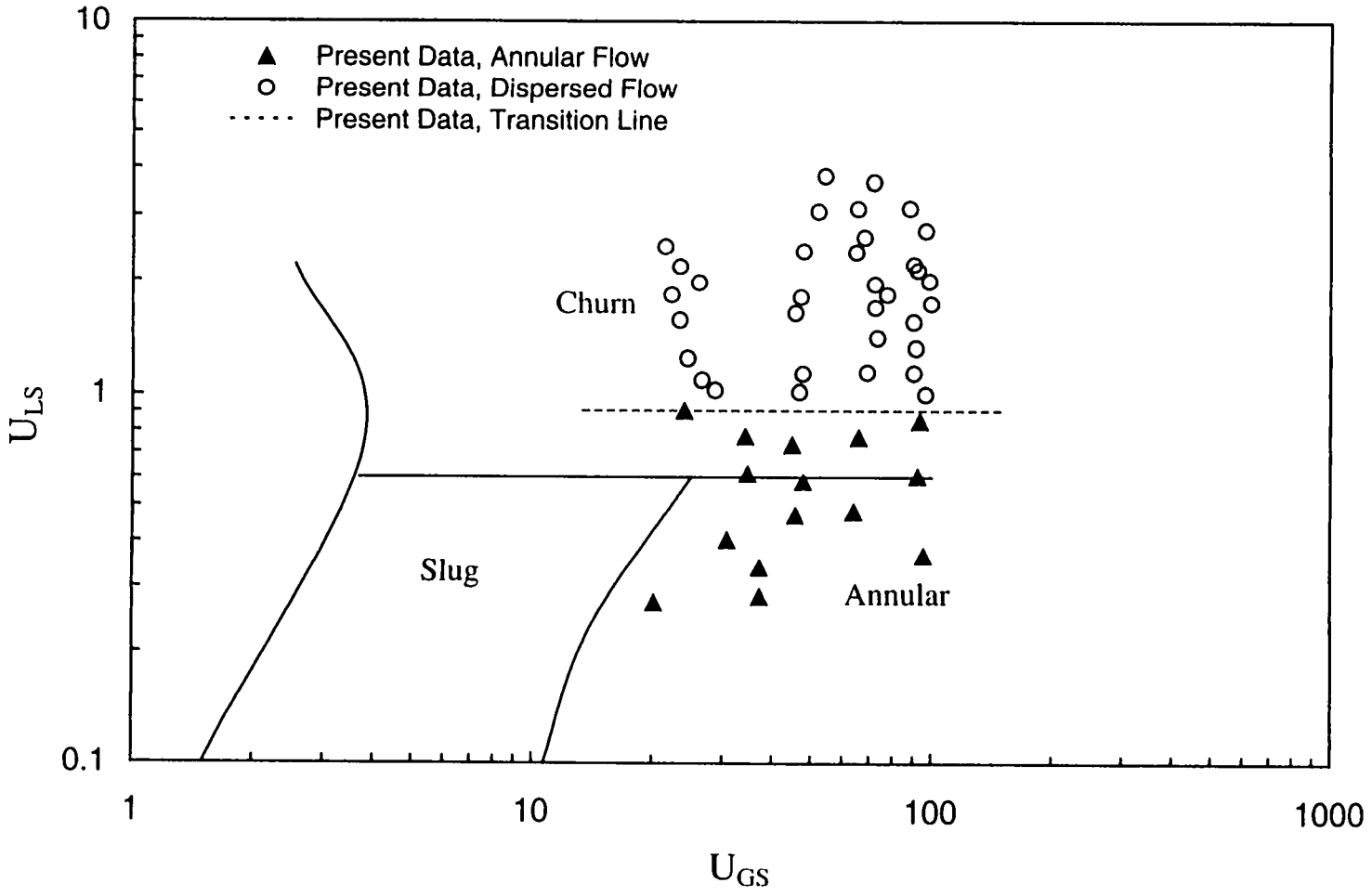

Figure 4.20. Comparison of Present Flow Regimes and Flow Pattern Transition Lines to the Flow Regimes and Transition Lines of Ekberg (1997) for the 1 mm Diameter Circular Test Section.

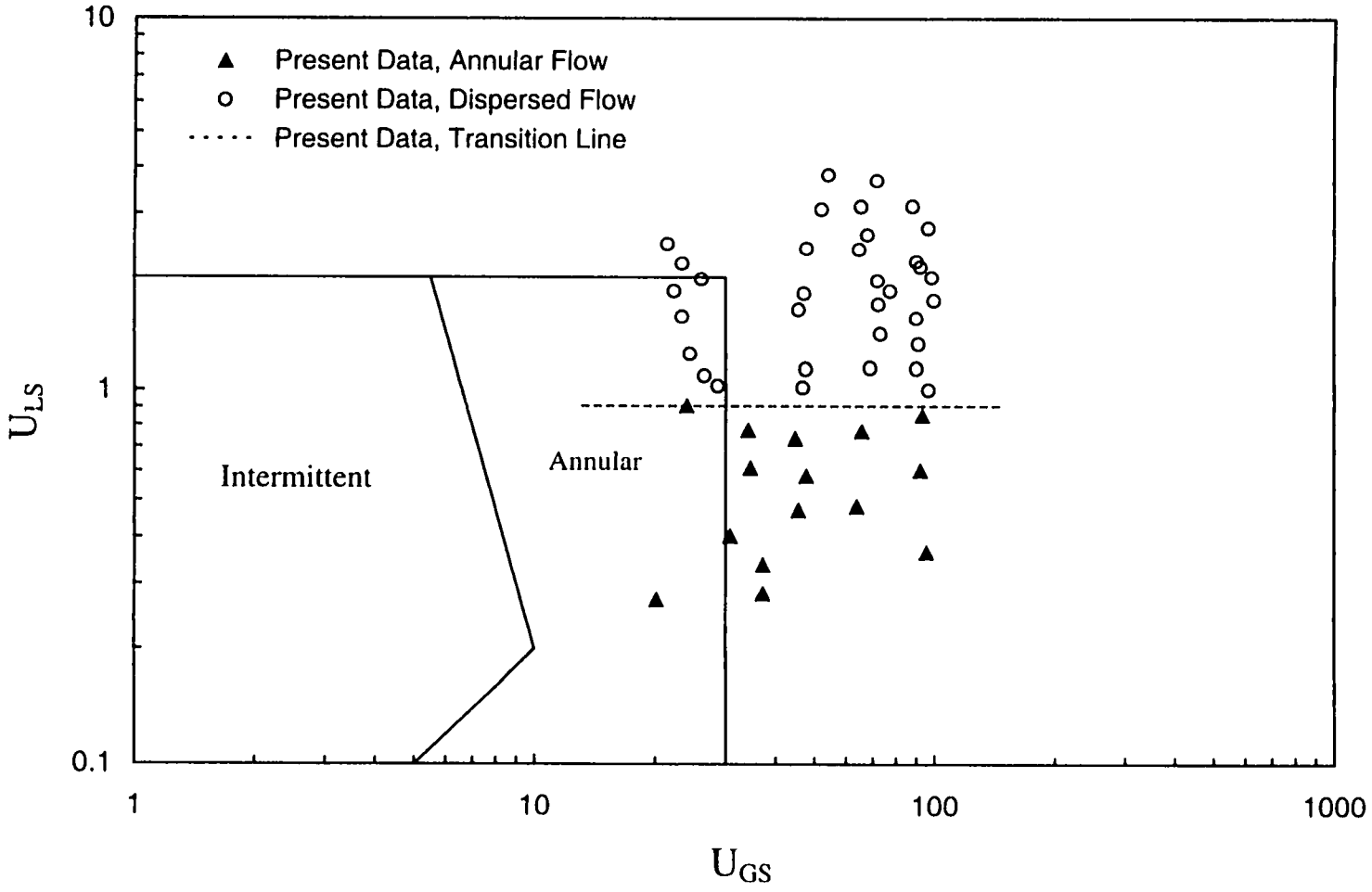

Figure 4.21. Comparison of Present Flow Regimes and Flow Pattern Transition Lines to the Flow Regimes and Transition Lines of Fukano and Kariyasaki (1993) for the 1 mm Diameter Test Section.

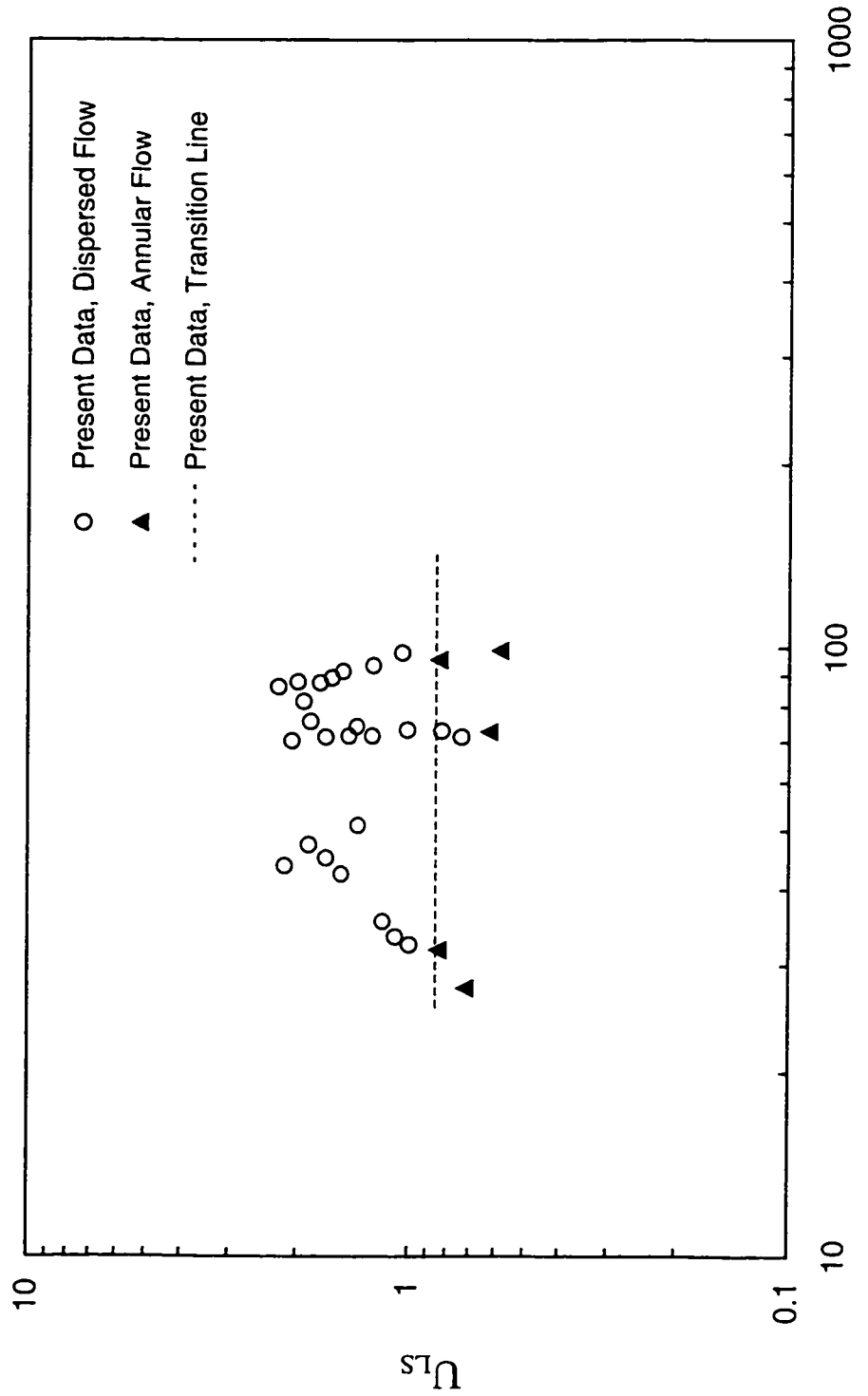

Figure 4.22. Flow Regimes and Flow Pattern Transition Line for the 800 μm Diameter Test Section.

U_{LS}= 0.28 m/s U_{GS}= 9.69 m/s D= 3 mm

Flow Regime= Pseudoslug Flow Run= 2

U_{LS}= 0.35 m/s U_{GS}= 9.12 m/s D= 3 mm

Flow Regime= Pseudoslug Flow Run= 4

U_{LS}= 0.45 m/s U_{GS}= 9.23 m/s D= 3 mm

Flow Regime= Pseudoslug Flow Run= 7

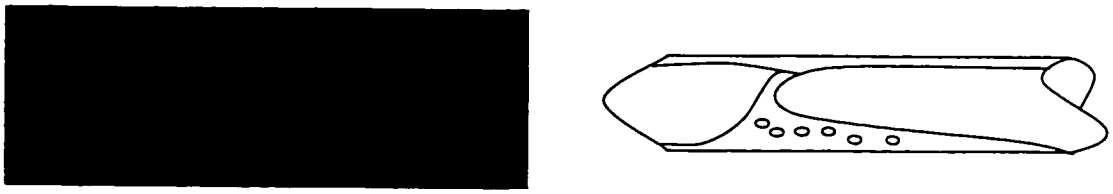

U_{LS}= 0.29 m/s U_{GS}= 12.82 m/s D= 3 mm

Flow Regime= Pseudoslug Flow Run= 20

Figure 4.23. Sample images for Pseudoslug Flow.

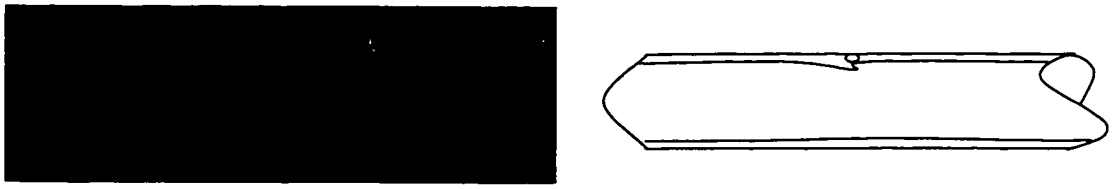

U_{LS}= 0.36 m/s U_{GS}= 14.14 m/s D= 3 mm

Flow Regime= Annular Flow Run= 35

U_{LS}= 0.32 m/s U_{GS}= 14.70 m/s D= 3 mm

Flow Regime= Annular Flow Run= 36

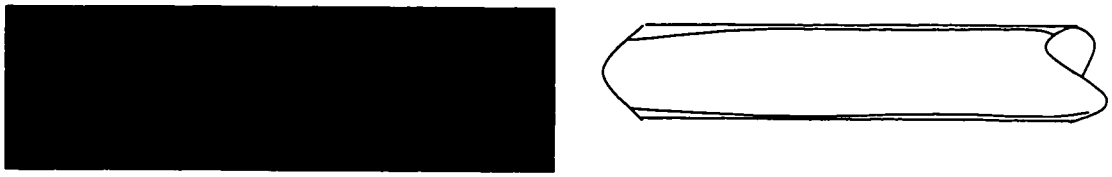

U_{LS}= 0.50 m/s U_{GS}= 13.36 m/s D= 3 mm

Flow Regime= Annular Flow Run= 37

U_{LS}= 0.59 m/s U_{GS}= 18.01 m/s D= 3 mm

Flow Regime= Annular Flow Run= 45

Figure 4.24. Sample images for Annular Flow.

U_{LS}= 1.14 m/s U_{GS}= 42.84 m/s D= 3 mm

Flow Regime= Dispersed Flow Run= 80

U_{LS}= 1.00 m/s U_{GS}= 62.20 m/s D= 3 mm

Flow Regime= Dispersed Flow Run= 88

U_{LS}= 0.73 m/s U_{GS}= 17.33 m/s D= 3 mm

Flow Regime= Dispersed Flow Run= 46

U_{LS}= 0.91 m/s U_{GS}= 18.08 m/s D= 3 mm

Flow Regime= Dispersed Flow Run= 48

Figure 4.25. Sample images for Dispersed Flow.

Table 4.1. Experimental and Model Predicted Two-Phase Pressure Drop Data of 3 mm Diameter Test Section.

Q_{air} (slpm)	Q_{water} (cc/min)	G_T (kg/m^2s)	G_L (kg/m^2s)	G_G (kg/m^2s)	x	P_I (kPa)	ΔP_{exp} (kPa)	ΔP_{Hom} (kPa)	$\Delta P_{Friedel}$ (kPa)	$\Delta P_{Chisholm}$ (kPa)
5.0	94.0	235.7	221.2	14.5	0.061	10.21	3.31	5.66	22.89	3.48
5.0	155.0	379.2	364.7	14.5	0.038	13.86	4.74	7.93	24.79	4.42
5.1	204.0	494.8	480.0	14.7	0.030	18.00	6.26	9.31	25.85	5.06
5.0	251.0	605.1	590.6	14.4	0.024	21.66	7.23	10.29	26.12	5.51
5.1	301.0	723.0	708.3	14.7	0.020	26.41	8.62	11.21	26.78	6.02
5.0	356.0	852.0	837.7	14.3	0.017	31.79	9.45	11.78	26.52	6.38
5.0	411.0	981.6	967.1	14.4	0.015	35.66	10.83	12.52	27.05	6.84
5.1	448.0	1068.9	1054.2	14.7	0.014	38.90	11.66	12.98	27.49	7.16
5.0	466.0	1111.0	1096.6	14.4	0.013	42.83	11.86	12.87	26.95	7.17
5.0	491.0	1169.8	1155.4	14.4	0.012	47.17	13.03	12.90	26.74	4.16
10.3	98.0	260.4	230.6	29.8	0.114	20.07	8.48	6.32	34.44	3.12
10.2	171.0	431.9	402.4	29.5	0.068	25.72	10.90	9.33	36.96	4.00
10.2	201.0	502.4	473.0	29.5	0.059	32.14	12.00	10.06	36.80	4.24
10.2	244.0	603.6	574.2	29.5	0.049	40.07	13.45	11.01	36.68	4.56
10.2	301.0	737.8	708.3	29.5	0.040	47.52	15.52	19.93	36.91	4.98
10.1	364.0	885.7	856.5	29.2	0.033	58.97	17.59	22.00	36.19	8.26
10.1	421.0	1019.8	990.7	29.2	0.029	65.17	19.52	24.35	36.37	8.76
10.2	467.0	1128.4	1098.9	29.5	0.026	71.24	21.03	26.19	36.51	9.15
10.0	482.0	1163.1	1134.2	28.9	0.025	78.97	21.38	25.51	35.19	9.04
10.1	498.0	1201.0	1171.9	29.2	0.024	86.21	21.66	25.58	34.67	9.08
15.7	128.0	346.6	301.2	45.4	0.131	38.90	11.24	14.10	42.60	4.09
15.6	148.0	393.3	348.3	45.1	0.115	45.59	13.03	15.17	42.13	4.27
15.1	196.0	504.8	461.2	43.6	0.086	50.55	14.97	18.30	42.57	4.76
15.2	230.0	585.1	541.2	43.9	0.075	56.97	16.69	20.41	42.81	5.08
15.2	323.0	804.0	760.1	43.9	0.055	68.76	21.03	25.97	43.55	5.85
15.1	344.0	853.1	809.5	43.6	0.051	76.21	21.31	26.28	42.57	9.24
15.1	410.0	1008.4	964.8	43.6	0.043	91.31	24.41	28.63	41.62	9.75
15.0	442.0	1083.4	1040.1	43.3	0.040	96.62	25.10	29.78	41.32	9.98
15.0	464.0	1135.2	1091.9	43.3	0.038	102.21	26.07	30.37	40.92	10.11

Table 4.1. Experimental and Model Predicted Two-Phase Pressure Drop Data of 3 mm Diameter Test Section. (Continued)

Q_{air} (slpm)	Q_{water} (cc/min)	G_T (kg/m^{2}s)	G_L (kg/m^{2}s)	G_G (kg/m^{2}s)	x	P_I (kPa)	ΔP_{exp} (kPa)	ΔP_{Hom} (kPa)	$\Delta P_{Friedel}$ (kPa)	$\Delta P_{Chisholm}$ (kPa)
15.3	482.0	1178.4	1134.2	44.2	0.038	104.83	27.45	31.61	41.40	10.35
20.5	100.0	294.5	235.3	59.2	0.201	45.59	13.52	14.05	46.48	4.08
20.4	170.0	459.0	400.0	58.9	0.128	53.24	18.62	20.63	49.48	5.11
20.2	200.0	529.0	470.6	58.4	0.110	68.76	19.86	21.43	47.19	5.25
20.1	240.0	622.8	564.8	58.1	0.093	78.21	22.21	23.77	46.85	5.59
20.2	302.0	769.0	710.7	58.4	0.076	89.93	24.97	27.61	46.99	6.12
20.2	344.0	867.8	809.5	58.4	0.067	104.76	27.24	28.93	45.66	6.32
20.3	398.0	995.2	936.6	58.6	0.059	111.86	30.34	32.17	46.09	6.73
20.2	442.0	1098.4	1040.1	58.4	0.053	119.79	32.00	34.11	45.76	10.90
20.2	463.0	1147.9	1089.5	58.4	0.051	128.97	30.14	34.27	44.86	10.96
20.3	485.0	1199.9	1141.3	58.6	0.049	136.14	33.31	34.91	44.45	11.09
25.2	110.0	331.6	258.8	72.8	0.219	63.79	18.76	16.46	49.40	7.00
25.2	157.0	442.2	369.4	72.8	0.165	74.14	21.31	20.60	50.56	8.06
25.2	194.0	529.3	456.5	72.8	0.138	87.45	23.45	22.90	49.86	8.62
25.2	244.0	647.0	574.2	72.8	0.113	96.41	26.69	26.68	50.42	9.45
25.2	299.0	776.4	703.6	72.8	0.094	104.48	30.28	30.72	51.01	10.26
25.2	347.0	889.3	816.5	72.8	0.082	122.34	32.48	32.40	49.42	10.63
25.2	376.0	957.6	884.8	72.8	0.076	136.69	34.21	32.82	47.97	10.75
25.2	433.0	1091.7	1018.9	72.8	0.067	148.41	36.14	35.69	47.72	11.31
25.2	456.0	1145.8	1073.0	72.8	0.064	156.83	37.10	36.28	47.09	11.44
25.3	465.0	1167.3	1094.2	73.1	0.063	158.90	37.93	36.78	47.13	11.53
31.3	138.0	415.1	324.7	90.4	0.218	92.28	24.76	20.69	52.49	5.13
31.3	165.0	478.7	388.3	90.4	0.189	109.52	26.41	21.90	50.91	5.35
31.2	195.0	549.0	458.9	90.1	0.164	125.79	28.76	23.26	49.60	5.58
31.3	244.0	664.6	574.2	90.4	0.136	139.59	32.55	26.60	49.73	6.07
31.3	297.0	789.3	698.9	90.4	0.115	152.00	36.76	30.05	49.86	6.54
31.3	367.0	954.0	863.6	90.4	0.095	160.69	40.28	35.11	50.84	11.26
31.3	387.0	1001.1	910.7	90.4	0.090	168.28	41.72	35.82	50.33	11.41
31.2	424.0	1087.9	997.7	90.1	0.083	173.17	43.72	38.15	50.55	11.84

Table 4.1. Experimental and Model Predicted Two-Phase Pressure Drop Data of 3 mm Diameter Test Section. (Continued)

Q_{air} (slpm)	Q_{water} (cc/min)	G_T (kg/m^2s)	G_L (kg/m^2s)	G_G (kg/m^2s)	x	P_l (kPa)	ΔP_{exp} (kPa)	ΔP_{Hom} (kPa)	$\Delta P_{Friedel}$ (kPa)	$\Delta P_{Chisholm}$ (kPa)
31.6	455.0	1162.0	1070.7	91.3	0.079	183.72	44.97	39.67	50.31	12.14
31.2	475.0	1207.9	1117.7	90.1	0.075	192.41	45.31	39.68	49.27	12.16
35.0	104.0	345.8	244.7	101.1	0.292	113.79	23.52	16.91	49.14	4.51
35.0	146.0	444.7	343.6	101.1	0.227	127.45	27.72	20.43	50.10	5.12
35.0	184.0	534.1	433.0	101.1	0.189	138.00	30.00	23.45	50.67	5.60
35.2	224.0	628.8	527.1	101.7	0.162	146.14	34.28	26.80	51.59	6.08
35.1	262.0	717.9	616.5	101.4	0.141	155.45	36.34	29.42	51.69	6.45
35.1	292.0	788.5	687.1	101.4	0.129	170.00	39.17	30.60	50.69	6.63
35.3	319.0	852.6	750.7	102.0	0.120	177.24	41.52	32.38	50.80	10.79
40.5	93.0	335.8	218.8	117.0	0.348	122.00	27.38	17.66	51.31	4.54
40.5	149.0	467.6	350.6	117.0	0.250	134.07	32.97	23.31	54.04	5.50
40.5	175.0	528.8	411.8	117.0	0.221	153.79	34.69	24.33	52.43	5.70

Table 4.2. Experimental and Model Predicted Two-Phase Pressure Drop Data of 1 mm Diameter Test Section.

Q_{air} (slpm)	Q_{water} (cc/min)	G_T (kg/m^2s)	G_L (kg/m^2s)	G_G (kg/m^2s)	x	P_I (kPa)	ΔP_{exp} (kPa)	ΔP_{Hom} (kPa)	$\Delta P_{Friedel}$ (kPa)	$\Delta P_{Chisholm}$ (kPa)
1.0	27.0	597.8	571.8	26.0	0.0435	42.83	26.00	31.39	163.10	19.40
1.0	39.0	851.9	826.0	26.0	0.0305	45.17	29.00	40.11	174.20	23.80
1.0	46.0	1000.2	974.2	26.0	0.0260	47.52	33.00	44.15	178.50	26.08
1.0	52.0	1127.3	1101.3	26.0	0.0231	49.59	34.10	47.21	181.50	27.94
1.0	61.0	1317.9	1291.9	26.0	0.0197	51.38	37.60	51.64	186.50	30.70
1.0	67.0	1444.9	1418.9	26.0	0.0180	55.03	39.20	53.52	187.20	32.27
1.6	20.0	465.2	423.6	41.6	0.0894	63.72	32.30	24.38	190.20	19.28
1.6	34.0	761.7	720.1	41.6	0.0546	68.21	38.70	35.90	207.50	25.28
1.6	41.0	909.9	868.3	41.6	0.0457	72.07	40.60	83.06	212.00	27.81
1.6	56.0	1227.6	1186.0	41.6	0.0339	76.41	51.00	108.68	222.40	33.00
1.6	78.0	1693.5	1651.9	41.6	0.0246	92.69	60.30	137.29	224.10	39.03
2.0	25.0	581.4	529.5	52.0	0.0894	70.62	38.50	64.12	224.70	33.19
2.1	37.0	838.2	783.6	54.6	0.0651	80.90	50.70	90.09	240.30	40.67
2.0	51.0	1132.1	1080.1	52.0	0.0459	89.24	57.20	111.61	240.10	44.97
2.0	60.0	1322.7	1270.7	52.0	0.0393	94.14	65.70	126.92	243.80	48.48
2.0	64.0	1407.4	1355.4	52.0	0.0369	100.21	67.90	131.06	241.50	49.52
2.5	23.0	552.1	487.1	65.0	0.1177	90.41	68.10	64.92	237.00	37.23
2.8	35.0	814.0	741.2	72.8	0.0894	102.14	81.60	97.99	266.00	96.74
2.5	47.0	1060.4	995.4	65.0	0.0613	110.21	82.50	112.33	253.40	99.10
2.7	52.0	1171.5	1101.3	70.2	0.0599	117.79	85.80	127.05	265.50	109.55
2.7	58.0	1298.5	1228.3	70.2	0.0541	121.03	95.00	138.69	268.60	114.89
3.3	26.0	636.4	550.6	85.8	0.1348	108.48	96.80	84.46	274.90	96.32
3.3	34.0	805.8	720.1	85.8	0.1065	117.59	115.10	102.34	280.20	106.72
3.3	50.0	1144.7	1058.9	85.8	0.0749	130.00	133.40	137.30	289.90	124.83
3.3	55.0	1250.6	1164.8	85.8	0.0686	140.83	136.90	143.40	285.30	127.81
3.3	60.0	1356.5	1270.7	85.8	0.0632	149.45	146.20	150.79	283.50	131.33
4.8	20.0	548.3	423.6	124.8	0.2276	174.14	111.50	74.13	276.80	106.02
5.0	43.0	1040.6	910.7	130.0	0.1249	196.14	149.80	134.29	310.40	149.22
5.0	53.0	1252.4	1122.4	130.0	0.1038	216.97	165.70	151.30	306.80	158.86
5.0	65.0	1506.6	1376.6	130.0	0.0863	233.59	176.70	173.35	307.30	170.65

Table 4.3. Experimental and Model Predicted Two-Phase Pressure Drop Data of 800 μm Diameter Test Section.

Q_{air} (slpm)	Q_{water} (cc/min)	G_T (kg/m^2s)	G_L (kg/m^2s)	G_G (kg/m^2s)	x	P_1 (kPa)	ΔP_{exp} (kPa)	ΔP_{Hom} (kPa)	$\Delta P_{Friedel}$ (kPa)	$\Delta P_{Chisholm}$ (kPa)
0.9	27.6	946.9	912.0	34.9	0.0369	67.33	43.40	41.10	194.60	67.33
1.2	21.0	742.0	695.2	46.7	0.0630	66.72	41.90	36.20	224.50	66.72
1.1	29.2	1010.9	966.6	44.3	0.0438	77.07	48.90	43.30	221.30	77.07
0.9	34.0	1162.2	1126.1	36.1	0.0311	77.97	50.90	45.50	199.00	77.97
0.8	37.6	1274.6	1242.9	31.7	0.0249	78.42	50.00	46.50	186.10	78.42
1.0	42.1	1433.5	1392.5	41.0	0.0286	96.18	61.10	50.00	210.80	96.18
0.9	46.3	1569.8	1532.4	37.4	0.0238	96.43	61.60	51.80	202.40	96.43
0.9	21.1	736.7	698.9	37.8	0.0513	101.91	66.00	28.80	168.00	101.91
1.0	26.1	904.1	864.3	39.8	0.0440	121.84	76.50	62.70	169.40	121.84
0.9	63.4	2133.9	2099.0	34.9	0.0164	123.27	91.90	133.00	189.90	123.27
1.5	60.3	2054.6	1995.7	58.9	0.0287	150.86	107.60	170.30	241.50	150.86
1.8	54.1	1863.2	1790.9	72.3	0.0388	148.90	106.90	181.50	271.60	148.90
1.8	52.2	1800.1	1727.0	73.1	0.0406	144.72	102.70	179.70	274.90	144.72
1.8	48.9	1691.9	1617.2	74.7	0.0442	143.86	103.40	172.30	275.80	143.86
1.8	43.1	1499.2	1426.9	72.3	0.0482	128.30	96.50	158.60	276.00	128.30
1.9	37.3	1312.1	1235.3	76.8	0.0585	110.77	83.60	157.00	296.40	110.77
1.9	34.6	1220.6	1144.6	76.0	0.0622	109.01	82.90	146.20	291.50	109.01
1.8	29.7	1055.1	981.1	73.9	0.0701	89.27	70.50	136.50	299.20	89.27
2.0	26.8	965.1	885.5	79.6	0.0825	82.90	67.80	136.80	316.80	82.90
1.7	20.6	750.8	681.3	69.5	0.0925	77.12	62.40	99.30	280.50	77.12
2.8	18.9	735.8	624.1	111.7	0.1518	86.35	68.60	133.00	370.70	86.35
2.8	26.5	991.3	875.9	115.4	0.1164	104.36	78.90	167.30	376.60	104.36
2.8	29.2	1076.6	964.9	111.7	0.1037	108.87	83.00	173.40	368.70	108.87
2.8	37.0	1336.8	1223.0	113.7	0.0851	125.21	91.30	202.40	369.10	125.21
2.8	42.2	1509.9	1395.8	114.1	0.0756	146.57	102.60	209.90	354.30	146.57
2.6	48.1	1696.5	1591.7	104.8	0.0618	147.61	106.30	220.60	342.80	147.61
2.8	51.0	1799.7	1688.0	111.7	0.0621	166.79	117.50	228.70	342.50	166.79
2.7	52.4	1841.1	1732.6	108.4	0.0589	173.08	117.60	223.80	331.50	173.08
2.8	58.5	2047.3	1934.8	112.5	0.0550	203.86	136.80	231.30	320.90	203.86
2.7	64.8	2252.4	2144.0	108.4	0.0481	203.12	138.50	248.30	320.60	203.12

Table 4.4. Two-Phase Flow Regime Data for 3 mm Test Section.

Run	Q_{air} (slpm)	Q_{water} (cc/min)	P_l (kPa)	T (°C)	U_G (m/s)	U_L (m/s)	x	Flow Regime
1	4.3	93.8	4.59	24	9.80	0.22	0.052	Pseudoslug
2	4.3	116.9	5.47	24	9.69	0.28	0.042	Pseudoslug
3	4.1	140.4	6.55	24	9.15	0.33	0.034	Pseudoslug
4	4.2	146.7	6.97	24	9.12	0.35	0.032	Pseudoslug
5	4.5	161.7	7.59	24	9.84	0.38	0.032	Pseudoslug
6	4.4	175.6	8.62	24	9.45	0.41	0.029	Pseudoslug
7	4.4	190.8	9.45	24	9.23	0.45	0.026	Pseudoslug
8	4.5	201.8	9.72	24	9.34	0.48	0.025	Pseudoslug
9	4.4	233.4	11.86	24	8.72	0.55	0.021	Pseudoslug
10	4.4	257.6	13.66	24	8.59	0.61	0.019	Pseudoslug
11	4.6	262.8	13.86	24	8.87	0.62	0.019	Pseudoslug
12	4.5	279.3	15.10	24	8.50	0.66	0.017	Dispersed
13	4.8	314.3	17.86	24	8.74	0.74	0.016	Dispersed
14	4.8	354.8	20.76	24	8.23	0.84	0.014	Dispersed
15	5.3	391.3	25.10	24	8.55	0.92	0.014	Dispersed
16	5.4	74.5	4.07	22	12.39	0.18	0.081	Pseudoslug
17	5.6	98.8	5.17	22	12.45	0.23	0.063	Pseudoslug
18	5.7	103.4	5.52	22	12.61	0.24	0.061	Pseudoslug
19	5.7	110.6	5.86	22	12.57	0.26	0.058	Pseudoslug
20	5.9	123.8	6.28	22	12.82	0.29	0.053	Pseudoslug
21	5.4	144.1	8.48	23	11.51	0.34	0.042	Pseudoslug
22	5.6	167.8	11.45	23	11.32	0.40	0.037	Pseudoslug
23	5.7	192.3	13.03	23	11.05	0.45	0.032	Pseudoslug
24	5.8	207.5	13.72	23	11.09	0.49	0.030	Annular
25	5.8	231.3	14.97	23	10.97	0.55	0.027	Annular
26	6.0	268.5	18.83	23	10.54	0.63	0.023	Annular
27	6.2	284.7	19.93	23	10.73	0.67	0.022	Annular
28	6.2	297.8	21.10	23	10.54	0.70	0.021	Dispersed
29	6.1	322.8	22.48	24	10.26	0.76	0.019	Dispersed
30	6.1	342.8	23.38	24	10.09	0.81	0.018	Dispersed
31	7.9	300.7	26.62	24	12.41	0.71	0.026	Dispersed
32	7.9	292.1	25.59	24	12.54	0.69	0.026	Dispersed
33	7.9	284.8	24.28	24	12.84	0.67	0.027	Dispersed
34	7.8	244.5	20.28	24	13.53	0.58	0.032	Annular
35	7.2	154.4	12.90	24	14.14	0.36	0.050	Annular
36	7.0	137.3	9.45	24	14.70	0.32	0.056	Annular
37	7.3	210.3	16.83	24	13.36	0.50	0.036	Annular
38	6.7	122.2	7.66	24	14.60	0.29	0.061	Annular
39	6.9	93.2	6.69	24	15.09	0.22	0.080	Annular
40	6.7	64.1	4.69	24	15.22	0.15	0.111	Annular
41	8.0	120.2	9.72	24	16.68	0.28	0.071	Annular

Table 4.4. Two-Phase Flow Regime Data for

3 mm Test Section. (Continued)

Run	Q_{air} (slpm)	Q_{water} (cc/min)	P_1 (kPa)	T (°C)	U_G (m/s)	U_L (m/s)	x	Flow Regime
42	8.4	152.3	13.03	24	17.99	0.36	0.058	Annular
43	8.4	184.7	16.07	24	17.66	0.44	0.047	Annular
44	8.7	205.7	19.24	24	17.85	0.49	0.043	Annular
45	9.3	249.3	25.10	24	18.01	0.59	0.036	Annular
46	9.3	309.7	30.34	24	17.33	0.73	0.028	Dispersed
47	10.1	347.5	35.93	24	18.13	0.82	0.026	Dispersed
48	10.4	386.8	40.00	24	18.08	0.91	0.024	Dispersed
49	10.6	425.6	44.41	24	17.94	1.00	0.021	Dispersed
50	10.6	470.2	46.83	24	17.57	1.11	0.019	Dispersed
51	10.5	116.9	16.41	22	21.88	0.28	0.089	Annular
52	11.5	154.9	22.90	22	22.54	0.37	0.070	Annular
53	8.0	189.2	27.24	22	15.14	0.45	0.040	Annular
54	11.9	213.2	31.03	22	21.95	0.50	0.051	Annular
55	12.6	255.5	37.31	22	22.26	0.60	0.043	Annular
56	13.8	316.3	47.17	22	22.78	0.75	0.036	Annular
57	13.8	350.6	51.10	22	22.09	0.83	0.032	Annular
58	15.0	392.2	59.24	22	22.89	0.92	0.029	Dispersed
59	14.8	427.2	63.45	22	21.98	1.01	0.026	Dispersed
60	16.5	482.7	74.00	22	22.97	1.14	0.024	Dispersed
61	15.4	116.1	29.66	21	28.72	0.27	0.114	Annular
62	16.0	143.6	33.66	20	28.79	0.34	0.095	Annular
63	16.9	207.9	44.00	20	28.32	0.49	0.066	Annular
64	18.6	276.8	56.28	20	28.72	0.65	0.051	Annular
65	18.9	299.6	60.07	20	28.39	0.71	0.047	Annular
66	20.0	348.7	69.24	21	28.53	0.82	0.041	Dispersed
67	20.4	382.3	74.62	21	28.27	0.90	0.037	Dispersed
68	21.7	422.0	83.66	21	28.62	0.99	0.034	Dispersed
69	22.1	450.0	88.07	21	28.39	1.06	0.032	Dispersed
70	22.3	474.8	91.66	21	28.11	1.12	0.030	Dispersed
71	26.2	112.4	49.45	23	42.63	0.26	0.264	Annular
72	27.7	154.4	57.38	23	42.87	0.36	0.276	Annular
73	29.7	201.3	67.52	23	43.22	0.47	0.278	Annular
74	32.3	269.2	82.14	23	43.22	0.63	0.263	Annular
75	34.2	305.7	91.45	23	43.48	0.72	0.273	Annular
76	35.3	330.1	96.21	23	43.90	0.78	0.290	Annular
77	37.7	389.9	108.69	23	44.04	0.92	0.283	Dispersed
78	38.5	414.8	112.55	23	44.16	0.98	0.294	Dispersed
79	39.4	444.5	118.69	23	43.97	1.05	0.301	Dispersed
80	38.0	485.3	116.55	23	42.84	1.14	0.296	Dispersed
81	41.8	111.3	66.55	23	61.14	0.26	0.741	Annular
82	45.0	154.5	79.38	23	61.16	0.36	0.690	Annular
83	48.5	197.7	91.59	23	61.75	0.47	0.654	Annular
84	49.0	274.8	90.48	23	62.62	0.65	0.596	Annular
85	49.6	300.5	90.69	23	63.40	0.71	0.593	Annular

Table 4.4. Two-Phase Flow Regime Data for

3 mm Test Section. (Continued)

Run	Q_{air} (slpm)	Q_{water} (cc/min)	P_t (kPa)	T (°C)	U_G (m/s)	U_L (m/s)	x	Flow Regime
86	48.5	358.4	91.38	23	61.73	0.85	0.558	Annular
87	45.5	383.8	78.97	23	61.99	0.90	0.556	Dispersed
88	46.5	424.8	81.93	23	62.20	1.00	0.545	Dispersed
89	46.8	448.5	80.97	23	62.98	1.06	0.547	Dispersed
90	45.8	480.1	78.90	23	62.41	1.13	0.540	Dispersed
91	48.5	118.7	76.76	24	71.18	0.28	0.850	Annular
92	47.4	208.5	81.31	24	71.94	0.49	0.773	Annular
93	47.6	292.5	75.93	24	73.12	0.69	0.720	Annular
94	42.7	339.3	74.35	24	73.90	0.80	0.700	Annular
95	42.5	407.4	72.07	24	74.58	0.96	0.671	Dispersed
96	44.2	435.3	75.79	24	75.40	1.03	0.667	Dispersed
97	43.0	467.6	72.00	24	75.33	1.10	0.659	Dispersed

Table 4.5. Two-Phase Flow Regime Data for 1 mm Test Section.

Run	Q_{air} (slpm)	Q_{water} (cc/min)	P_1 (kPa)	T (°C)	U_G (m/s)	U_L (m/s)	x	Flow Regime
1	1.8	19.0	25.86	27	30.77	0.40	0.09	Annular
2	1.0	12.8	3.86	27	20.16	0.27	0.08	Annular
3	1.2	42.7	8.21	27	23.98	0.91	0.03	Annular
4	1.9	13.3	13.86	27	37.14	0.28	0.14	Annular
5	1.9	28.8	19.93	27	34.59	0.61	0.06	Annular
6	1.9	15.9	15.52	27	37.14	0.34	0.12	Annular
7	1.9	36.5	22.69	27	34.17	0.77	0.05	Annular
8	1.6	48.4	25.66	27	28.65	1.03	0.03	Dispersed
9	1.5	51.5	26.62	27	26.53	1.09	0.03	Dispersed
10	1.4	58.6	28.90	27	24.40	1.24	0.02	Dispersed
11	1.4	73.7	31.79	27	23.34	1.56	0.02	Dispersed
12	1.4	70.6	35.45	27	22.28	1.50	0.02	-
13	1.4	86.4	38.28	27	22.28	1.83	0.01	Dispersed
14	1.9	93.2	59.86	27	26.10	1.98	0.02	Dispersed
15	1.7	103.2	61.93	27	23.34	2.19	0.01	Dispersed
16	1.6	117.1	66.14	27	21.43	2.48	0.01	Dispersed
17	3.0	22.2	44.21	27	45.62	0.47	0.11	Annular
18	3.2	27.5	47.17	27	47.75	0.58	0.09	Annular
19	3.1	34.6	53.52	27	44.78	0.74	0.07	Annular
20	3.5	47.9	67.66	27	46.69	1.02	0.05	Dispersed
21	3.8	53.5	76.48	27	47.53	1.14	0.05	Dispersed
22	4.2	77.1	104.62	27	45.62	1.64	0.03	Dispersed
23	4.5	85.2	113.93	27	47.11	1.81	0.03	Dispersed
24	5.5	113.8	158.55	27	47.75	2.41	0.02	Dispersed
25	5.2	145.3	124.28	27	51.99	3.08	0.02	Dispersed
26	6.2	180.0	154.00	28	54.11	3.82	0.02	Dispersed
27	8.2	173.6	155.45	28	71.73	3.68	0.02	Dispersed
28	6.3	147.8	116.34	28	65.36	3.14	0.02	Dispersed
29	5.8	124.1	90.74	28	67.91	2.63	0.03	Dispersed
30	5.2	113.1	78.69	28	64.72	2.40	0.04	Dispersed
31	5.5	92.4	69.86	28	72.15	1.96	0.08	Dispersed
32	5.7	86.5	64.9	28	77.46	1.84	0.12	Dispersed
33	5.3	79.7	64.55	28	72.36	1.69	0.15	Dispersed
34	5.0	66.3	51.86	28	73.21	1.41	0.21	Dispersed
35	4.5	54.0	44.21	28	68.97	1.15	0.27	Dispersed
36	3.8	36.2	29.31	28	65.78	0.77	0.38	Annular
37	3.5	22.7	20.21	28	63.87	0.48	0.52	Annular
38	5.3	17.2	23.59	28	95.49	0.37	0.71	Annular
39	5.5	28.4	33.45	28	92.31	0.60	0.61	Annular
40	5.9	40.1	40.55	28	93.37	0.85	0.55	Annular
41	6.3	47.2	45.72	28	96.55	1.00	0.54	Dispersed

Table 4.5. Two-Phase Flow Regime Data for

1 mm Test Section. (Continued)

Run	Q_{air} (slpm)	Q_{water} (cc/min)	P_1 (kPa)	T (°C)	U_G (m/s)	U_L (m/s)	x	Flow Regime
42	6.1	53.7	51.10	28	90.19	1.14	0.51	Dispersed
43	6.8	62.4	65.79	28	91.25	1.32	0.50	Dispersed
44	7.0	73.0	72.41	28	90.19	1.55	0.47	Dispersed
45	8.4	81.6	88.76	28	99.74	1.73	0.48	Dispersed
46	8.8	94.2	98.28	28	98.68	2.00	0.46	Dispersed
47	8.9	100.8	115.24	28	92.31	2.14	0.44	Dispersed
48	9.1	104.6	124.28	28	90.19	2.22	0.44	Dispersed
49	11.2	129.4	158.07	28	96.55	2.74	0.42	Dispersed
50	10.8	148.2	174.41	28	88.07	3.15	0.37	Dispersed

Table 4.6. Two-Phase Flow Regime Data for 800 μm Test Section.

Run	Q_{air} (slpm)	Q_{water} (cc/min)	P_l (kPa)	T (°C)	U_G (m/s)	U_L (m/s)	x	Flow Regime
1	1.2	21.6	47.74	25	27.52	0.72	0.0450	Annular
2	1.4	25.3	48.06	25	31.83	0.84	0.0445	Annular
3	1.4	30.0	53.06	25	32.49	1.00	0.0385	Dispersed
4	1.5	32.7	55.89	25	33.49	1.08	0.0366	Dispersed
5	1.6	35.3	54.55	25	35.48	1.17	0.0359	Dispersed
6	2.3	41.3	54.00	25	51.06	1.37	0.0438	Dispersed
7	1.9	45.9	58.26	25	42.44	1.52	0.0331	Dispersed
8	2.1	50.5	61.81	25	45.09	1.68	0.0320	Dispersed
9	2.3	56.1	66.94	25	47.41	1.86	0.0304	Dispersed
10	2.1	64.9	61.46	25	43.77	2.15	0.0244	Dispersed
11	3.7	62.1	82.44	25	70.29	2.06	0.0402	Dispersed
12	3.9	55.5	80.13	25	75.60	1.84	0.0480	Dispersed
13	3.7	50.6	77.59	25	71.29	1.68	0.0495	Dispersed
14	3.6	43.8	72.26	25	71.62	1.45	0.0571	Dispersed
15	3.6	41.6	68.65	25	74.27	1.38	0.0620	Dispersed
16	3.1	37.7	47.81	25	71.62	1.25	0.0657	Dispersed
17	3.0	30.4	43.04	25	73.28	1.01	0.0818	Dispersed
18	2.9	24.9	38.60	25	72.95	0.82	0.0980	Dispersed
19	2.9	22.1	38.40	25	71.29	0.73	0.1065	Dispersed
20	2.9	18.7	35.57	25	72.61	0.62	0.1256	Annular
21	4.1	17.6	43.16	25	98.81	0.58	0.1724	Annular
22	4.2	25.3	49.82	25	95.49	0.84	0.1228	Annular
23	4.4	31.4	52.88	25	98.15	1.04	0.1036	Dispersed
24	4.3	37.5	57.14	25	93.50	1.24	0.0846	Dispersed
25	4.3	45.5	61.45	25	91.51	1.51	0.0693	Dispersed
26	4.2	48.7	62.59	25	89.19	1.62	0.0635	Dispersed
27	4.2	52.4	64.90	25	87.54	1.74	0.0582	Dispersed
28	4.0	57.9	70.01	25	81.57	1.92	0.0496	Dispersed
29	4.3	60.0	70.20	25	87.87	1.99	0.0515	Dispersed
30	4.4	67.4	74.61	25	86.21	2.23	0.0452	Dispersed

CHAPTER V

CONCLUSIONS AND FUTURE DIRECTIONS

The present research yields considerable insight into the behavior of two-phase flow in mini- and micro-channels. In the short term, the outcome of this research will have a direct impact on the methodology used in the design of two-phase mini- and micro-channel systems. In the long term, the proposed research will serve as a baseline for studies of two-phase flow and heat transfer characteristics in mini- and micro-channels. This will lead to more reliable flow identification techniques and more universally valid flow regime maps. Also, it would lead to more accurate heat and flow models in mini- and micro-channels.

A new test facility was designed and constructed to investigate the two-phase flow and heat transfer in mini- and micro-channels, in both the short and long terms. After the completion of the test facility, two-phase frictional pressure drop measurements, as well as flow regime map experiments were performed with three different test sections which were 3 mm, 1 mm, and 800 μm in diameter. The pressure drop measurements were compared with the most widely used two-phase pressure drop correlations, namely: the homogenous, the Friedel (1979), and the Chisholm (1967) model. The homogenous model was the best model to predict the frictional pressure drop with an average error of 1.2%, 15.6%, and 24.1% for the 3 mm, 1 mm, and 800 μm test sections, respectively. However, it was also observed that the standard deviation of the errors increased as the

channel diameter decreased. The Friedel (1979) model over-predicted the pressure drop for every test section, while the Chisholm (1967) model mostly under-predicted the pressure drop data. The average error and the standard deviation of the results increases while the channel diameter decreases. Therefore, the homogeneous model is not appropriate for the prediction of experimental results in smaller channels.

The flow regimes were observed for high gas superficial velocities ($U_{GS} \geq 10$ m/s). There were three flow regimes and two transition regions observed in the 3 mm test section, which, when compared, were in fairly good agreement with the experimental data obtained by Damianides (1987). There were two flow regimes and one transition region observed in the 1 mm and the 800 μm test sections. Also, the flow regime transition region from annular to dispersed flow observed in the 1 mm test section was in fairly good agreement with the previous experimental data obtained by Damianides (1987), Fukano (1993), and Ekberg (1997) for the 1 mm circular test sections. However, in the present experiment, the transition from annular to dispersed was observed when the superficial water velocity was slightly higher than that observed in the experiments conducted by Damianides (1987), and Ekberg (1997). Finally, the transition region from the annular to the dispersed flow regime in the 800 μm test section occurred when the superficial water velocity was approximately 0.9 m/s, which coincided with the results obtained in the 1 mm test tube. This difference observed in the position of the flow regime transition regions may be explained by the different flow regime determination techniques used in the mentioned studies. A pressure traces method was used by Damianides (1987) for small channels, while a high-speed digital camera was used by

Ekberg (1997) for the visualization of images, and a 3CCD analog camera was used for the visualization of images in the present study. Also, due to the complex nature of the gas-liquid interface and especially due to the high velocities that are associated with annular and dispersed flow, the visual observation for the flow regime determination became very difficult for the mini- and micro-channels. It is important to note that determining most of the flow regimes was finalized with the unaided eye, so establishing the flow regimes in this way varies from researcher to another, since everybody has their own individual judgment about which flow regime they are observing.

FUTURE DIRECTIONS

Since most of the time for this research was spent on the design and the construction of the test facility, only a limited amount of time was designated for the actual experimental study, which in turn limited the number of the test sections used, the number of the parameter configurations employed, as well as the range of the test matrix.

Using smaller test sections (600 μm to 10 μm), changing the cross-section geometry of the test sections, as well as enlarging the range of the test matrix are all recommended extensions of this study. These suggestions can be implemented simply by changing the flow meters and test sections. If pursued, these studies could further examine the characteristics of the frictional pressure drop using more data and smaller test sections. Also, one should develop a mathematical model to predict the frictional pressure drop in mini- and micro-channels from the vast pool of data that will be produced in the future. The additional experimental data produced would contribute to the expansion of the

range of flow regime maps, and would ultimately lead to a universal flow regime map for two-phase flow in micro-channels. Lastly, studies on the experimental void fraction should be conducted.

To deepen the knowledge available thus far on the subject of boiling two-phase flow, the test facility could be used without the air supply line and with the addition of heat exchangers. This would permit the acquisition of data for the heat transfer characteristics of mini- and micro-channel two-phase flow. Also, instead of using water as a two-phase flow component, the tests could be run with different fluids, such as coolants. The test facility was designed to perform a wide variety of experiments pertaining to two-phase flow, by simply changing one or more parameters of the test facility.

REFERENCES

Agrawal, S. S., Gregory, G. A. and Govier, G. W., "An analysis of horizontal stratified two-phase flow in pipes", The Canadian Journal of Chemical Engineering, Vol. 51, 1973, pp. 280-286.

Al-Sheikh, J. N., Saunders, D. E. and Brodkey, R. S., "Prediction of flow patterns in horizontal two-phase pipe flow", The Canadian Journal of Chemical Engineering, Vol. 48, 1970, pp. 21-29.

Annunziato, G. and Girardi, G., "Horizontal two-phase flow: a statistical method for flow pattern recognition", Proceedings of the Third International Conference on Multi-Phase Flow, Paper F1, The Hague, Netherlands, 1987, pp. 169-185.

Alves, G. E., "Cocurrent liquid-gas flow in a pipeline contractor", Chemical Engineering Progress, Vol. 50, No. 9, 1954, pp. 449-456.

Baker, O., "Simultaneous flow of oil and gas", The Oil and Gas Journal, Vol. 53, 1954, pp. 185-195.

Barnea, D., Luninski, Y. and Taitel, Y., "Flow pattern in horizontal and vertical two-phase flow in small diameter pipes", The Canadian Journal of Chemical Engineering, Vol. 61, 1983, pp. 617-620.

Baroczy, C. J., "A systematic correlation for two-phase pressure drop", Chemical Eng. Progress Symposium Series, Vol. 62, No. 64, 1966, pp. 232-249.

Beattie, D. R. H. and Whalley, P. B., "A simple two-phase frictional pressure drop calculation method", Int. J. Multiphase Flow, Vol. 8, 1982, pp. 83-89.

Bergelin, O. P., Gazley, C. Jr, "Cocurrent gas-liquid flow –I: Flow in horizontal tubes", Proceedings of the Heat Transfer and Fluid Mechanics Institute, June22-24, Berkeley, California, 1949, pp. 5-12.

Chisholm, D., "A theoretical basis for the Lockhart Martinelli Correlation for two phase flow", Int. J. of Heat and Mass Transfer, Vol. 10, 1967, pp. 1767-1778.

Choe, W. G., Weinberg, L. and Weisman, J., "Observation and correlation of flow pattern transitions in horizontal cocurrent gas-liquid flow", Two-Phase Transport and Reactor Safety (Edited by Verizoglu, T. N., and Kakak, S.), Hemisphere, Washington, 1978.

Coleman, J. W. and Garimella, S., "Characterization of two-phase flow patterns in small diameter round and rectangular tubes", Int. J. Heat Mass Transfer, Vol. 42, No. 15, 1999, pp. 2869-2881.

Corradini, M. L., "Multiphase flow and heat transfer", Lecture Notes, University of Wisconsin, http://courses.engr.wisc.edu/ecow/get/neep/520/corradini/notes/, 2002.

Damianides, C., "Horizontal two-phase flow of air-water mixtures in small diameter tubes and compact heat exchangers", Ph.D. Thesis, University of Illinois at Urbana-Champaign, 1987.

Damianides, C. and Westwater, J.W., "Two-phase flow patterns in a compact heat exchanger and in small tubes", Proceedings of the Second U.K. National Conference On Heat Transfer, Vol. II, Glasgow, Scotland, 1988, pp. 1257-1268.

Duckler, A. E. and Hubbard, M. G., "The characterization of flow regimes for horizontal two-phase flow –I: Statistical analysis of wall pressure fluctuations", Proceedings of the Heat Transfer and Fluid Mechanics Institute, Edited by Saad, M. A. and Miller, J. A., Stanford University Press, 1966, pp. 100-121.

Eaton, B. A., Andrews, D. E., Knowles, C. R., Silberberg, I. H. and Brown, K. E., "The prediction of flow patterns: Liquid holdup and pressure losses occuring during continuous two-phase flow in horizontal pipelines", Journal of Petroleum Technology, Vol.19., 1967, pp. 815-828.

Ekberg, N. P., "Two-phase flow regime maps and pressure drop in micro-channels", Master Thesis, Georgia Tech., 1997.

Ekberg, N. P., Ghiassian, S. M., Abdel-Khalik, S. I. and Yoda, J., "Gas-liquid two-phase flow in narrow horizontal annuli", Nuclear Engineering and Design, Vol.7., 1999, pp. 112-121.

Fukano, T., Kariyasaki, A. and Kagawa, M., "Flow patterns and pressure drop in isothermal gas-liquid concurrent flow in a horizontal capillary tube", ANS Proceedings 1989 National Heat Transfer Conference, Vol. 4, 1989, pp. 153-161.

Govier, G. W. and Omer, M. M., "The horizontal pipeline flow of air-water mixtures", The Canadian Journal of Chemical Eng., Vol. 40, 1962, pp. 93-104.

Govier, G. W. and Aziz, K., "Flow of complex mixtures in pipes", Van Nostrand-Reinhold Co., New York, 1972, pp. 554-613.

Harms, T. H., "Heat transfer and fluid flow in deep rectangular liquid cooled micro-channels etched in a (110) silicon substrate", Master Thesis, University of Tennessee, 1995.

Hughes, R. R., Evans, H. D. and Sternling, C. V., "Flash vapourization analysis of fluid mechanical and mass transfer problems", Chemical Eng. Prog., Vol. 49, No.2, 1953, pp.78-87.

Hoogendoorn, C. J., "Gas-liquid flow in horizontal pipes", Chemical Eng. Science, Vol. 9., 1959, pp. 205-217.

Johnson, H. A. and Abou-Sabe, A. H., "Heat transfer and pressure drop for turbulent flow on air water mixtures in a horizontal pipe", Trans. of the American Society of Mechanical engineers, Vol. 74, 1952, pp. 977-998.

Kosterin, S. I., "An investigation of the influence of the diameter and inclination of a tube on the hydraulic resistance and flow structure of gas-liquid mixtures", Izvestia Akad.Nauk SSSR, Vol. 12, 1949, pp. 87-102.

Lockhart, R. W. and Martinelli, R. C., "Proposed correlation of data for isothermal two-phase, two-component flow in pipes", Chemical Engineering Progress, Vol. 45, No. 1, 1949, pp. 39-48.

Mandhane, J. M., Gregory, G. A. and Aziz, J., "A flow pattern map for gas-liquid flow in horizontal pipes", International Journal of Multiphase Flow, Vol. 1, 1974, pp. 537-553.

Martinelli, R. C., Boelter, L. M. K., Taylor, T. H. M., Thomsen, E. G. and Morrin, E.H., "Isothermal pressure drop for two-phase two-component flow in a horizontal pipe", Transactions of the American Society of Mechanical Engineers, Vol. 66, No. 2, 1944, pp. 139-151.

Mishima,K., Kibiki, T. and Nishirara, H., "Some characteristics of gas-liquid flow in narrow rectangular ducts", Int. J. Multiphase Flow, Vol. 19, 1993, pp. 115-124.

Nicholson, M. K., Aziz, K. and Gregory, G.A., "Intermittent two-phase flow in horizontal pipes: predictive models", The Canadian Journal of Chemical Engineering, Vol. 56, 1978, pp. 653-663.

Scott, D. S., "Properties of cocurrent gas-liquid flow", Advances in Chemical Eng., Vol. 4., 1963, pp. 208-211.

Simpson, H. C., Rooney, D. H., Grattan, E. and Al Samarrae, F., "Two-phase flow in large diameter horizontal tubes", Paper A6 presented at the European Two-Phase Flow Group Meeting, Grenoble, June 1977.

Suo, M., and Griffith, P., "Two-phase flow in capillary tubes", Transactions of the ASME-Journal of Basic Engineering, Vol. 86, 1964, pp. 576-582.

Tabatabai, A. and Faghri, A., "A New two-phase flow map and transition boundary accounting for surface tension effects in horizontal miniature and microtubes", Transaction of the ASME, 2001.

Taitel, Y. and Duckler, A. E., "A model for predicting flow regime transitions in horizontal and near horizontal gas-liquid flow", AIChE Journal, Vol. 22, No. 1, 1976, pp. 47-55.

Taitel, Y., Barnea, D. and Dukler, A. E., "Modeling flow patterns transitions for steady upward gas-liquid flow in vertical tubes", AIChE J1 22, 1980, pp. 47-55.

Troniewski, L. and Ulbrich, R., "Two-phase gas-liquid flow in rectangular channels", Chem. Eng. Sci., Vol. 39, 1984, pp. 751-765.

Wambsganss, M. W., Jendrzejczyk, J. A., France, D. M. and Obot, N. T., "Two-phase flow patterns and frictional pressure gradients in a small, horizontal, rectangular channel", Argonne National Lab. Report ANL-90/19, 1990.

Weisman, L., Duncan, D., Gibson, J. and Crawford, T., "Effects of fluid properties and pipe diameter on two-phase flow patterns in horizontal lines", International Journal of multiphase flow, Vol. 5, 1979, pp. 437-462.

Wilmarth, T. and Ishii, M., "Two phase flow regimes in narrow rectangular vertical and horizontal channels", Int. J. Heat Mass Transfer, Vol. 37, 1994, pp. 1749-1758.

White, P. D. and Huntington, R. L., "Horizontal cocurrent two-phase flow of fluids in pipe lines", The Petroleum Eng., Vol. 27, 1955, pp. D40-D45.

Xu, J. L., Cheng, P. and Zhao, T. S., "Gas liquid two-phase flow regimes in rectangular channels with mini/micro gaps", Int. J. of Multiphase Flow, Vol. 25., 1999, pp. 411-432.

Xu, J., "Experimental study on gas-liquid two-phase flow regimes in rectangular channels with mini gaps", Int. J. Heat and Fluid Flow , Vol. 20, 1998, pp. 422-428.

Appendix A

House Calibration of the Main Components

The flow meters and the differential pressure transducers were chosen after a very careful and precise research. The most accurate and reliable instruments in their classes, which were specifically built for research purposes, were supplied for the test facility. Even though, the manufacturer companies and the products were reliable products in the market, there was a need for house calibration of the devices as to not leave any hesitation or question as to the experimental certainty.

Water flow meters are the devices that measure the flow rate per minute, so if we could measure the actual flow rate and compare this data with the reading, we would be able to calibrate the flow meters.

The water flow meters were directed inside a high precise measuring tube. After collecting certain amount of water, and dividing this amount by the time calculated with the timer clock which gave us the actual flow rate. The reading mostly doesn't remain perfectly constant or steady, so the average reading value is considered as the reading.

The calibration charts are plotted as below for the water flow meters. Please note that, the small accuracy of reading from the measuring tube, and the procedure followed to find the average reading were the main sources of error during this calibration.

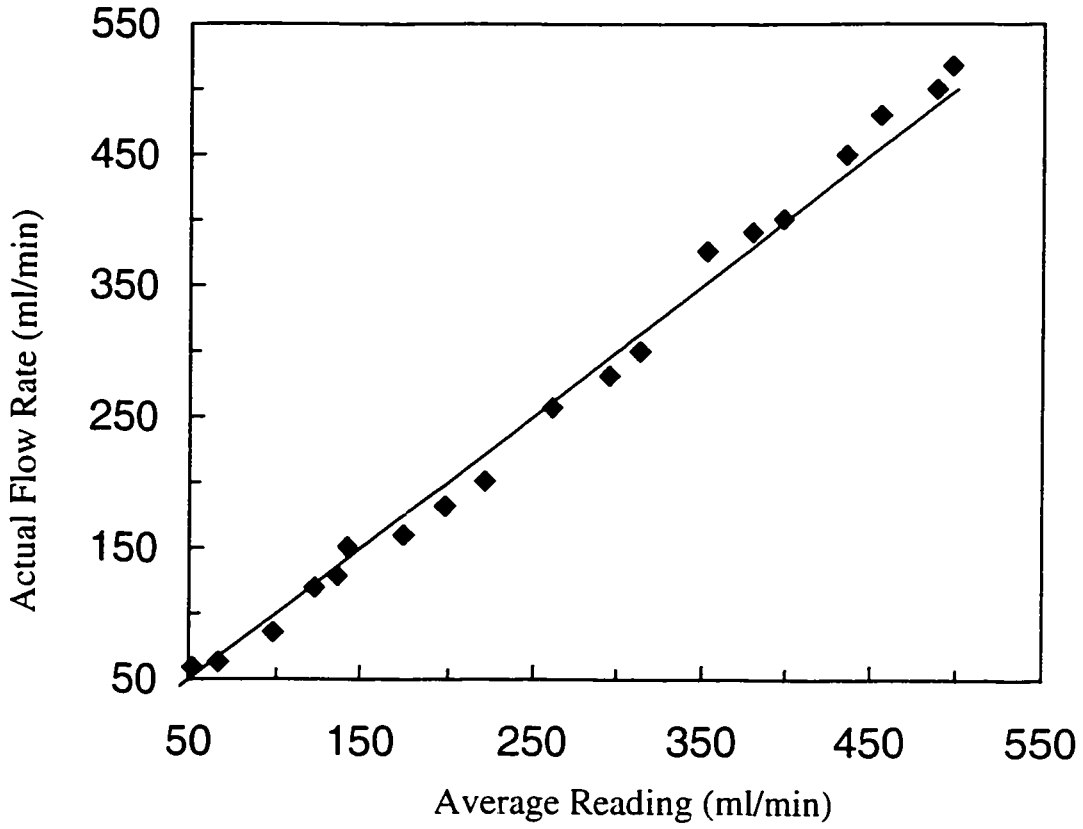

Figure A.1. Water Flow Meter Calibration Chart (50-500 ml/min).

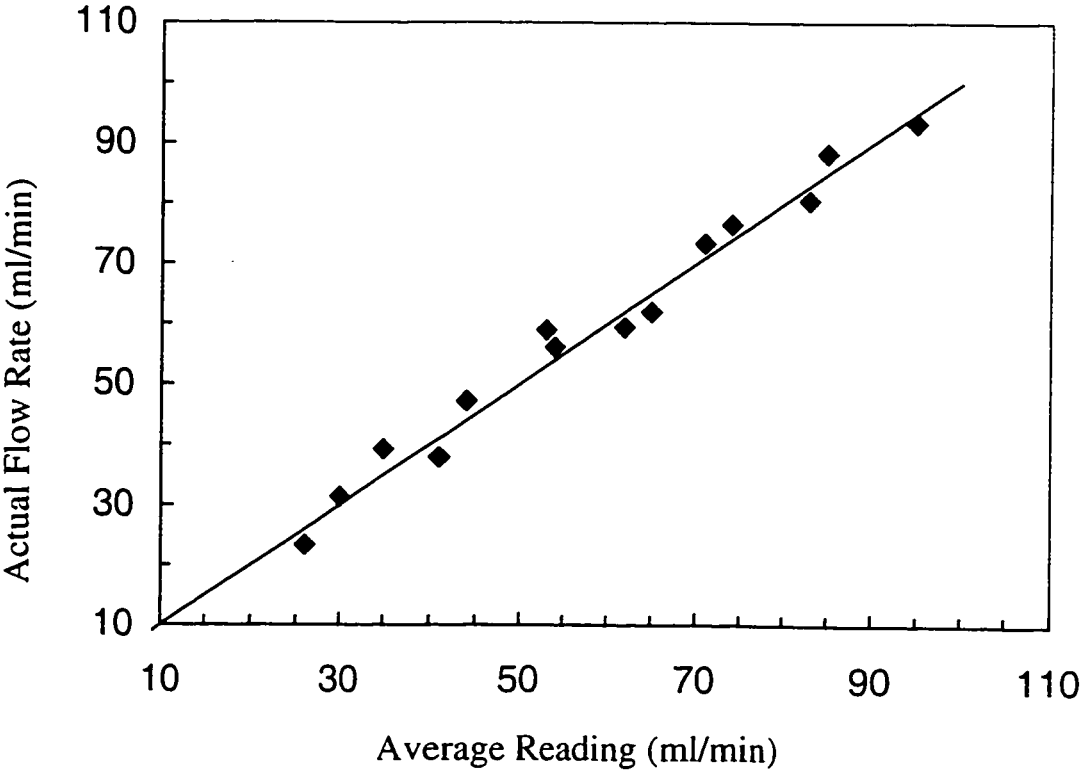

Figure A.2. Water Flow Meter Calibration Chart (15-100 ml/min).

The differential pressure transducer is the device measuring the pressure from both sides (inlet-outlet) and calculating the difference as a pressure drop. These differential transducers are also very accurate devices with high repeatability and they are able to work with air-water mixture. The calibrations for these devices were mostly done to be certain about the programming of the digital meter than the calibrating of the differential pressure transducer.

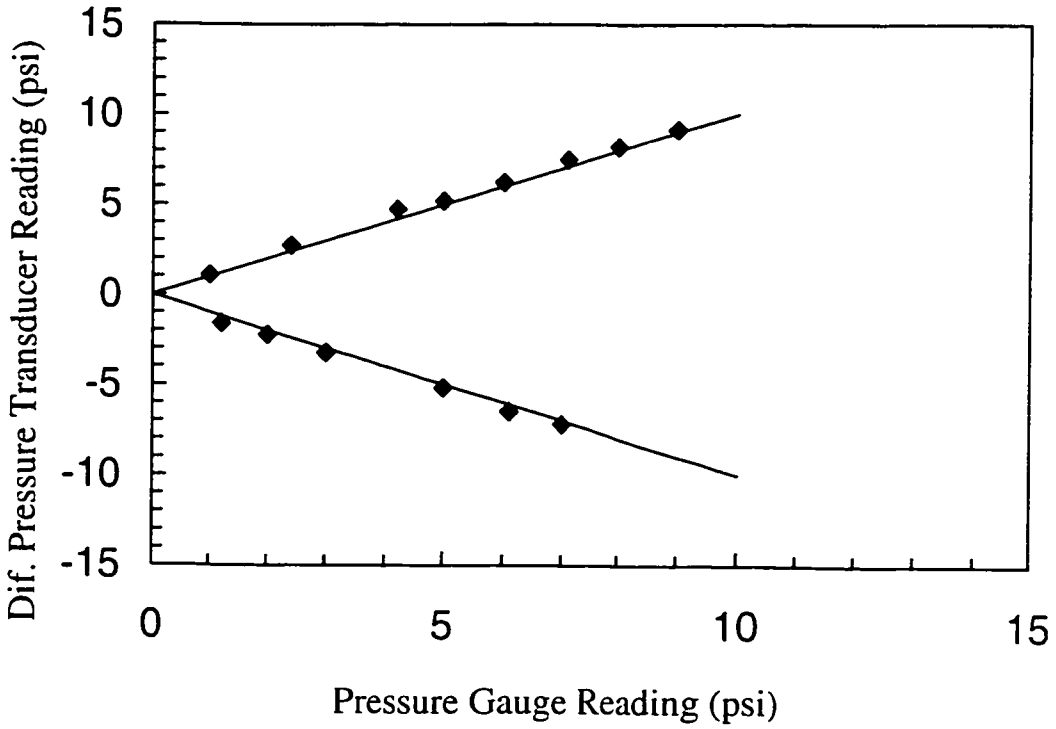

Figure A.3. Differential Pressure Transducer Calibration with a Pressure Gauge.

The method used to make the calibration was very simple. The procedure was using the differential transducer as a pressure gauge by leaving one of the sides to the atmosphere. The regulated pressurized air (by using the pressure regulator) was installed either the inlet or the exit side of the pressure transducer and the other side of the pressure

transducer was left open to the atmosphere. So the reading from the pressure gauge installed on the pressure regulator presents the actual pressure, the reading from the differential pressure transducer presents the experimental reading as plotted above. Please note that, the uncertainty of the pressure gauge is very high compared to that of the digital reading from the differential pressure transducer. After considering the reading error of the pressure gauge and looking at the Figure A.3, there was no more doubt about the differential pressure transducers and the digital meters.